Functionalization of In-plane Photonic Microcantilever Arrays for Biosensing Applications

Stanley J. Ness

A dissertation submitted to the faculty of
Brigham Young University
in partial fulfillment of the requirements for the degree of

Doctor of Philosophy

Gregory P. Nordin, Chair
Aaron R. Hawkins
Brian A. Mazzeo
Richard K. Watt
Adam T. Woolley

Department of Electrical and Computer Engineering

Brigham Young University

November 2012

ABSTRACT

Functionalization of In-plane Photonic
Microcantilever Arrays for
Biosensing Applications

Stanley J. Ness
Department of Electrical and Computer Engineering, BYU
Doctor of Philosophy

Microcantilevers have been investigated as high sensitivity, label free biosensors for approximately 15 years. In nearly all cases, a thin gold film deposited on the microcantilevers is used as an intermediate attachment layer because of the convenience of thiol-gold chemistry. Unfortunately, this attachment chemistry can be unstable when used with complex sample media such as blood plasma. The Nordin group at BYU has recently developed an all-silicon in-plane photonic microcantilever (PMCL) technology to serve as a platform for label-free biosensing. It has the advantage of being readily scalable to simultaneous readout of many PMCLs in array format, and allows integration with polymer microfluidics to facilitate the introduction of biological samples and reagents. An essential processing step for the transformation of the PMCL into a practical biosensor is the ability to effectively immobilize active biological receptors directly on silicon PMCL surfaces such that ligand binding generates sufficient surface stress to cause measureable PMCL deflection. This dissertation presents the development of a method to functionalize the sensor surface of all-silicon in-plane photonic microcantilever (PMCL) arrays.

This method employs a materials inkjet printer for non-contact jetting and a fluid that is custom designed for ink-jetting and biological applications with approximately 1 pL droplet size. The method facilitates the application of different receptors on select PMCLs with drop placement accuracy in the +/- 7.5 μm range. The functionalization fluid facilitates further processing using humidity control to achieve full coverage of only the PMCL's top surface and removal of dissolved salts to improve uniformity of receptor coverage and to prevent fouling of the sensor surface.

Once a functionalization method was successfully developed, a series of experiments were performed to investigate the amount of surface stress that can be generated when receptors are immobilized directly to the silicon surface. In one series of experiments, a 4.8 μM streptavidin solution was used with biotin immobilized on multiple PMCLs to demonstrate adsorption-induced surface stress and concomitant deflection of the PMCL. The group observed ~ 15 nm PMCL deflection on average, with a corresponding surface stress of approximately 4 mN/m. These experiments yield the sensor response in real-time and employ a combination of multiple PMCLs functionalized as either sensors or unfunctionalized to serve as references. Investigation of various attachment chemistries is included, as well as a comparison with and without passivation of non-sensor surfaces. Investigated passivation strategies prevented ligand binding from generating a differential surface stress. Failure modes and physical mechanisms for adsorption-induced surface stress are discussed.

Immobilization and passivation strategies for antibody-based biosensing are demonstrated with fluorescence microscopy and a corresponding PMCL sensing experiment using rabbit anti-goat F(ab') fragments as the receptors and Alex Fluor 488 labeled goat anti-rabbit IgGs as the ligand. While the results of these experiments remain inconclusive, suggestions for future research involving the PMCL sensor array are recommended.

Keywords: Stanley J. Ness, microcantilever, inkjet functionalization, in-plane photonic transduction, photonic microcantilever, biosensor, PDMS microfluidics, streptavidin, biotin, organosilane, CVD, antibody fragment immobilization, F(ab') fragment, adsorption-induced surface stress

ACKNOWLEDGMENTS

First and foremost, I would like to acknowledge the hand of God in all things, yes, even in science, engineering and university research.

I appreciate my family, friends and colleagues whose support has sustained me and allowed me to complete my formal education. I feel very fortunate to have as my advisor, Dr. Gregory P. Nordin, and thank him for his guidance and encouragement. I have been consistently impressed with his technical acumen combined with his patient and effective leadership of our research group. I would like to thank the members of my graduate committee, Dr. Aaron Hawkins, Dr. Brian Mazzeo, Dr. Richard Watt, and Dr. Adam Woolley for their comments, suggestions and guidance. My special thanks goes to Dr. Seunghyun Kim, who was so very instrumental in the success of this microcantilever project in a variety of ways.

I cannot thank enough the members of my research group and students in other research groups for their dedication and willingness to train me in their areas of expertise. Additionally, I am very grateful for the professional competence of the ECEn Department staff who are always supportive and easy to work with.

Unequalled was the contribution of my lovely wife, Jennifer, and three adorable daughters, Sami, Abby, and Lydia. I am truly grateful for their sacrifice, love and support that allowed me to spend many a long night completing experiments, analyzing data and writing papers.

Finally, I would like to acknowledge the financial support from NSF grants ECS-0602261 and IIS-0641973, and DARPA grant 66001-04-8933 that funded parts of the research for this dissertation.

TABLE OF CONTENTS

LIST OF TABLES

LIST OF FIGURES

1 INTRODUCTION

Optical and electronic sensors enhance almost every aspect of human life. We use IR sensors to change the TV channel, RF sensors to open and start our vehicles, and motion sensors to aid in the operation of our phones and other hand-held devices. The area of healthcare is no exception. From advanced imaging systems to glucose sensors, there are many sensor-based devices to help medical professionals diagnose and treat their patients.

In general, a sensor is a device that detects and measures a physical quantity of energy or matter and then converts that measurement into a signal to be read by the observer. New methods to detect and characterize natural phenomena at a lower limit of detection form the backbone of advancing science and technology. A microcantilever (MCL) is a mechanical device that can be used as the basis of a sensor. This dissertation focuses on the transformation of a simple MCL into a biosensor.

1.1 Motivation

In 2009, the United States spent $7,960 per capita on healthcare [1]. With high costs driving the fast paced growth of biotechnology and pharmaceuticals, opportunities for cost reduction abound. A nano/micro-scaled diagnostic sensor capable of detecting biomolecules at very low concentrations (pico- to femto-molar range) could enable a cost savings through faster, more reliable and accurate diagnosis of a patient's condition and reduced consumption of reagents in the lab.

Microcantilevers (MCLs) have been successfully demonstrated as nanomechanical biosensors based on a variety of biomolecular interactions, including DNA hybridization [2-4], DNA-protein [5,6], protein-protein [7,8], and antibody-antigen [3,7,9,10]. The two most common readout methods involve reflecting a laser beam from a MCL onto a position sensitive detector (optical lever method) or measuring min changes in resistance of a piezoresistor embedded in the MCL [11]. The optical lever method provides much higher responsivity, i.e., change in normalized output signal per change in deflection, (the best reported values are 10^{-3} nm^{-1} vs. ~$4x10^{-6}$ nm^{-1}, respectively) [12] but does not scale well to simultaneous readout of multiple MCLs.

The Nordin research group has recently developed a new differential MCL transduction mechanism based on photonic MCLs (PMCLs) with integrated waveguides [12-14] designed to allow simultaneous readout of tens to hundreds of PMCLs on a single chip [15]. Moreover, the responsivity is comparable to the best reported for the optical lever method [12], which has enabled the group to readily measure differential surface stress changes as small as 0.23 mN/m with a 16-MCL array [17].

These PMCL arrays are designed to operate based on static deflection due to receptor/ligand adsorption (static mode), rather than measuring a shift in resonance frequency (dynamic mode). Static mode is typically preferred for sensing in liquid due to the damping effect that liquid has on microcantilever vibration which decreases the quality factor, Q, of the fundamental mode microcantilever resonance [17]. To induce static deflection, a MCL must have receptor molecules attached to only one side of the MCL, such that receptor uptake of the ligands creates a change in surface stress on only that side. The result is a differential surface stress between the functionalized and unfunctionalized sides of the MCL, which creates a net

bending of the MCL. Hence molecular adsorption is converted into mechanical deflection of the MCL, which is then transduced with the in-plane differential photonic read out mechanism.

In the vast majority of cases reported in the literature, receptor molecules for microcantilever biosensors are attached to a MCL by first depositing a thin layer (<40 nm) of gold followed by reaction of proteins, DNA, antibodies, and/or molecular linkers that have an attached thiol group with the gold layer [2-10,17-20]. This method has the advantage of exploiting the well-known gold-thiol binding chemistry to form the desired reactive receptor layer on the surface of the cantilever. Moreover, it is an especially simple and convenient method of attaching reactive molecules to just one side of a MCL while immersing the MCL in the functionalization fluid since the gold-thiol interaction drives assembly of molecules on only those portions of the surface coated with the gold layer (typically either the top or bottom surface of the MCL). However, serious disadvantages of this approach include large deflection sensitivity to changes in temperature [21, 22], instability of the receptor gold-thiol linkage in the presence of thiols in complex sample media such as blood plasma [47], and susceptibility of the gold-thiol bond to air oxidation [23].

In summary, PMCLs are of interest as biosensors due to their potential for label-free sensing, fast response, high sensitivity, small size, scalability and compatibility with "lab-on-a-chip" microfluidic systems. This, along with their potential use in both gaseous and liquid media, presents an important advancement opportunity with scientific and healthcare applications. However, a method to modify the PMCL surface to facilitate its use as a biosensor, in a process termed "functionalization", must be developed before their full potential can be realized.

1.2 Overview of Dissertation

This dissertation introduces an improved functionalization method specifically designed for an all-silicon PMCL array and presents the results of actual sensing experiments using biotin/streptavidin and polyclonal IgG as the receptors/ligands. The dissertation is organized as follows.

In chapter 2, I review background information on PMCL fabrication, primary mode of operation, transduction and readout, including adsorption-induced surface stress, biochemistry, surface chemistry, and the role of microfluidic integration.

In chapter 3, I demonstrate the single-sided inkjet functionalization of PMCL array with discussion of the experimental approach, results and conclusions.

In chapter 4, I present the Nordin group's streptavidin sensing results with the in-plane silicon PMCL including my selection of successful reagents, possible passivation molecules, discussion of the results and conclusions.

In chapter 5, I present a strategy to immobilize an IgG based receptor/ligand system in an oriented fashion for use with the PMCL and results of a sensing experiment to determine the degree of adsorption-induced surface stress generated by an IgG based system.

The final chapter, chapter 6, provides a summary of this work and discusses potential research opportunities.

1.3 Contributions

My specific contributions to the research and development of biosensors based on PMCL arrays are as follows:

1) Developed and demonstrated a jettable fluid for the Dimatix Fujifilm DMP-2831 Materials Printer and its corresponding 1 pL drop volume cartridge (DMC-11601)

that is biologically compatible, tailorable to various aqueous reaction requirements (pH, buffer concentration, % organic solvents, etc.) and capable of remaining hydrated on a MCL during an incubation period.

2) Developed and demonstrated the method and print patterns to accurately place any number of 1–2 pL drops of jettable fluid on MCLs that are 45 μm wide x 100 – 500 μm long, including a mathematical coverage model and equations relating functionalization coverage to deflection.
3) Developed and demonstrated a method to consistently deposit a monolayer film of amino-silane on released PMCL arrays while maintaining the functionality of the die and activity of the surface.
4) Developed and demonstrated a method to expand functionalization fluid to near full and uniform coverage after inkjet deposition, including a method to prevent buffer salts from aggregating on the sensor surface and fouling receptors.
5) Demonstrated different functionalization chemistries that resulted in adsorption-induced surface stress and PMCL deflection upon adsorption of the target molecule.
6) Provided design and processing inputs for the PMCL die and PDMS microfluidic layouts with respect to functionalization and fluid handling requirements.
7) Characterized surface roughness and demonstrated its effect on PMCL deflection.
8) Developed a method to immobilize oriented IgG F(ab') fragments on one side of a PMCL.

2 BACKGROUND

Functionalizing a PMCL biosensor requires extensive knowledge concerning the fundamental operation of MCLs, adsorption-induced surface stress, PMCL fabrication, transduction and readout details, organic and biological chemistry, surface modification/characterization, micro-fluidics and micro-deposition systems. This chapter provides background information on these areas, especially as they relate to functionalizing PMCL biosensors.

2.1 Microcantilever Beam Theory

A MCL is a horizontal beam that is clamped or fixed at one end and free in six-degrees at the other. MCLs may be micro-machined in a variety of materials such as silicon (Si), silicon dioxide (SiO_2), silicon nitride (SiN), and even various polymers. They are commonly found as atomic force microscopy (AFM) tips that range from 1 - 8 μm thick, 20–50 μm wide, and 100–500 μm long depending on the mode of operation.

The fundamental behavior of the MCL is effectively modeled by Euler–Bernoulli beam theory (classical) as a first-order approximation, but with the advent of computer aided design (CAD), this is often superseded by finite element analysis (FEA) to match the intricacies of the design that may fall outside of classical underlying assumptions. Classical beam theory can lead to a number of closed-form equations to describe MCL motion based on a specific loading or applied force. The equation,

$$\kappa = \frac{1}{R} = \frac{6\sigma_f h_f (1-\nu^2)}{E t_s^{\,2}}, \tag{2-1}$$

as derived from classical beam theory by G. Stoney [37] and later revised by R. Koch [38], X. Feng [39], and K. Kitahara [49] to account for biaxial stress, is of primary concern for a PMCL undergoing adsorption-induced surface stress.

This form of Stoney's equation models the curvature (κ) of a MCL with an applied tensile or compressive stress in a thinly adsorbed film, where R is the radius of curvature, σ_f is the axial stress generated inside the adsorbed thin film, h_f is the thickness of the adsorbed layer, ν is Poisson's ratio, E is the Young's elastic modulus, and t_s is the thickness of the substrate from which the MCL is fabricated.

For the PMCLs, the orientation of the silicon-on-insulator (SOI) wafer is [110] with respect to the long axis of the PMCL, hence the elastic modulus is 169 GPa and Poisson's ratio is 0.064 [40]. Using the small angle approximation and equation for arc length, equation 2-1 can be integrated to find the tip deflection (w) when assuming a uniform applied surface stress over the entire length (L) of the MCL, yielding

$$w = \frac{3\sigma_f h_f L^2 (\nu^2 - 1)}{E t_s^{\,2}} \,. \tag{2-2}$$

Based upon classical beam theory, the underlying assumptions for these equations are as follows:

1) The adsorbed film and substrate have the same radius of curvature, R.
2) The film thickness h_f and substrate thickness t_s are uniform, and $h_f << t_s << R$, thus eliminating the need to offset the neutral plane and enabling the use of the small angle approximation.
3) The film and substrate are linearly elastic, homogeneous and isotropic.

4) Strains, rotations and out-of-plane stresses are negligible.

Local surface stress at the base of the MCL contributes to a larger portion of the total deflection than does local surface stress at the tip. Figure 2-1 shows a general schematic of a slightly deflected cantilever.

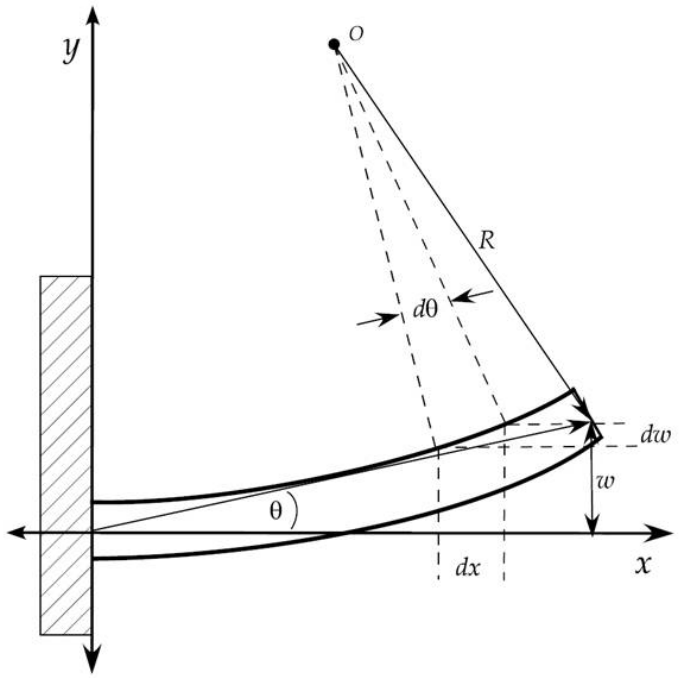

Figure 2-1: Schematic of deflected cantilever beam with parameters defined.

Assuming a uniform surface stress across the width of the beam, equation 2-1 can be integrated between two arbitrary points (x_1 and x_2) along the length of the MCL to give the expression

$$w(x_1, x_2) = \frac{3\,\sigma_f\, h_f\,(x_1 - x_2)(x_1 - 2L + x_2)(\nu^2 - 1)}{E\, t_s^{\,2}}, \tag{2-3}$$

which describes the deflection due to the local surface stress across the portion of the MCL bounded by the two points.

If one normalizes for length and total deflection of the MCL, one can see that the first half of the MCL from the fixed-end is responsible for 75% of the maximum possible deflection as shown in Figure 2-2. The last 20% of the MCL from the base only contributes 4%, thus illustrating the need for complete coverage, particularly at the base of the MCL, to achieve as much deflection as possible.

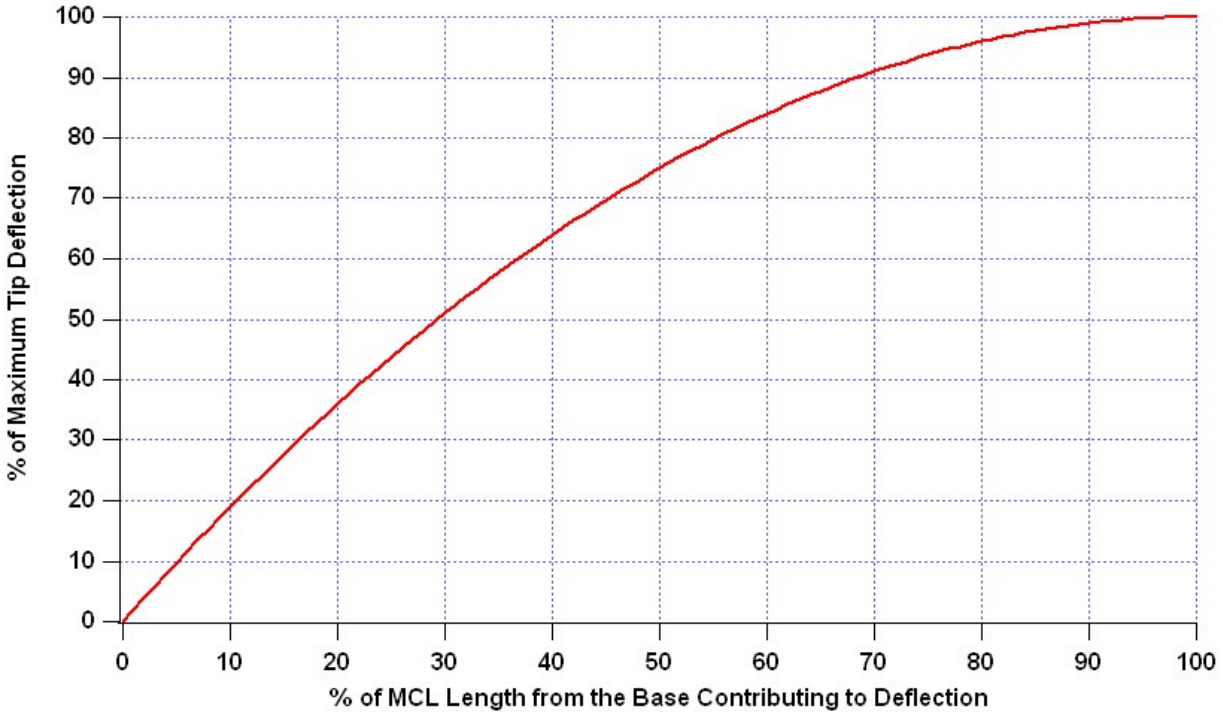

Figure 2-2: Normalized contribution of local surface stress as a function of position on the long axis of an MCL—cumulative starting at the base of the MCL.

2.2 Photonic Microcantilever

The PMCL is a unique type of microcantilever that is micro-machined in the plane of a SOI chip. Light propagating along a ridge waveguide on the surface of the chip traverses the gap at the free end of the PMCL, couples into a multi-mode step waveguide to be split and read out by a linear InGaAs focal plane array camera. The difference between the split signals scales

monotonically based on PMCL deflection. If only one surface of the PMCL is modified to induce a surface stress upon adsorption of a target molecule, then the chemical reaction will induce a corresponding mechanical deflection. The PMCL transduces the differential surface stress and corresponding deflection into an optical signal that the linear InGaAs focal plane array camera then transduces into an electrical signal for processing and storage. To give the reader a better understanding of the PMCL, this section outlines the fabrication and operation of the PMCL.

2.2.1 Fabrication of Multiple PMCL Array Chip

There are many fabrication challenges to overcome when constructing a PMCL array chip. This section presents information about the fabrication process of the specific devices used for this dissertation based on operational requirements and the impact fabrication may have on functionalization of the PMCL. Because an independent method of quantifying induced surface stress does not exist, I had to rely on the PMCL sensor platform itself for feedback. In order to increase the number of opportunities to test different functionalization protocols, the group modified the chip layout to provide two to three independently addressable arrays with 8 to 16 PMCLs in each array.

Figure 2-3 (a – e) shows the progression of the chip layout over the course of 3-4 years of experiments. The first generation chip featured 35 μm x 100 μm PMCLs in a 2 x 8 array configuration. Later, the width of the PMCLs was increased to 45 μm. For the second generation, room was made for an additional array of eight (8) PMCLs. The third generation increased the number of PMCLs in one of the three arrays to sixteen (16), thus providing 1 x 16 and 2 x 8 PMCL arrays on a single die. Additionally, an experiment to functionalize longer PMCLs (200 μm to 500 μm) was accomplished. Based on fabrication yield, the PMCL length of subsequent

generations was increased to 300 μm. A design having eight PMCLs available to serve as sensor and eight others to serve as reference PMCLs in a single array, allowed a clearer picture of sensor response by providing a better statistical average, even if 1 or 2 PMCLs in an array were lost. The benefit of this redundancy prompted the design of the fourth generation chip with 2 x 16 PMCL arrays. The 2 x 32 PMCL chip was designed, but never produced for experiments.

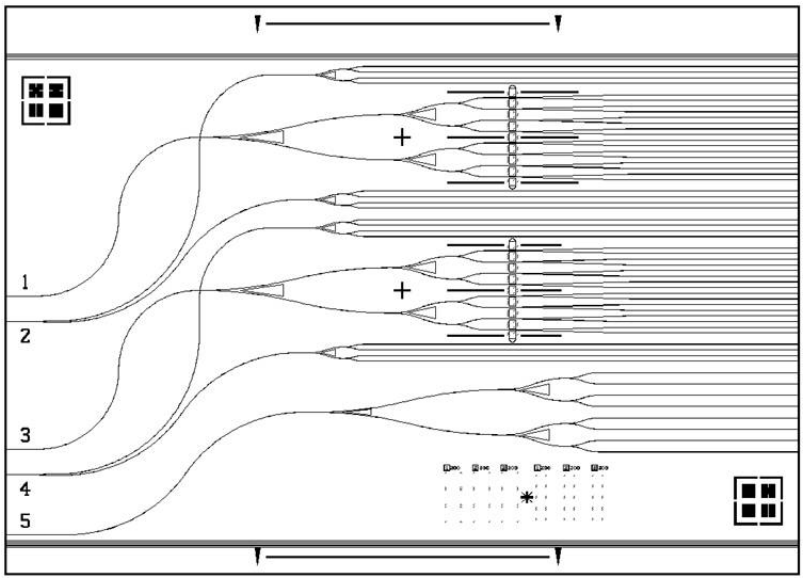

(a)

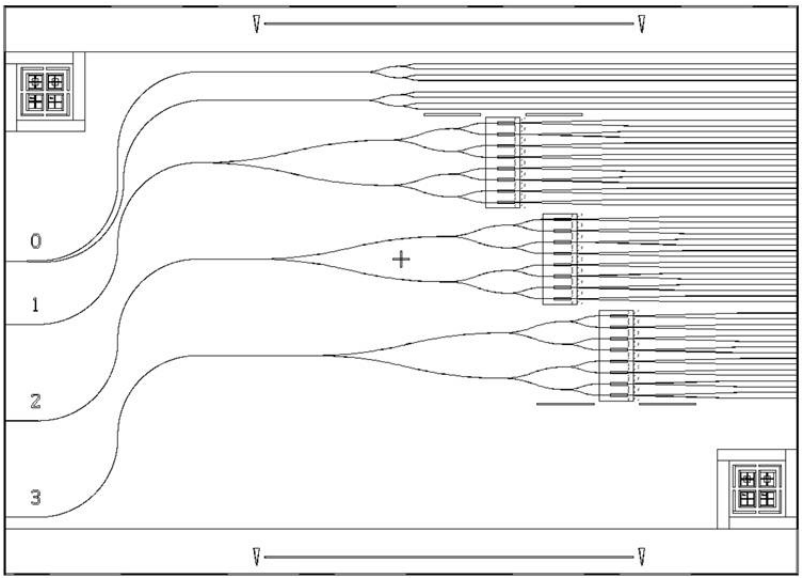

(b)

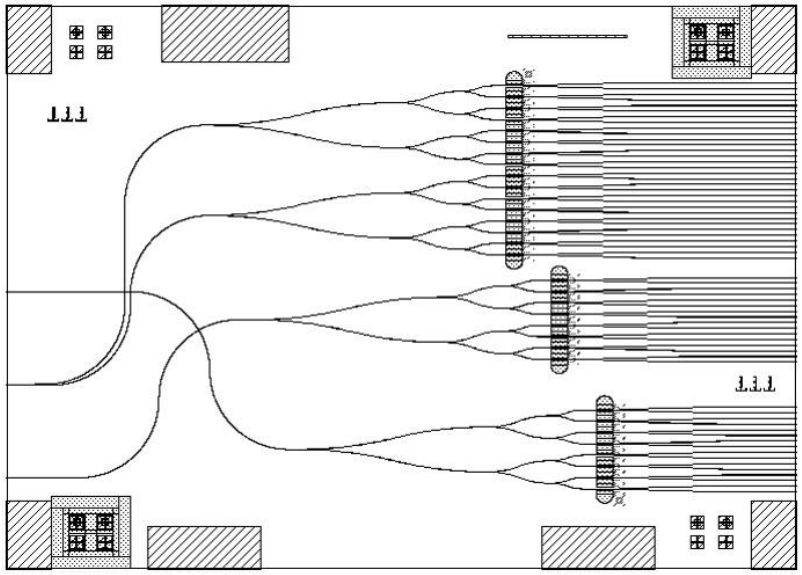

(c)

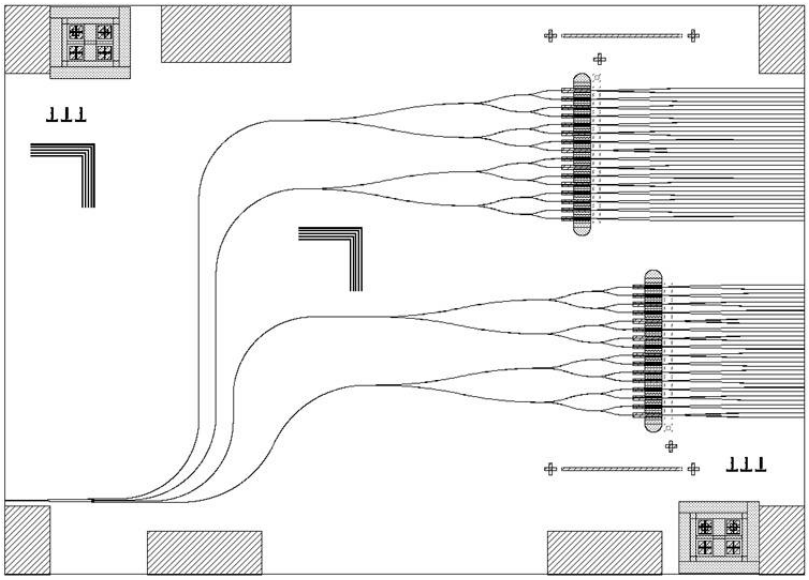

(d)

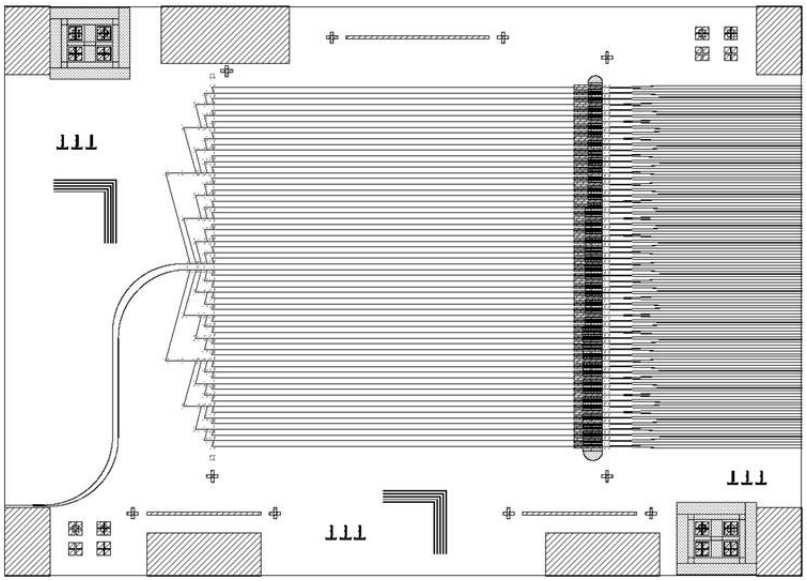

(e)

Figure 2-3: Successive PMCL die designs starting with (a) V.1 (2 x 8 PMCL arrays), (b) V.2 (3 x 8 PMCL arrays), (c) V.3 (1 x 16, 2 x 8 PMCL arrays), (d) V.4 (2 x 16 PMCL arrays) and (e) V.5 (2 x 32 PMCL arrays, which can be read out as a 64 PMCL array).

The processing steps for the different die layouts are basically the same. They can be divided into two categories: wafer-level processing and die-level processing. Wafer-level processing steps include ion implantation around the waveguide area, patterning of the waveguides and the gold alignment marks which are used for electron-beam lithography (EBL) during die-level processing to pattern fine features such as the multi-step ridge waveguide or features that may vary from die to die such as PMCL length and width. The steps for the wafer-level processing are as follows:

1) Photoresist is patterned to cover the area where future waveguides and PMCL arrays will be formed on a 100 mm SOI wafer with a 750 nm single crystal silicon top layer and a 3 μm buried oxide layer. This patterned photoresist is to protect the waveguide and PMCL areas against ion implantation. Boron ions are implanted in the field (minus the waveguide and PMCL areas) to reduce light scattering in the top silicon

layer and noise in the waveguide outputs via free-carrier absorption. Photoresist is applied by first dehydrating the wafer at 120 °C for 20 min, applying hexamethyldisilazane (HMDS) to promote adhesion and then spinning on S1813 photoresist at 2000 RPM for 60 sec Following a 1 min soft-bake at 115 °C, the photoresist is exposed for 12 sec at 10 mW/cm^2 of UV light in a MA150 CC Karl Suss contact aligner in hard contact mode, developed in MF319 developer for 60 sec and hard-baked at 120 °C for 40 min on a hot plate. Wafer doping is perform by Core System Inc. to a level of at least 5x10^{18} ions/cm^3. Boron is implanted twice to produce a relatively uniform distribution of ions through the thickness of the top silicon layer. The first dose imparts 3x10^{15} ions/cm^2 at 200 keV and the second dose imparts 3x10^{14} ions/cm^2 at 50 keV. The photoresist is then stripped and the wafer cleaned in Piranha solution (1:1 sulfuric acid: hydrogen peroxide) overnight at 130 °C.

2) EBL alignment marks are patterned at the same time as the rib waveguides so that the fine features will be as closely aligned with the waveguides as is possible. A 10 nm thick layer of chrome, followed by a 40 nm thick layer of gold are deposited on top of the wafer with a Denton e-beam evaporator. The chrome layer is used to improve gold adhesion. After dehydration and HMDS application, photoresist (AZ-701 @ viscosity of 11 cPs) is spun on the wafer at 4000 RPM for 60 sec. This is followed by a 1 min soft-bake at 90 °C, exposure in the contact aligner for 9 sec at 10 mW/cm^2 in hard contact mode, post-exposure-bake at 110 °C for 1 min, and developed in AZ-300 MIF for 90 sec. The chrome/gold layer is wet etched, leaving pads that will be

formed to make the EBL alignment marks in the next step. The photoresist is then stripped and the wafer cleaned in Piranha solution.

3) AZ701 is then spun on the wafer and patterned with a GCA 8500 DSW stepper at North Carolina State University to create the waveguides and differential splitters. After developing, the chrome/gold layer is wet etched to form the EBL alignment marks. To form the waveguide and splitter network, the top silicon layer is etched down 100 nm in a Surface Technology Systems (STS) inductively coupled plasma reactive ion etcher (ICP-RIE) using 90 sccm of C_4F_8, 50 sccm of SF_6, 800 W coil power, 15 W platen power, 15 mT pressure and 15 sec of etching time. The photoresist is then stripped and the wafer cleaned in Piranha solution.
4) Next, the wafer is coated with a sufficiently thick layer of photoresist to protect the surface while the wafer is diced into individual die using the Disco DAD 320 dicing saw.

Die-level processing creates the asymmetric double-step area of the multimode waveguide, patterns the outline of the individual PMCLs, polishes the input/output edges of the die for good optical transmission, undercuts the fixed-fixed micro-beam to remove the oxide layer, cuts one end of the micro-beam to form the free-end of the MCL and compensates excess upward deflection of individual MCLs with ion implantation. Details of each step are as follows:

1) EBL is used to create the asymmetric double-step multimode waveguide just across the gap of the free-end of the PMCL. This is done by spinning a positive resist (ZEP 520A) suitable for EBL on the die at 4000 RPM for 1 min and then soft baking at 180 °C for 2 min. A water soluble conductive polymer (aquaSAVE53za) is spun on top of the resist, followed by 30 sec at 90 °C on a hot plate to prevent charging of the

surface during EBL. A Nanometer Pattern Generation System (JC Nabity NPGS) and field emission environmental scanning electron microscope (FEI/Philips XL30 ESEM-FEG) are used to expose the positive resist. After adjusting the fine focus and astigmatism, an electron beam at 30 keV potential with a spot size of one is used to directly write the pattern with a dose of 60 $\mu C/cm^2$. The exposed sample is then developed in ZED-N50 (n-Amyl Acetate) for 2 min, followed by rinsing in ZMDD (Methyl Isobutyl Ketone). A 30 sec ICP-RIE dry etch using the same parameters as used for the waveguides is applied to create a 200 nm etch step. The photoresist is then stripped and the die cleaned in Piranha solution.

2) Photolithography is used to form the outline (length and width) of the individual PMCLs. A die is dehydrated at 120 °C for 20 min followed by spinning on Surpass 4000 (Step 1: 500 RPM at 110 RPM/sec for 5 sec, Step 2: 1000 RPM at 550 RPM/sec for 60s, Step 3 6000 RPM at 5500 RPM/sec for 12 sec) and then AZ701 is spun on at for 1 min at 400 RPM. The photoresist is then soft baked for 1 min at 90 °C, exposed for 7 sec in the contact aligner (soft contact mode), and developed for 15 sec with MIF3000. After a DI H_2O rinse and N_2 dry, the die is dry etched 650 nm in the STS ICP-RIE using 110 sccm of C_4F_8, 50 sccm of SF_6, 800 W coil power, 14 W platen power, 15 mT pressure and 3 min 30 sec etching time. The photoresist is then stripped and the wafer cleaned in Piranha solution.

3) Protective resist is applied over the face of the die in preparation for polishing the input and output edges of the die. Polishing is done on an oscillating CMP at a speed of 50 - 80 RPM with oscillations at ~ 0.5 Hz for ~90 min During the polishing process, water continuously rinses the diamond pad, starting with a 10 μm grit pad

and then a 1 μm grit pad. The photoresist is then stripped and the die cleaned in Piranha solution.

4) The oxide under the PMCLs is removed by applying a ~30 μL drop of 49% HF for 120 sec with a steady flow of air across the die to prevent HF fumes from under-cutting the edges of the die. The die is rinsed in DI H_2O, transferred to IPA and dried in a Tousimis Autosamdri 815B critical point dryer (CPD)
5) At this point, the PMCLs are fixed-fixed micro-beams arrays. To cut the trailing end (with respect to light propagation) of the micro-beam, a focused ion beam (FIB) was used to mill through the thickness of the beam. The die is prepared with conductive polymer (aquaSAVE53za) as previously described. Milling is done in a FEI Helios Nanolab 600 with FIB at 30 kV (900X magnification) and 28 pA with a Z-size of 2 μm for silicon.
6) Due to internal stress of the top SOI layer, the initial deflection of a 300-μm-long PMCL is on average 1 μm upward, which is outside of the transduction range of the PMCL. To compensate for this upward deflection, Ga^+ ions are implanted in a 64 μm x 45 μm area at the base of the PMCL with the FIB. A single FIB scan at 30kV (2000X magnification) and 2.7 pA is used to bombard this area and typically results in a 100 nm downward deflection, therefore, multiple scans may be necessary. Compensation is performed during the same FIB session as milling of the gap, so no additional die preparation is required. The conductive polymer is then stripped and the die cleaned in Piranha solution. The die is then rinsed in DI H_2O, transferred to IPA and dried in the CPD.

In later experiments, the dies were modified with an optional deep silicon etching (DSE) process that expands the etched region under the PMCL arrays, through the SiO_2 layer and into the silicon substrate. This process begins after step 2 in the above procedure (before the buried oxide is wet etched) and continues with the next step (HF wet etch of the buried oxide).

1) The die is cleaned with acetone, IPA and then dehydration baked for 15 min at 120 °C. A layer of SU-8 3005 is then applied by a spin-on process, first at 500 RPM and 125 RPM/sec for 5 sec, then a 200 RPM spin with 500 RPM/sec acceleration for 60 sec and finally a 6000 RPM spin with a 4000 RPM/sec acceleration for 2 sec to help eliminate ridges of the SU-8 along the edges of the die. The SU-8 is then soft-baked for 5 min at 65 °C. The temperature is then is increased to 95 °C and continues to bake at 95 °C for another 5 min.
2) The die is exposed with a Karl Suss Mask Aligner MA 150 for 30 sec in soft contact mode with a 70 μm gap and hard-baked following the same soft-bake procedure.
3) The SU-8 is then developed for 1 min in SU8 developer, rinsed with IPA and dried with an N_2 stream. The SU-8 coated die is now ready for etching as shown in Figure 2–4(a).
4) The etch process is relatively long, so that the edges of the die must be protected. After the die is mounted on a carrier wafer with thermal paste, the edges are covered with Kapton tape. The die and carrier wafer are placed in a Trion Technology Minilock Phanton III RIE/ICP for anisotropic dry etching of the SiO_2 buried oxide. The SiO_2 etch process is done for 5 min using CF_4 at 50 sccm with an RIE power of 75 watts, an ICP power of 550 watts, and a pressure of 12 mT.

5) The die is removed from the Trion to the STS Multiplex ICP-RIE to dry etch the underlying silicon substrate in a semi-isotropic process. The die is etched for 28 min with a SF_6 flow rate of 130 sccm, at 30 mT pressure, a coil power of 700 W and a platen power of 10 W.
6) The die is then cleaned in Nanostrip at 90 °C for 12 hours followed by a DI H_2O rinse and very gently dried with an N_2 stream.
7) The remaining oxide under the PMCL is then removed with 49% HF for 2 min, then rinsed with DI H_2O and very gently dried with N_2 stream.

Figure 2–4(a) shows a portion of the PMCL array with developed SU8-3005 over the area where dry etching of the buried oxide and underlying silicon substrate occurs. Figure 2-4 (b) shows the same area after dry etching.

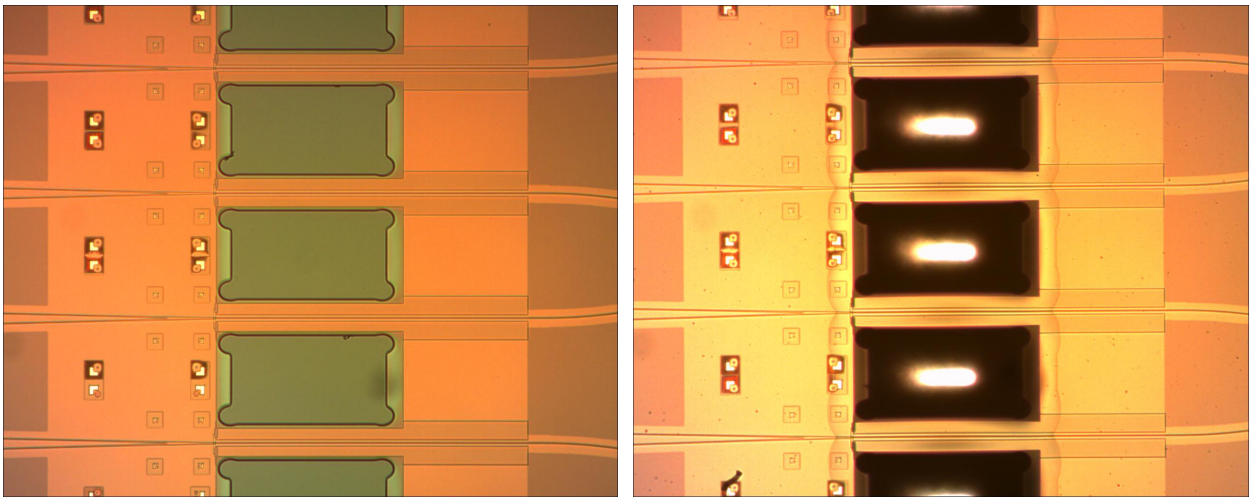

Figure 2-4: Optical microscope image of a die (45 x 300 µm PMCLs) with patterned photoresist (a) before and (b) after etching of the sacrificial oxide layer and underlying silicon substrate.

In summary, the sensor surface is exposed and possibly modified during fabrication by coatings of chrome/gold, and several different photoresists. The final processing step culminates in exposure to HF, which will strip the native oxide and lift off any residues. The native oxide then reforms after exposure to air and is thus ready for functionalization.

2.2.2 PMCL Transduction and Readout Method

The PMCL transduction method begins with a super-luminescent light-emitting diode (SLED) at 1550 nm as the light source, which is coupled into the single-mode waveguides at the edge of the die on the cantilever side of the gap with a single mode optical fiber (core diameter of 8-10 μm). As light propagates along the waveguides and crosses the gap, the light is captured by the asymmetric double-step multimode rib waveguide (ADSW) opposite the free end of the PMCL. The ADSW is made by etching down 200 nm for half the width of a 3-μm-wide multi-mode waveguide and the surrounding area as shown in the SEM image in Figure 2–5.

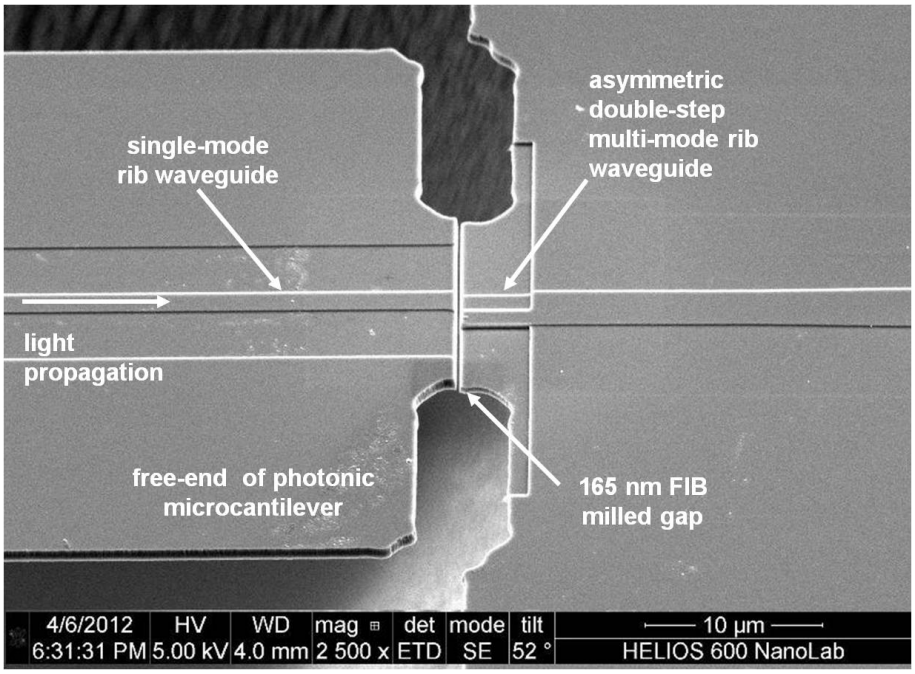

Figure 2-5: SEM image of the free-end of a PMCL with a patterned ADSW.

After passing this section of the optical path, the light is split by a Y-branch 1 x 2 optical power splitter to provide two optical outputs, P_1 and P_2, as shown in Figure 2-6.

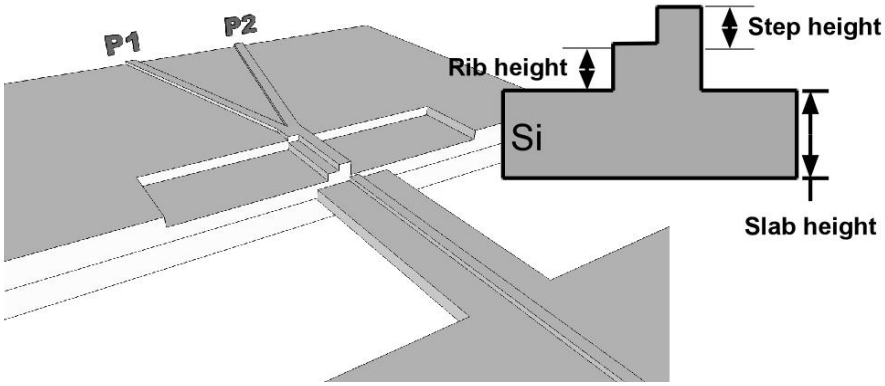

Figure 2-6: Schematic of free-end of a PMCL, ADSW and optical splitter with outputs P_1 and P_2.

The output face of the die is imaged on a linear InGaAs focal plane array camera and the power of each optical output is measured. Due to the geometry of the PMCL and ADSW, the transverse electric (TE) field distribution into P_1 and P_2 changes with respect to PMCL deflection. As seen in Figure 2–7, the individual output power profiles of P_1 and P_2 are Gaussian in nature with peak values that are slightly offset as indicated by Δ (0.035 μm).

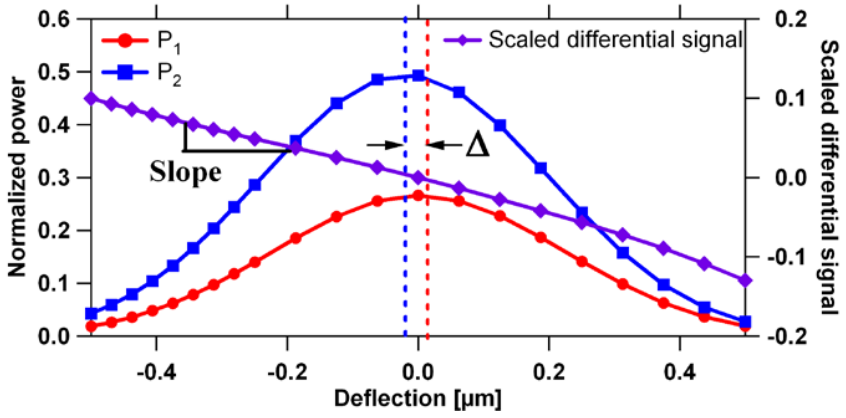

Figure 2-7: Typical optical outputs for P1 and P2 with respect to deflection state and associated scaled differential signal.

This offset can be used to compute a scaled differential signal (η_{scaled}) which is monotonically dependent on the PMCL deflection state:

$$\eta_{scaled} = \frac{P_2 - \alpha P_1}{P_2 + \alpha P_1} \quad . \tag{2-4}$$

The scaling factor (α) is defined by

$$\alpha = \frac{P_{20}}{P_{10}}, \tag{2-5}$$

where P_{10} and P_{20} are the output powers of P_1 and P_2 at an arbitrary reference deflection for any given PMCL and is necessary to compensate for variations in optical loss from one PMCL to another within an array. This reference deflection should preferably be taken at or near zero deflection where the signals for both P_1 and P_2 are strongest. Figure 2–8 shows the scaled differential signal with respect to PMCL deflection for an array of PMCLs during a push-down test where deflection state is determined by a piezo-driven probe.

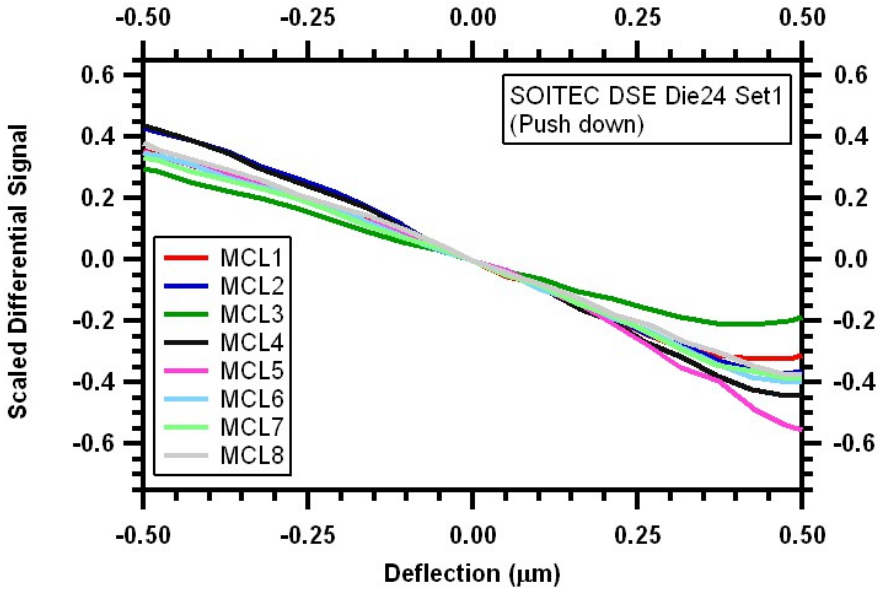

Figure 2-8: Typical scaled differential signal with respect to PMCL deflection for an array of eight PMCLs.

2.3 Surface Chemistry

Finding an appropriate chemistry to maximize the density and activity of bound receptor molecules in the sensor area played a central role in the research. This section covers what chemical reactions were considered and the various methods to modify the sensor surface with those chemistries.

Because the native silicon oxide layer presents a chemically inert surface to biological molecules, a silane linking molecule must first be applied to the surface before a bio-receptor can be immobilized. This linking molecule should have a terminal group opposite the silane that is reactive to chemistries commonly used for bio-conjugation in order to exploit the breadth of options used in this field of science to covalently immobilize receptors to the PMCL surface. There are several available organo-functional alkoxy-silanes that could potentially fill this role, examples of which are described in this section.

Figure 2–9 shows a diagram of *3-glycidoxypropyl-trimethoxysilane (GOPS)*. Sensor surfaces prepared with an active glycidyl (or epoxy) can react directly with primary amine groups that are typically available on protein surfaces and sulfhydryl groups. Amine groups react best with epoxies in the pH range of 8.6 – 8.9 and sulfhydryl groups at pH 7.0 – 8.0. The reaction is slow compared to N-hydroxysuccinimide ester (NHS) and maleimide chemistries, but has the advantage of protein immobilization without additional activation steps. [32]

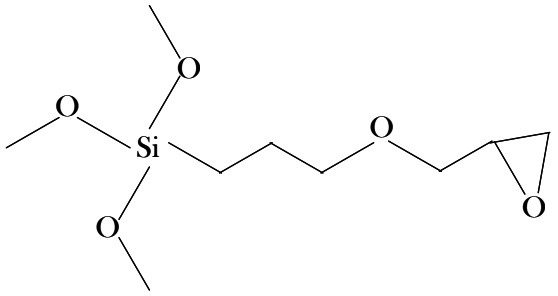

Figure 2-9: Model of the 3-glycidoxypropyl-trimethoxysilane (GOPS) molecule.

Figure 2–10 shows a diagram of *3-aminopropyl-triethoxysilane (APTES)*. An amine functionalized surface requires an intermediate activation step when immobilizing proteins. A plethora of strategies have been investigated. Some of the more commonly used strategies involve homobifunctional reagents containing reactive groups such as aliphatic aldehydes (e.g. glutaraldehyde), NHS esters and 1,4-Phenylene diisothiocyanate (DITC). Alternatively, a hetrobifunctional reagent can be used where one end reacts with the amino-functionalized surface and the other end reacts with sulfhydryl on the protein (e.g. 3-maleimidopropionic acid N-hydroxysuccinimide ester (MPA-NHS). [32]

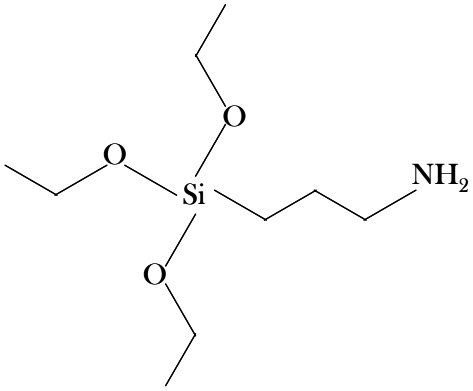

Figure 2-10: Model of the 3-aminopropyl-triethoxysilane (APTES) molecule.

Figure 2–11 shows a diagram of *3-aminopropyl-trimethoxysilane (APTMS).* This molecule provides the same functionality as APTES, but is more reactive with the silicon substrate due to its smaller molecular weight.

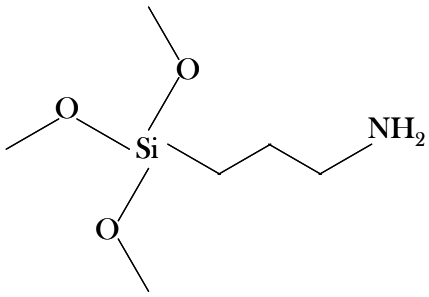

Figure 2-11: Model of the 3-aminopropyl-trimethoxysilane (APTMS) molecule.

Figure 2–12 shows a diagram of *3-aminopropyl-diisopropylethoxysilane (APDIES)*. APDIES is a monofunctional silane with only one ethoxysilane group attached to the silicon atom. Depending on the purity of the solution, it will resist forming long polymer chains in the presence of stray water in the reaction vessel during incubation. This makes it ideal for liquid deposition of a monolayer since the multilayer effect seen with trifunctional silanes is due to cross polymerization instead of reacting solely with the silicon surface.

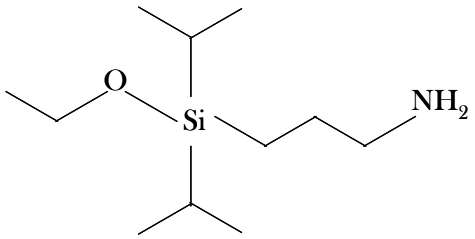

Figure 2-12: Model of the 3-aminopropyl-diisopropylethoxysilane (APDIES) molecule.

Figure 2–13 shows a diagram of *3-iodopropyl-trimethoxysilane (IPTMS).* IPTMS is another potential linker that may be used for oriented immobilization of proteins. Iodopropyl groups may react with free sulfhydryls by nucleophilic substitution of iodine with a thiol group, resulting in a stable thioether bond. Iodopropyl groups are most specific for sulfhydryl groups at pH 8.3. However, if there are excess iodopropyl sites after the bulk of sulfhydryls are reacted, the iodopropyl group can react with amino acids in the unprotonated form above pH 7. As with GOPS, this type of activated surface is less stable and should be protected from contamination until proteins can be applied.

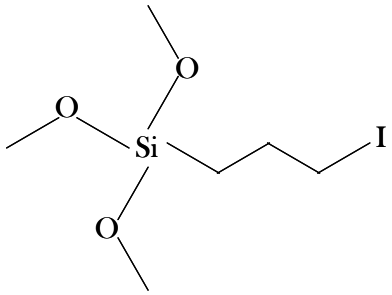

Figure 2-13: Model of the 3-iodopropyl-trimethoxysilane (IPTMS) molecule.

Figure 2–14 shows a diagram of *3-mercaptopropyl-trimethoxysilane (MPTMS).* MPTMS may be a better option than IPTMS for oriented protein immobilization. Like IPTMS it will selectively bind to –SH groups to form a disulfide bond at physiological conditions (pH 7.3) but will not form bonds with amines. Again, this type of prepared surface is less chemically stable than the amine coated surface and should be protected from contamination until proteins can be applied.

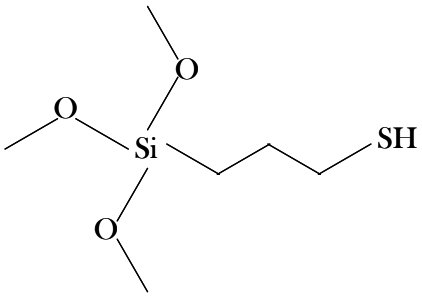

Figure 2-14: Model of the 3-mercaptopropyl-trimethoxysilane (MPTMS) molecule.

2.4 Chemical Deposition Methods and Systems

The two most common methods to deposit monolayer films of organo-functional alkoxy-silanes are chemical vapor deposition (CVD) and liquid phase deposition (LPD). Most research groups opt for the liquid phase deposition because there is no need to invest in capital equipment aside from what would normally be found in a basic laboratory environment. This section

provides background on these two methods and the three different systems/protocols investigated and used for this dissertation.

Complete dehydration of the native SiO_2 surface and the deposition chamber, whether for LPD or CVD, is key to obtaining a complete silane/substrate bond that is stable after exposure to atmospheric moisture and is limited to a monolayer thickness. Excess moisture in the deposition chamber leads to polymerization of a tri-functional silane.

Another key aspect is pre-processing—the silicon surface must be extremely clean with activated hydroxyl (-OH) groups for the reaction to occur. There are a number of methods to activate the surface with hydroxyls. These include an air/O_2 plasma with water vapor present, UV/ozone exposure and exposure to an acid solution such as Pirahna or Nanostrip (aqueous sulfuric acid and hydrogen peroxide). Low-power water vapor plasma following a cleaning in Nanostrip was the most convenient and adequately effective for our application. Nanostrip performs the bulk of the cleaning while the plasma removes any remaining residue just before deposition.

Depending on the size of the deposition chamber, chemical usage for a CVD process is typically less than 1% of the amount needed for LPD processes. CVD processes are typically done at a higher temperature (110 - 160 °C) than LPD, which drives the reaction and completes the process in a shorter time than LPD. There are drawbacks with a CVD process that are easily avoided with a LPD process. One is the difficulty of completely cleaning a CVD vacuum oven chamber to avoid cross-contamination when switching between different silanes—fluoro-silanes are particularly troublesome due to their reactive nature. Another drawback is that the need to extract a sample at elevated temperatures (i.e. before the oven has cooled) tends to accelerate the surface contamination by atmospheric pollutants. For most applications, this may not be an

issue, but with PMCL functionalization, where close packing of receptor sites is highly desired, it was a concern and seemed to be the primary factor with film reproducibility.

Figure 2-15: Yield Engineering System's YES-1224P CVD oven with integrated plasma. (YES stock photo)

Initial efforts to deposit an organo-silane were performed in a very sophisticated CVD oven made by Yield Engineering Systems (YES)—the YES-1224P CVD oven with an integrated plasma function (see Figure 2-15). The CVD process begins with several purge cycles to dehydrate the injection lines for the silane product and the chamber is then primed with the silane. Next, the sample is placed in the oven and a plasma cleaning cycle is used to clean and activate the sample surface. This is best done on a non-active floating plate to avoid over etching of the sample. The chamber is then evacuated to low pressure and refilled with dry N_2 three times to completely remove water vapor. Once the purge cycles are finished, the system pumps the silane directly from the source bottle, which is capped with a septum, to the heated vaporization chamber thus preventing any exposure to water vapor. The YES-1224P can accommodate two chemical source bottles as well as wide variations of vapor pressures among different silanes. Processes can be programmed and saved for repeatability using a touch screen GUI.

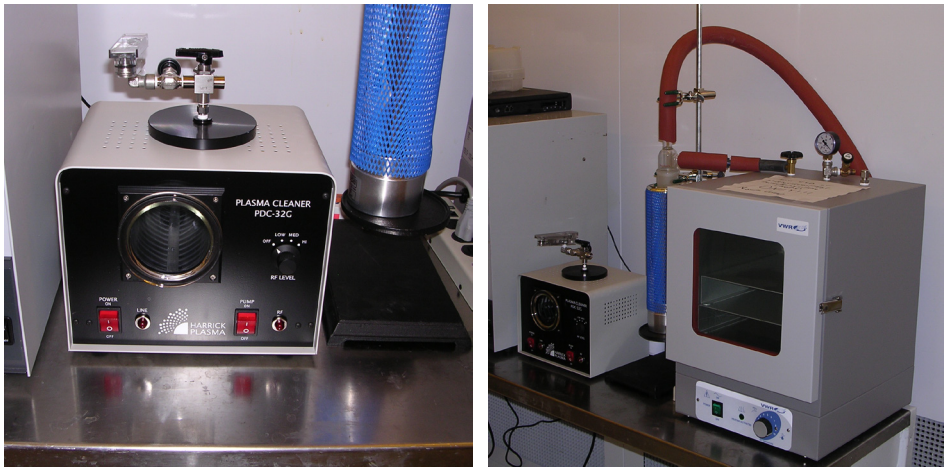

Figure 2-16: Dedicated CVD system with Harrick PDC-32G Plasma Cleaner and a VWR 1400E economy vacuum oven.

Despite its elegant design, the YES-1224P I was unable to use it due to cross-contamination issues caused by other users. Therefore, a dedicated system using a Harrick PDC-32G Plasma Cleaner, a VWR 1400E economy vacuum oven, an Edwards E2M2 vacuum pump, a 1-liter Dewar flask for LN_2, cold finger condenser and various valves and fittings (see Figure 2-16) was assembled. The process is basically the same with more manual inputs. After a 3 min plasma at 18 W (high power) in the Harrick plasma cleaner, the sample is placed in the VWR oven preheated to 150 °C, purged three times with N_2, evacuated to low pressure (< 200 mT) and 0.5 ml of silane product is injected through a PTFE/silicone septum into the VWR oven with a gas-tight glass syringe and needle. The reaction is allowed to proceed for 30 min after which the oven is purged again and allowed to cool before removing the sample. Repeatability and film thickness was quite good at first, but suffered as silane build-up in the chamber (probably in and around the gaskets—maybe the trap or gauges) caused increasing variability.

Liquid deposition was the final method investigated. Inexpensive 50 ml glass jars with polypropylene lids and retrofitted with PTFE liners served as the deposition chamber. First, the jar is rinsed with acetone and IPA, N_2 dried, plasma cleaned in the Harrick and dehydrated in a

dedicated dehydration oven at 150 °C for 3 – 4 hours. After removing the jar from the oven, it is immediately filled with a 5% silane solution in dry HPLC grade toluene and the lid placed on the jar. A PMCL die that was previously cleaned in Nanostrip and dried in a CPD dryer was then activated in the Harrick (3 min plasma at 18 W) and immediately placed in the jar, once again replacing the lid. The reaction is much slower and the use of a CPD is required, but monolayer coverage and repeatability was greatly improved, especially when using a mono-functional silane (APDIES) in which the reaction is naturally limited to a monolayer. Figure 2-17 shows the progression of APDIES deposition on silicon slides using the LPD process as a function of reaction time. The final values corresponded nicely with reported values in the literature. [42]

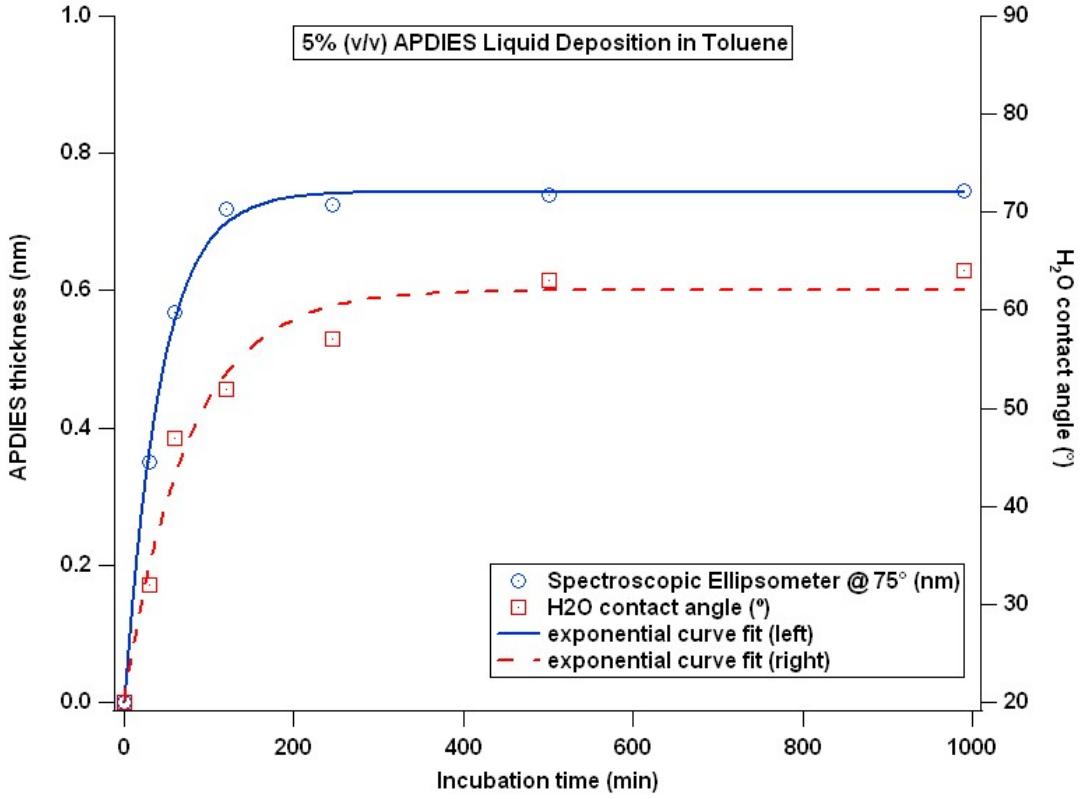

Figure 2-17: APDIES film thickness with respect to reaction time on silicon slides using the LPD process.

2.5 The Human Serum Proteome

A major frontier for solid-state biosensors is the ability to detect and quantify the numerous types of proteins found in blood plasma. Blood tests have long been a medical standard for disease diagnosis due to the safety in which a sample can be taken from a live patient and the comprehensive nature in which a person's blood reflects the health and general state of the body. Figure 2-18 provides a clear perspective of the concentration at which some proteins of interest occur in human plasma [51].

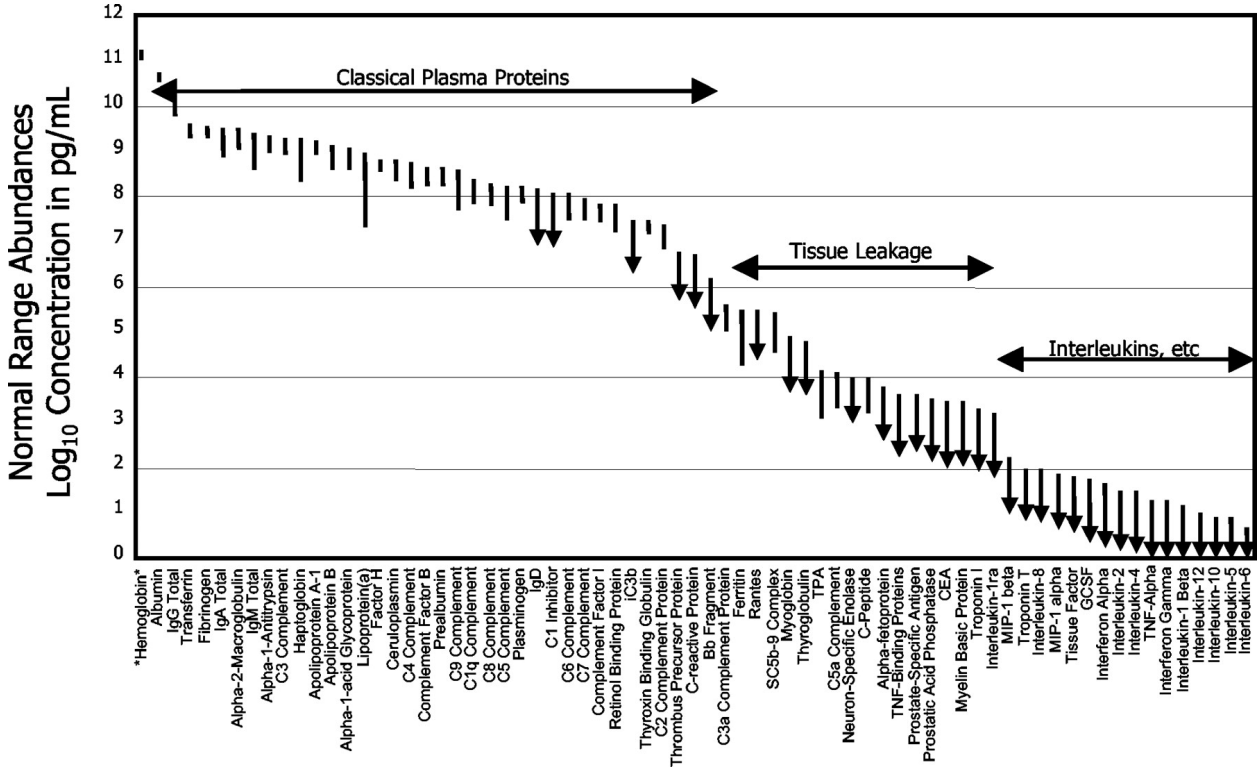

Figure 2-18: Concentration of various proteins found in the human serum proteome. [51]

At the abundant end of the spectrum, serum albumin is normally found at 35–50 x 10^9 pg/ml, while at the low end, interleukin 6 has a normal range of 0–5 pg/ml and indicates an inflammation or infection in the body [51]. This underscores two fundamental requirements a comprehensive biosensor must fulfill: specificity and sensitivity.

Specificity is addressed by refining the receptor production process or whatever means of identification is used to distinguish one protein from the next if receptors are not used. Examples might include affinity purified IgG's that have been absorbed against the antibodies of other organisms that are not to be detected, thereby minimizing cross-reactivity. Or in the receptor-free case, an example might be the development of new spectra for peptides and proteins for gas chromatography, liquid chromatography or mass spectroscopy.

Sensitivity can be approached in a variety of ways, but for the PMCL platform, the Nordin group reduced noise from optical scattering, increased the slope of the signal response and used microfluidics to recycle the sample volume over the sensor surface. Figure 2-18 shows that sub-pg/ml sensitivities are required for complete coverage of the human plasma proteome.

2.6 Bio-conjugation

The development of fluorescent detection probes for Western blotting, ELISA and laboratory research on protein structure and interactions, has led to a wide range of labeling chemistries employed to covalently bond, or crosslink, various proteins and other bio-molecules together. Crosslinking molecules have two or more reactive sites capable of chemically bonding to specific functional groups on proteins or other molecules. This section describes some of these functional groups and the structure of some of the commercially available crosslinkers of interest to my application. [50]

The structure of proteins can be quite complex with a variety of possible sequences and number combinations of the 21 different amino acids utilized by the human body. Despite this wide variation, there are only four chemical functional groups commonly used for practical bio-conjugation: primary amines ($-NH_2$), carboxyls (–COOH), sulfhydryls (–SH), and carbonyls (–CHO). [50]

Primary amines exists at the N-terminus of each polypeptide chain and are referred to as α-amines. When the protein is translated from messenger RNA, it is created from N-terminus to C-terminus. The side chain of lysine also contains a primary amine and are referred to as ε-amines. At physiological pH, primary amines are positively charged causing them to usually face outward from the centroid of the protein and are therefore accessible for conjugation without denaturing the protein. [50]

Carboxyls exist at the C-terminus of each polypeptide chain and in the side chains of aspartic and glutamic acids. Like primary amines, they are found on the surface and are available for conjugation, but their charge is negative. Amines and carboxyls are the most commonly used binding sites on proteins. [50]

Sulfhydryls are found in the side chain of cysteine. Cysteines are responsible for a polypeptide folding back on itself via disulfide bonds (S–S) when two cysteines join to form a cystine. The same interaction may occur between two different peptides if the separate disulfide bonds are first reduced to sulfhydryls and then react to from a crosslink. [50]

Carbonyls are composed of a carbon atom double-bonded to an oxygen atom and characterize functional groups such as aldehydes, ketones, esters, amides and carboxylic acid. For bio-conjugation these are formed on glycoproteins by oxidizing their polysaccharide with sodium meta-periodate. [50]

Due to its high binding efficiency with streptavidin and relative low cost, biotin is often used in bioconjugation. As I was able to deposit a uniform monolayer of amino-terminated silane, the large selection of amine biotinylation reagents became of interest. Sulfosuccinimidyl-2-(biotinamido)-ethyl-1,3'-dithiopropionate (Sulfo-NHS-SS-Biotin), modeled in Figure 2-19, has a medium length spacer arm that contains a cleavable disulfide bond. The N-hydroxysuccinimide

ester (NHS) reacts specifically with α-amines and ε-amines to form a stable amide bond and is most efficient in the range of pH 7-9.

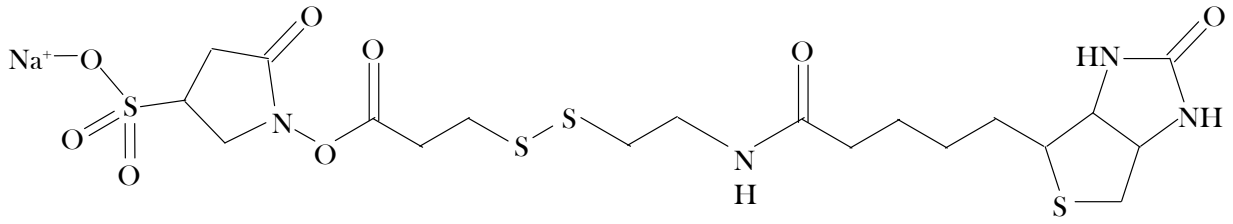

Figure 2-19: Molecular model of Sulfo-NHS-SS-Biotin (M.W. 606.69, Spacer Arm: 24.3 Å).

Another available biotinylation reagent is TFP-PEG$_3$-Biotin, which is a tetrafluorophenyl ester of biotin with a triethyleneglycol spacer. The polyethylene glycol (PEG) spacer arm is hydrophilic and improves water solubility of the biotinylated molecule. The tetrafluorophenyl (TFP) ester also reacts with α-amines and ε-amines to form a stable amide bond and is most efficient at pH 7-9.

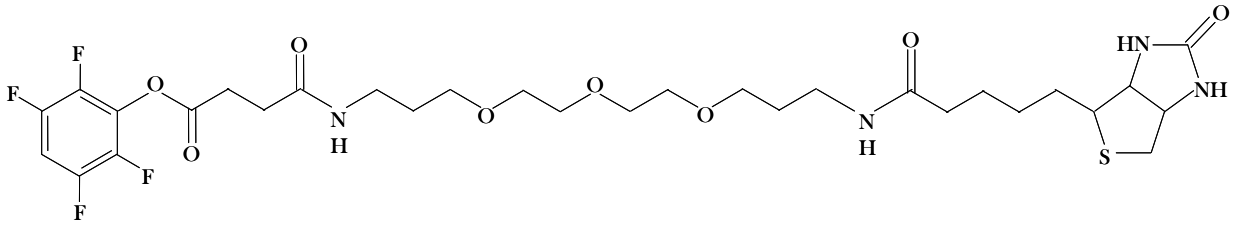

Figure 2-20: Molecular model of TFP-PEG3-Biotin (M.W. 694.74, Spacer Arm: 32.6 Å).

Since both TFP and NHS esters are reactive in aqueous media with a half-life of 2-3 hours, they must be kept dry until just before the reaction is to occur. Any remaining reagent must be discarded afterward.

Another option is to have the reactive group deposited on the surface of the PMCL die as in the case of GOPS, which terminates in a reactive epoxy ring. An important consideration with this approach is to deposit the biotinylation reagent before the reactive epoxy surface is fouled by

atmospheric contaminants. The advantage here is having a more stable biotin solution that does not need to be discarded within a few hours after preparation. Amine-PEG_3-biotin (Figure 2-21) is one example of a biotinylation reagent that could be used with this strategy and is most efficiently and specifically reacted with the epoxy ring at pH 8.5 – 8.9. [32]

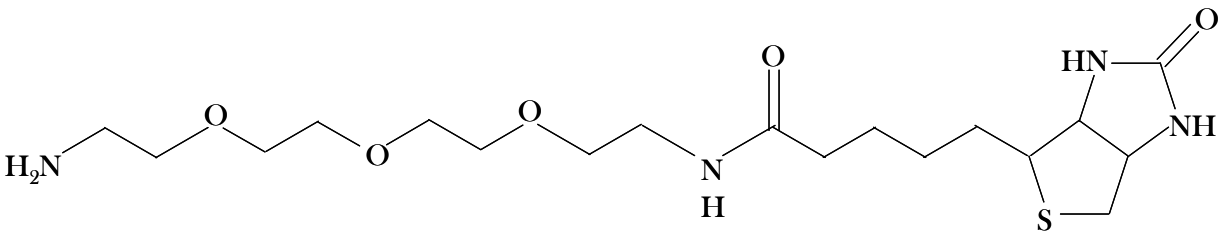

Figure 2-21: Molecular model of Amine-PEG3-Biotin (M.W. 418.55, Spacer Arm: 22.9 Å).

2.7 Micro- / Nano-spotting Systems

Several commercially available micro- / nano-spotting systems were considered for fluid placement on the top surface of the PMCLs. Three of these are presented here:

BioForce Nanosciences makes a spotting system called the Nano eNabler™ capable of dispensing attoliter to femtoliter volumes of biomolecules or nanoparticles suspended in a fluid onto a surface that has at least some affinity for the solution being deposited. Their system uses an atomic force microscopy (AFM) tip that has been micro-machined with a micro-well like a fountain pen would have as shown in Figure 2-22. They typically use surfactant (e.g. 0.5% Tween 20) in their spotting solutions, but do not require thickeners for achieving a specific viscosity. Alignment and inspection optics operate in real time and magnify 150x – 1000x, which is a little more than what is needed for the PMCL die. The GUI is excellent, the positioning is more than adequate at +/- 20 nm, and even comes with a 25-80% RH humidifier to maintain fluid in the microwell and substrate. In general, I found their system to be an excellent spotting

system for rigid surfaces, but problematic while spotting the tip of our PMCL. This system requires physical contact with the surface and because our surface is a MCL with spring constant of ~0.02 N/m (0.025 N/m non-etched and 0.017 N/m etched), the spotting AFM tip could not pull away cleanly from the PMCL tip due to surface tension of the fluid and hydrophilicity of the two surfaces.

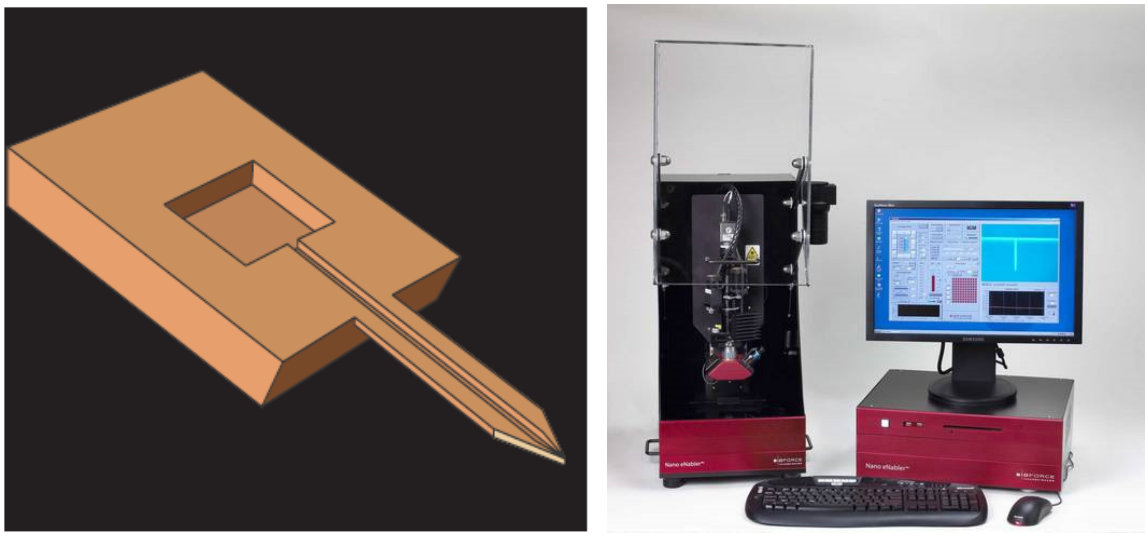

(a) **(b)**

Figure 2-22: (a) Micromachined fluid dispensing AFM tip, and (b) image of BioForce Nanoscience's Nano eNabler™ and control console. (BioForce stock photos)

Sonoplot has a spotting system, the GIX Microplotter II (Figure 2-23), which initially appeared to be ideal for my application. It uses an ultrasonic emitter to pump fluid to the tip of a sharp glass micropipette, where a meniscus is bowed out and then touched off to the substrate to form a drop or dragged across to form a continuous line or arc. The tip of the micropipette does not come in direct contact with the substrate, but rather indirectly through the meniscus of the liquid. Some of its key features are the 5 μm positioning accuracy and the ability to program cleaning steps between drawing fluid from a microtiter plate for multiplexed functionalization without changing tips. The GUI is user-friendly and the optics operate in real-time, but do not

magnify sufficiently and are unable to mount at 0° angle of incidence to the plane of the PMCL die, thus the image was very dark. After a live demonstration, it was determined that the indirect non-contact method was unsuitable for MCLs that may have a bit of upward deflection. Figure 2-24 shows several broken MCLs during the test, which may have been due to a fixable software glitch.

(a) **(b)**

Figure 2-23: The (a) Sonoplot GIX Microplotter II spotting system and (b) image of ultrasonic spotting tip depositing an array of drops. (Sonoplot stock photos)

Figure 2-24: Broken MCLs during a test run with the GIX Microplotter II.

After further review of spotting systems, it was determined that a non-contact solution was a hard requirement. The Dimatix Fujifilm DMP-2831 Materials Printer appeared to be the most cost effective non-contact solution on the market at the time (2007). Some of its key features include: a nominal 1 pL drop volume with DMC-11601 cartridge, 1.5 ml user-fillable replaceable cartridge, and a +/- 25 µm drop placement repeatability. The error in repeatability comes largely from backlash in the acme screw that moves the platen stage in the y-direction (orthogonal to the printhead direction of motion) to the next line of printing. With some investigation of the system and proper formulation of a jettable fluid, I brought the repeatability to about +/- 7.5 µm for the first pass of the printhead after a calibration cycle. The +/- 7.5 µm is largely due to pixel ambiguity of the fiducial camera used for alignment of the substrate. The GUI is user-friendly with a native pattern programming environment. It does suffer from the requirements to develop a jettable fluid, change to a new cartridge for multiplexed spotting, and slightly less than desirable resolution on the optics. Despite these resolvable shortcomings, the need for an affordable, non-contact, and small volume (~ 1 pL) dispensing system led the Nordin group to select the DMP-2831 (see Figure 2-25).

(a) **(b)**

Figure 2-25: The (a) Dimatix Fujifilm DMP-2831 Materials Printer and (b) 1.5 ml DMC-11601 cartridge for 1 pL drop volume dispensing. (Dimatix stock photos)

2.8 Microfluidics

Microfluidics play an important role in any micro/nano biosensing application by enabling precise flow control of μL volumes and increasing sensor response time via flow-induced advection to the sensor surface. The significance of flow-induced advection vs. diffusion can be seen in Figure 2-26 of analytical and simulated values of molecular flux as a function of volumetric flow rate to a 35 μm wide surface in a 2D simulation. The simulated particle is prostate specific antigen (PSA) at a concentration of 10 pM. Flow rates of 1-2 μL/min are typical during a sensing experiment for the microfluidics and the PMCLs used in this dissertation, which provides nearly four orders of magnitude greater particle flux to the sensor surface than would a diffusion limited system would provide, thereby dramatically increasing response time.

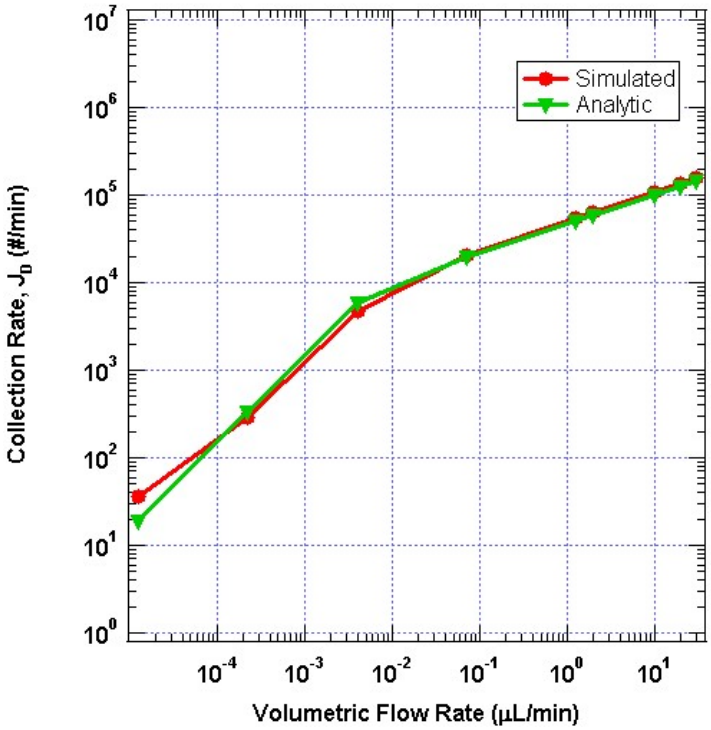

Figure 2-26: Simulated and analytical values of molecular flux to a surface vs. volumetric flow rate.

The relatively simple microfluidic design consists of two bonded layers of PDMS. The bottom layer (fluid layer) forms the fluid microchannels when bonded with the silicon die, while the upper layer (control layer) forms the control channels and reservoirs that serve as valves when aligned across a segment of microchannel in the bottom layer as seen in Figure 2-27. The cross section of a typical fluid microchannel is 60 µm high at the center and 600 µm wide. Valves are actuated with pneumatically pressurized DI water which expands the reservoir and collapses the flexible fluid layer, which in consequence closes off the channel thereby directing sample fluids through the desired microchannel.

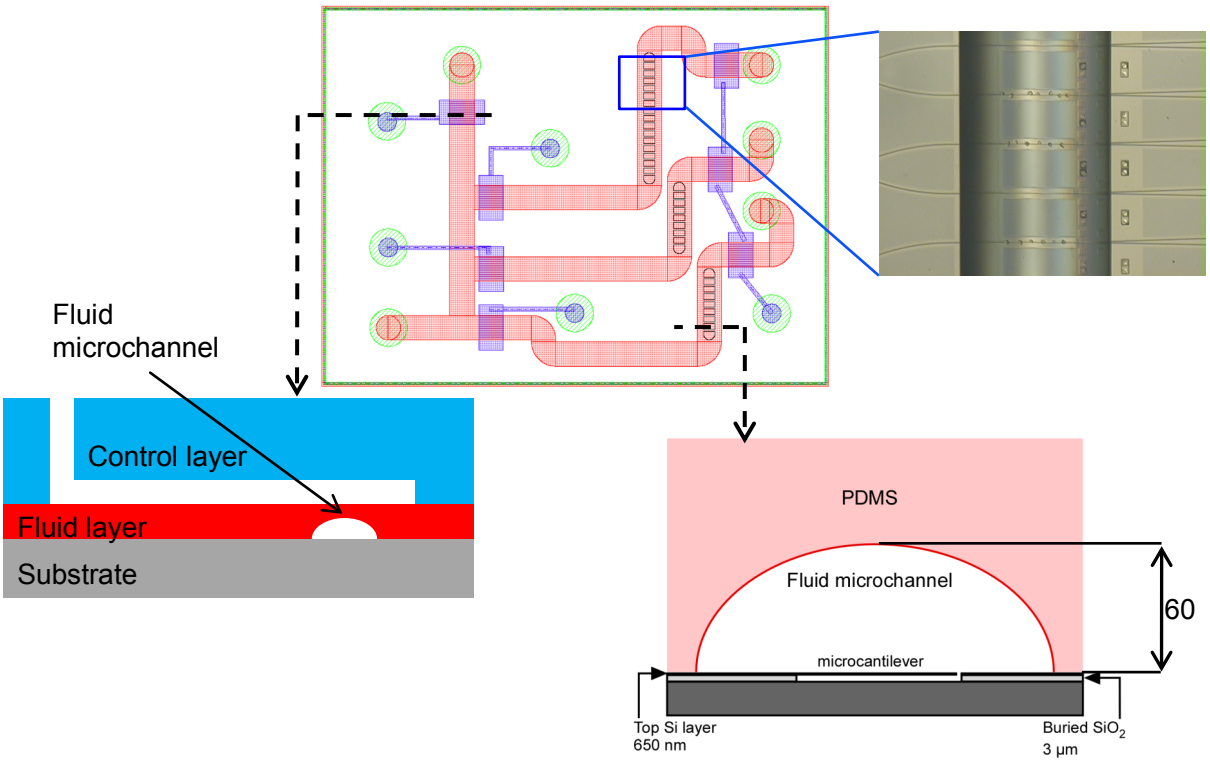

Figure 2-27: Schematic of microfluidic layout with cross-sectional and micrographic insets.

Using photolithography to pattern a positive photoresist (AZ 50XT; AZ Electronic Materials) on a 4 inch silicon wafer, a master mold containing 41 usable single-chip patterns is created for the fluid layer. Following photoresist development, the mold is reflowed on a hot plate at 125 °C for 3 min, resulting in a semicircular cross-section, which is necessary to allow the microchannel to completely close a during valve actuation. The fluid mold is coated with a silane ((tridecafluoro-1,1,2,2-tetrahydrooctyl) 1-tricholorosilane) to facilitate release of the cured PDMS. The PDMS base material and curing-agent (Sylgard 184 kit; Dow Corning Corp.) are then mixed at a 10:1 ratio for the fluid layer, degassed for 1 hour, spun onto the fluid mold at 900 RPM and cured at 80 °C for one hour.

The control layer is created in similar fashion with a negative photoresist (SU8 25; MicroChem). The control channels and reservoirs do not require a semi-circular shape, but have a rectangular cross-section and thus no reflow step is performed. Each reservoir that constitutes a valve is 30 μm tall, 600 μm wide, and 1200 μm long. The PDMS base and curing-agent for the control layer is mixed at a 4:1 ratio, degassed for 1 hour, poured over the control layer mold at the bottom of a cylindrical container and cured at 80 °C for one hour.

After curing, the PDMS layers are removed from the molds, cut into single pieces with a razor blade and hole punched where pneumatic and fluid channels begin and/or end using a 21 gauge Nordson EFD precision dispensing tip and generic punch press.

The control layer is bonded with the fluid layer by stamping the control layer on a thin film of curing-agent spun onto a 4 inch silicon wafer at 4000 RPM for 30 sec [38]. Prior to bonding, the two PDMS layers are properly oriented relative to each other with the aid of a custom-built alignment stage, assembled and then cured at 80 °C for one hour. This microfluidic piece may then be bonded to the PMCL die using the same stamp and alignment process but

cured at room temperature to preserve the activity of the functionalization. The PMCL/microfluidic assembly is then mounted in a small spring load vise with a 1 mm thick glass piece on top of the PDMS. The glass piece has holes drilled through it to match the holes in the PDMS where connections are made with 24 AWG thin wall PTFE tubing (Cole-Parmer Item# 06417-21). Holes in the PDMS for valve actuation connect with a pneumatic solenoid valve manifold (LFMX0510438BF, LHDA1211111H, The Lee Company). Holes for the fluid input and outputs connect to a syringe pump (Harvard 33 Twin Syringe Pump, Harvard Apparatus) and waste beaker, respectively. Figure 2-28 shows a CAD image of the microfluidic layout for two different PMCL chip designs,

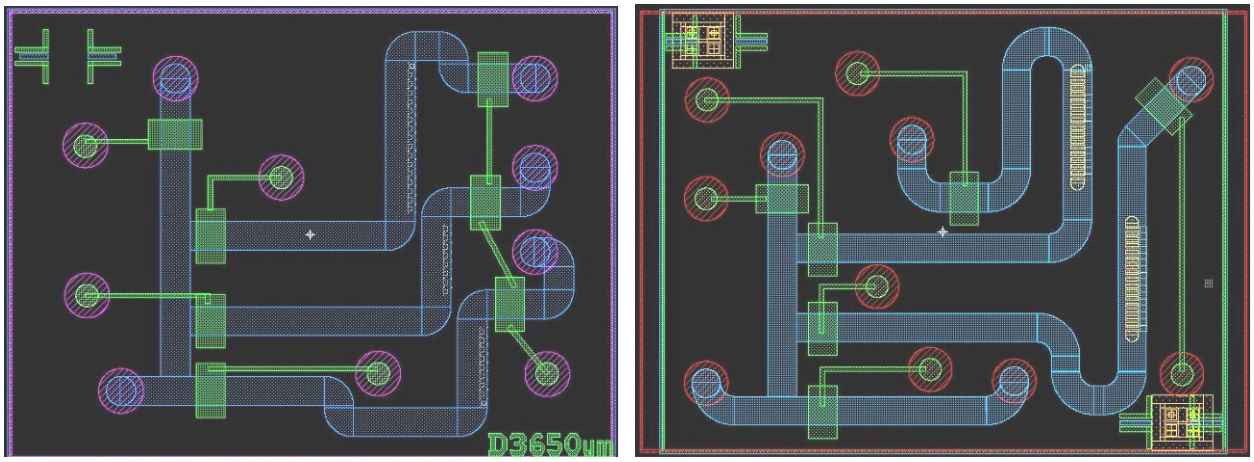

(a) **(b)**

Figure 2-28: CAD image of microfluidic layout for (a) 1 x 16, 2 x 8 and (b) 2 x 16 PMCL chip designs.

A deep silicon etching (DSE) process used while forming the PMCLs enhances stability of the sensor response by equalizing the analyte transport to both the top and bottom of the PMCLs. This processing step not only removes the buried oxide, but also a portion of the bulk silicon substrate thus placing the PMCLs mid-level vertically in the microfluidic channel. The value in doing this extra step is demonstrated in Figure 2-29. The graph on the left (a) shows simulation results for normalized concentration of BSA around a microcantilever during the

initial introduction of BSA in the microfluidic channel without a deeply etched volume under the PMCLs.

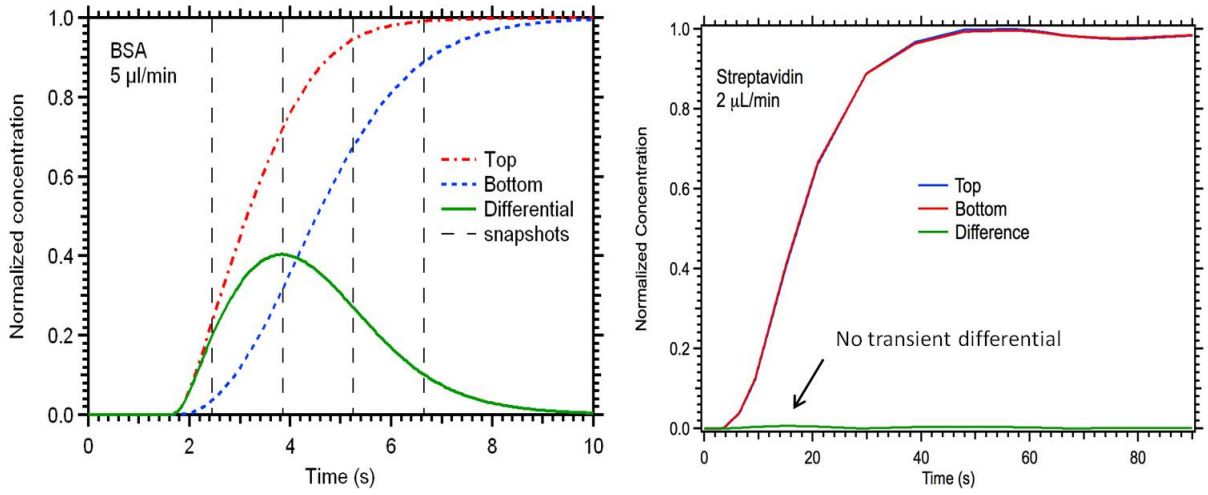

(a) **(b)**

Figure 2-29: (a) 3D FEA simulation of concentration gradient for non-DSE case and (b) 2D FEA simulation for the DSE case.

The figure on the right (b) shows similar simulation results for streptavidin with a deeply etched volume under the PMCLs. Notice the transient differential response (green line) in the first figure on the left and the lack of a transient response in the second image on the right.

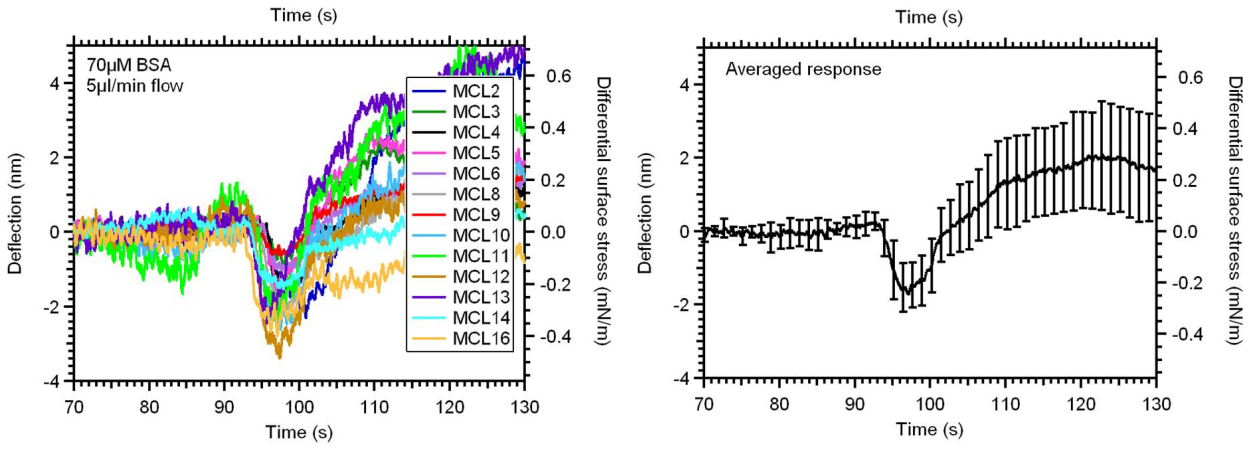

(a) **(b)**

Figure 2-30: (a) Response of individual PMCLs in a 1 x 16 array (non-DSE) to the change in fluid concentration and (b) the averaged response with error bars. [38]

A transient PMCL response due to concentration differential was demonstrated experimentally by Andersen et al. [38] and is shown in Figure 2-30.

3 SINGLE-SIDED INKJET FUNCTIONALIZATION OF SILICON PHOTONIC MICROCNTILEVERS

3.1 Motivation

This chapter is adapted from a peer-review journal article published in Sensors and Actuators B: Chemical. It examines inkjet functionalization of silicon PMCLs with no intermediate gold layer. Criteria for successful functionalization include receptor attachment to only one side of each PMCL and high uniformity and density of active receptor sites. A previous attempt at inkjet functionalization has been reported in which dispensed droplets were large enough that they overfilled the PMCL surfaces [24]. However, use of a gold coating on the top PMCL surface and thiolated receptor molecules in the jetted fluid allowed functionalization of only the gold-coated surface. In the case of the PMCL, I relied on jetting small enough droplets that only the top PMCL surface is wetted as a means to limit direct receptor attachment to just the top surface. The typical PMCL dimensions are 100 to 400 μm long and 45 μm wide. Hence dispensed droplets must be smaller than 45 μm in diameter once on the PMCL surface and droplet placement accuracy must be sufficient for a droplet to not overlap the edge of a MCL since in that case some or all of the fluid can wick around to the back surface. Consequently, the group chose to use a Dimatix DMP-2831 materials inkjet printer with 1 pL dispensing DMC-11601 cartridges which typically yield approximately 30 μm diameter droplets on our MCL surfaces (refer to discussion in Chapter 2).

Reliable droplet dispense from the Dimatix inkjet head requires functionalization fluid with substantially higher viscosity and lower surface tension than aqueous-based solutions. The former is obtained with the addition of glycerol, and the latter with surfactant. In this chapter I specifically examine details of inkjet fluid formulation and spotting to achieve single-sided MCL coverage, followed by droplet swelling using humidity control during incubation to uniformly fill the MCL surface and create a region at the base of each MCL for salt accumulation during drying, and the effect of buffer species and pH on receptor uniformity and relative density. Biotinylated bovine serum albumin (bBSA) and Alexa Fluor 514 labeled streptavidin are used as a model receptor/ligand system to permit fluorescence-based analysis of MCL coverage uniformity and relative density.

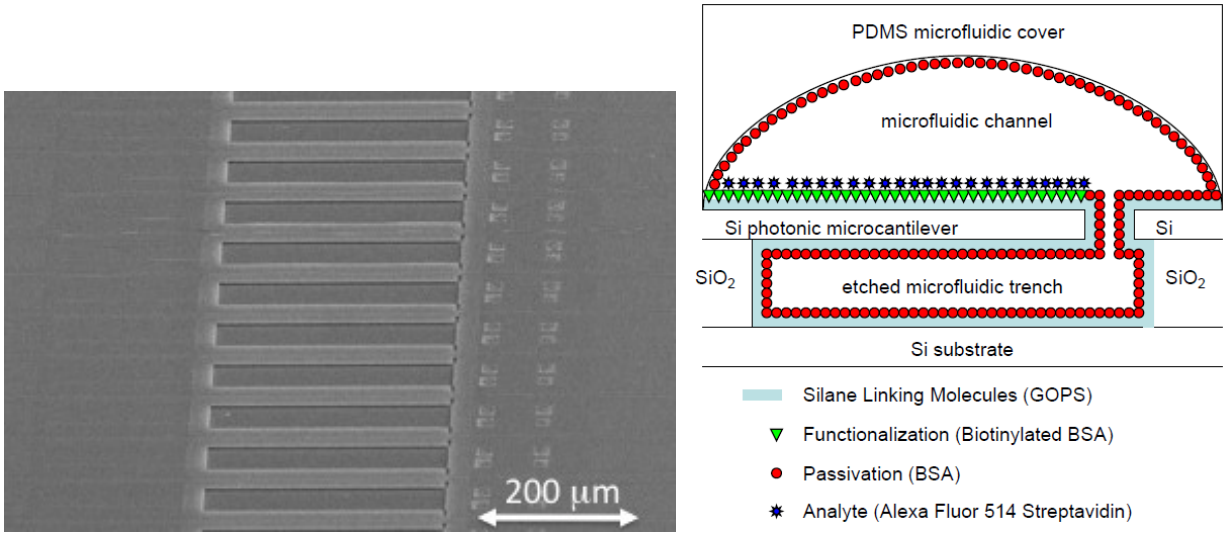

(a) **(b)**

Figure 3-1: (a) Scanning electron microscope (SEM) image of microcantilever array. (b) Cross-sectional schematic of silicon microcantilever, PDMS microfluidic channel, and molecular layers.

It may also be noted that the inkjet functionalization techniques developed in this dissertation can be applied to not only microcantilevers read out with other techniques (e.g., optical lever and piezoresistive methods), but also to alternate sensor approaches including

ELISA microarrays [25], Mach-Zehnder interferometers (MZIs) [26], ring resonators [27], whispering gallery mode resonators [28], and multiplexed surface acoustic wave (SAW) sensors [29].

3.2 Materials and Methods

Despite its size, the PMCL array sensor chip is complex system integrating MEMS, microfluidics, optical devices, bio/chemical lab equipment and proteins. The following sections outline the experimental setup.

3.2.1 Photonic Microcantilever Arrays

PMCL arrays are fabricated from 100 mm SOI wafers with 0.75 μm silicon and 3 μm silicon dioxide layers. Fabrication details are discussed in Chapter 2 and other references [12,14]. Each PMCL die has three PMCL arrays with eight PMCLs in each array. All PMCLs are 45 μm wide with the first, second, and third arrays having PMCLs with 200 μm, 300 μm, and 400 μm lengths, respectively. Figure 3-1 shows a fabricated PCML array and cross sectional schematic illustration of the various molecular layers on PCML and flow channel surfaces. Details of the PCML and microfluidic geometry are given in Chapter 2 and other references [16].

3.2.2 Chemicals

(3-glycidoxypropyl) trimethoxysilane (GOPS) and Brij 35 were purchased from Sigma-Aldrich; and Triton X-100, Tween 20 and glycerol were purchased from Fisher Scientific. Alexa Fluor 514 labeled streptavidin and BSA were obtained from Invitrogen, and bBSA was purchased from Thermo Scientific. All reagents were used as received.

3.2.3 Surface Preparation and GOPS Coating

Surface preparation of a fabricated PMCL die begins with cleaning in Nanostrip at 90 °C for 1 hour, followed by a DI water rinse. The die is then transferred into isopropyl alcohol (IPA) and dried in a Tousimis Autosamdri-815 Series B supercritical point dryer. Next, the die surface is activated with silanol groups by placing it in a Harrick Plasma Cleaner (PCD-32G) at 18 W for 3 min Immediately thereafter, chemical vapor deposition (CVD) of GOPS is performed in a VWR vacuum oven (Model 1400E), modified with a PTFE coated silicone septum injection port and preheated to 155 °C. After placing a die in the oven, the pressure is brought to less than 200 mTorr (0.27 mbar) at which time all valves are closed and 300 μL of GOPS solution is injected into the oven and held for 30 min After purging the chamber, the die is removed and taken to the Dimatix inkjet printer to spot PMCLs with fluid containing 2 mg/ml bBSA. A blank silicon witness sample is included with the PMCL die during GOPS deposition to characterize the GOPS layer. Ellipsometry measurements are taken with a J.A. Woollam manual angle M-2000 spectroscopic ellipsometer at an angle of 70°. The average GOPS film thickness of 28 different CVD cycles is 1.14 nm with a standard deviation of 0.23 nm, which corresponds well with reported values for a self-assembled monolayer of GOPS [30]. Water contact angle (static sessile drop) as measured with a Ramé-Hart Model 100 goniometer is typically in the range of 53° - 58°, which is on par with 55° as reported by [31].

3.2.4 Formulation of Jettable Functionalization Fluid

The functionalization fluid must meet a variety of criteria. First, Dimatix recommends jetting fluids with a viscosity between 10 and 12 cPs and a surface tension of 28 to 33 dynes/cm. Next, covalently binding protein to the GOPS thin film requires the fluid to have a low evaporation rate, and maintain a pH of 8.6 – 8.9 [32] for an efficient epoxide-amine reaction

during incubation. Moreover, while an ionic concentration greater than 100 mM mostly eliminates electrostatic interactions between suspended and immobilized molecules for better covalent coupling [33], I found that a high concentration of dissolved salt can foul deposited proteins as the solvent dries. Hence a salt concentration trade-off must be made. In addition, solutions containing more than 0.2% (w/w) dissolved solids (not including buffer salts) begin to suffer from unreliable and inaccurate jetting, but, on the other hand, enough protein must be present in solution to provide sufficient surface coverage of the receptor upon reaction. Finally, surfactant used to lower the surface tension and permit free flow of fluid during jetting must not interfere with pH and viscosity, or, at the very least, adjustments should be made to accommodate their presence in the solution. As an example of the need for surfactant, consider Figs. 3-2(a) and 3-2(b) in which the lack of surfactant (Fig. 3-2(a)) results in pooling of liquid around nozzles on an inkjet printhead thereby preventing jetting, while, as shown in Fig. 3-2(b), the presence of 0.135 mg/ml (0.2%) Triton X-100 surfactant in the fluid eliminates such pooling.

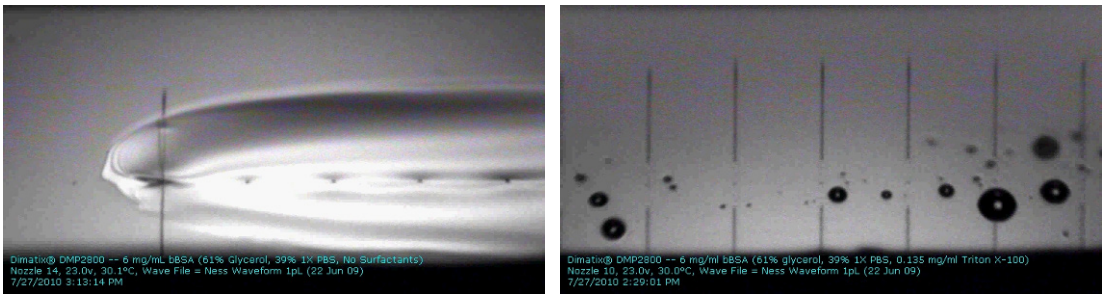

(a) **(b)**

Figure 3-2: Images of printheads jetting fluid (a) with and (b) without Triton X-100 in the fluid. Jetted fluid is directed upward in the photos and consists of thin vertical lines. Reflected images of jetted fluid are also visible in the lower portion of each photo.

To address these criteria, I evaluated several different buffer systems, surfactants and thickeners. For example, successful jetting is achieved with carbonate, citrate and phosphate buffers, but borate dries and skins over the printhead which blocks all nozzles. Buffer systems

containing amines are not considered since they compete with amines on bBSA to bind with the epoxides of the GOPS thin film. The surfactants I tried were Tween 20, Triton X-100, and Brij 35—all of which are nonionic for ease of use in maintaining desired pH. I found that the concentration of surfactant necessary to achieve the lowest possible surface tension is too small to affect viscosity. Successful jetting is achieved with Tween 20 and Triton X-100 down to their critical micelle concentration (CMC), but Brij 35 causes the fluid to skin over in the nozzles and prevents jetting.

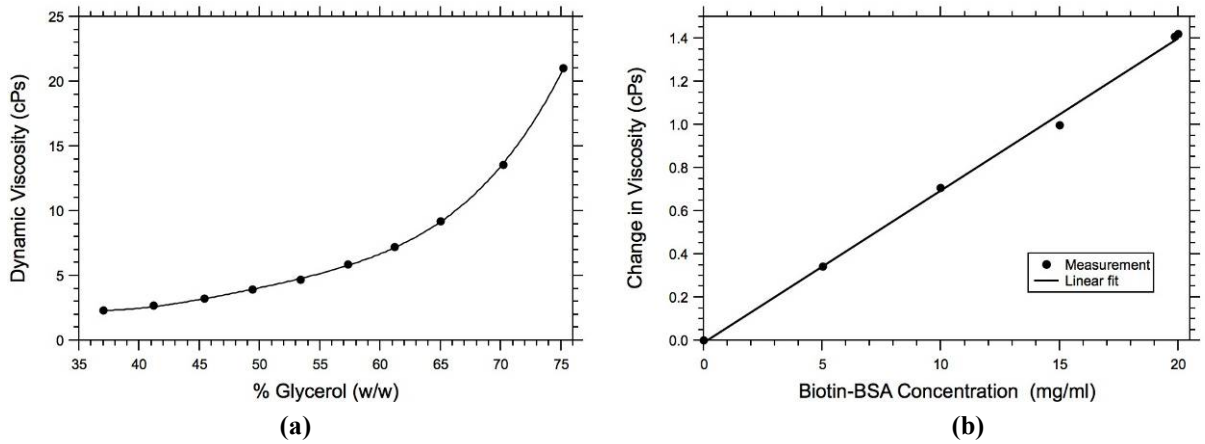

Figure 3-3: (a) Measured viscosity of aqueous glycerol solution as a function of glycerol content at 30 ºC and (b) measured change in viscosity as a function of bBSA concentration for a 61% glycerol solution with 0.06 mg/ml Tween 20.

I chose glycerol as a thickening agent because it is hygroscopic, adequately viscous, non-denaturing to proteins, and eventually can be made to evaporate, which is important for droplet drying following incubation and before PDMS integration. The latter factor is decisive in choosing glycerol over higher molecular weight alternatives such as polyethylene glycol. Figure 3-3(c) shows measured viscosity as a function of glycerol content (w/w). To match manufacturer guidelines of viscosity of 10 – 12 cps, 66% to 68.5% glycerol is needed. However, after experimentation I determined that 61% (w/w) glycerol gives the most reliable jetting performance. The measured viscosity with surfactant is ~8 cPs with a surface tension of ~38

dynes/cm. The surface tension increases to ~50 dynes/cm when protein is added (2 mg/ml), but no significant change in jetting performance is observed. Figure 3-3(d) shows the measured change in viscosity as a function of protein concentration. For 2 mg/ml the change is only 0.13 cPs. Viscosity is measured with a Cannon-Manning semi-micro E140 viscometer. Surface tension is measured with a Ramé-Hart Model 100 goniometer in conjunction with the pendant drop method [34], a CCD camera and custom processing software using MATLAB.

3.2.5 Spotting PMCLs with Dimatix Printer

The Dimatix printer ejects droplets from the printhead while the printhead is in motion. The printhead direction is along the x-axis. Samples are placed on a platen which moves in the y-direction and is stationary during droplet dispensing (i.e., any motion in the y-direction is completed before droplet dispense begins). I found that PMCLs must be oriented length-wise along the x-axis for droplet deposition because the small amount of x-axis momentum imparted by the moving printhead causes droplets to skid a few microns after landing. If the PMCLs are oriented in the y-axis direction the amount of skid is often enough to cause a droplet to move partially off the edge of a PMCL, which in turn causes the droplet to wick to the back surface of the PMCL. Figure 3-4(a) shows a line of drops on each of three PMCLs which are oriented in the x-direction. The print head travels from left to right along the length of each microcantilever and deposits 10 drops, ~30 μm in diameter and 45 μm apart, on a 45 x 400-μm PMCL during a single pass. The two rightmost droplets on the third lowest PMCL have agglomerated into a single larger droplet. An unspotted PMCL is shown in the lower part of the frame below the crosshairs. The horizontal line in the middle of each PMCL is a single mode rib waveguide. The rectangles in the right portion of the figure are alignment marks used during PMCL fabrication.

3.2.6 Fluorescent Imaging

The following components constitute the fluorescent imaging system used to evaluate ligand to receptor binding on PMCLs: Navitar Video ZFL Scope, Infinity 2-2M 2.0 Megapixel CCD Monochrome Camera, X-Cite 120Q microscope light source, liquid light guide and Chroma filter set 41001 FITC/ RSGFP/ Bodipy/ Fluo 3/ DiO. Images are taken with 500 ms exposure at maximum gain and lowest gamma correction at 7X magnification.

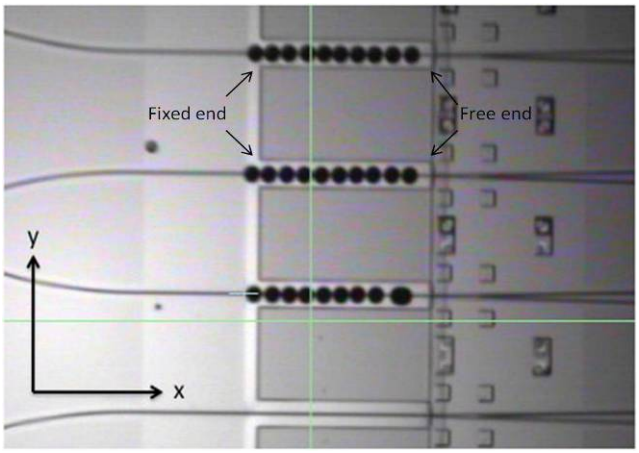

(a)

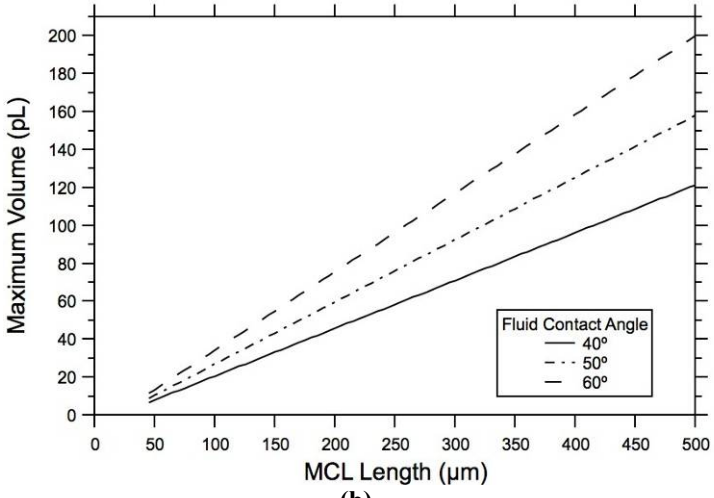

(b)

Figure 3-4: (a) Three PMCLs spotted with 2 mg/ml bBSA jettable fluid and one unspotted PMCL. (b) Maximum calculated fluid volume as a function of MCL length for various contact angles.

3.3 Results and Discussion

Having demonstrated that inkjet spotting on the top surface of a PMCL in an array is possible, I then addressed the issues of (1) uniformly filling each PMCL surface with fluid and (2) evaluating the uniformity and relative active site density of receptors by fluorescent imaging of tagged ligands bound to receptors.

3.3.1 Droplet Swelling

I began by calculating the theoretical maximum amount of fluid that can be dispensed onto a PMCL for a given fluid contact angle. First, I determine the volume of a single dispensed droplet. Assuming that a single droplet resting on a flat surface is otherwise spherical in nature, the volume of a droplet with a contact angle, θ, and diameter, D, can readily be calculated as

$$V_{drop} = \frac{\pi D^3}{24}\left(\frac{\cos^3\theta - 3\cos\theta + 2}{\sin^3\theta}\right) \quad . \tag{3-1}$$

The typical contact angle for tested solutions is ~ 40° and the drop diameter ranges from 24 to 30 μm, which puts the droplet volume between one and two pL. I found that droplet volume varies between these limits from cartridge-to-cartridge and fluid-to-fluid and that I must therefore deposit and measure a number of calibration droplets to determine the average dispensed droplet volume for a specific cartridge and fluid before dispensing droplets onto PMCLs.

The maximum volume of fluid that a 45-μm-wide MCL can hold based on its length and the fluid contact angle is also readily calculated. Figure 3-4(b) shows the calculated fluid volume as a function of PMCL length for three different contact angles. As an example, a 45 x 200 μm MCL can hold a maximum of 45.8 pL if the fluid has a 40° contact angle with the surface. This

corresponds to between 23 and 46 droplets dispensed by the printhead. However, I found that as the PMCL begins to fill up with fluid, the addition of further droplets increases the probability that fluid will spill over to the underside of the MCL. Hence in practice it is not useful to attempt to fill the PMCL surface solely through droplet dispense. I will discuss an alternate approach later in this section using substantially fewer droplets based on the hygroscopic nature of glycerol.

I now determined the minimum receptor concentration in the functionalization fluid to achieve full coverage of the PMCL surface with receptor molecules. Based on its average size, a bBSA molecule occupies roughly 110 nm^2 when immobilized on a surface [29]. Dividing the area of the PMCL by the bBSA footprint gives the approximate number of required bBSA molecules, which in the case of a 45 μm x 200 μm PMCL is 8.18×10^7 molecules, or 9.45 pg. If 100% surface coverage was possible and all molecules in the functionalization fluid found their way to the surface, the minimum required bBSA concentration would be 9.45 pg/45.8 pL = 0.206 mg/ml assuming the maximum fluid volume on the microcantilever is achieved solely with dispensed droplets. However, each of these assumptions is unlikely to be realized in practice such that the actual needed concentration will likely be greater. My approach is therefore to use the highest concentration possible within the solubility limits of the protein and consistent with reliable jetting performance. For bBSA this turns out to be approximately 2 mg/ml, which is more than sufficient. In the case of other receptor molecules with lower solubility limits, it may be necessary to perform multiple droplet dispense/rinse/dry cycles to build up to maximum active site density.

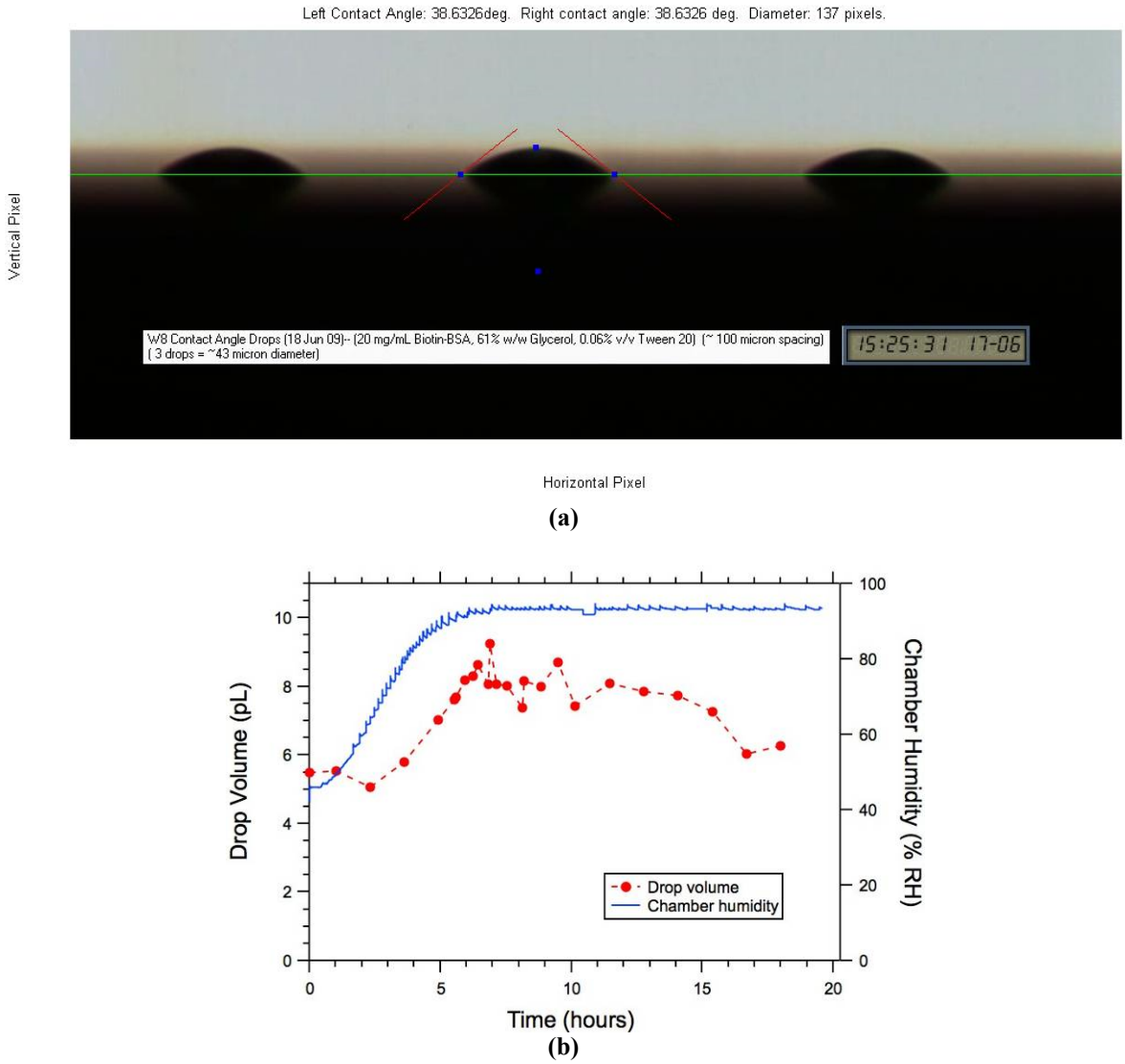

Figure 3-5: (a) A single frame from the monitoring video during incubation and (b) droplet volume and relative humidity as a function of time during an incubation period in which the humidity is slowly ramped up during the first 7 hours.

Less than the theoretical maximum fluid volume can be deposited on a PMCL when a hygroscopic functionalization fluid is used because increasing the ambient humidity causes the droplets to swell. This effect can be used to fill the entire top surface of the PMCL with functionalization fluid resulting in uniform fluid coverage. To gain a rough idea of how much swelling is possible a silicon slide is CVD coated with GOPS and a small array of ~45-µm-diameter droplets are deposited near the edge of the slide. A custom goniometer with a

microscope objective is focused on the drops and the contact angle and diameter are monitored as a function of time throughout an incubation cycle while the humidity is increased from 47 to 93 %RH. Figure 3-5(a) shows one frame of the monitoring video from which both the contact angle and droplet diameter are measured at that instant in time. As shown in Fig. 3-5(b) for a 19 hour incubation period, the droplet volume increases with increasing humidity until the humidity reaches its maximum at 7 hours, after which the volume slowly decreases as fluid evaporates from the droplet. The maximum increase in droplet volume is approximately 1.6 times the initial volume.

To demonstrate the technique on microcantilevers, four different fluids are jetted onto 200 μm long PMCLs in an 8-PMCL array, with each individual fluid being dispensed onto two PMCLs. The fluids all consist of 2 mg/ml bBSA, 61% glycerol, 39% aqueous buffer and 0.06 mg/ml Tween 20, but vary in their buffer species, ionic strength, and/or pH. Details are shown in Table 3-1. The specified ionic concentrations are for the final fluids including glycerol. For each fluid, a series of calibration droplets is first dispensed and measured to determine the average droplet volume, which is then used to estimate the number of droplets to dispense for that fluid to reach approximately half the maximum calculated volume that each 45 μm x 200 μm PMCL can hold (45.8 pL).

Table 3-1: Functionalization fluid details

PMCLs	Buffer Species	NaCl Ionic Strength (mM)	Buffer Ionic Strength (mM)	Total Ionic Strength (mM)	pH	Number of droplets dispensed	Total volume dispensed (pL)
1, 2	Citrate	0	0.14	0.14	5	15	22.6
3, 4	Phosphate	69.9	6.7	76.6	7	16	26.7
5, 6	Carbonate	0	46.6	46.6	10	12	23.5
7, 8	Carbonate	37.8	48.4	86.2	10	12	23.1

Figure 3-6(a) shows the PMCL array just after fluid spotting. In each case individually dispensed droplets have agglomerated into between one and three larger droplets on a given PMCL. I found that for a given fluid and number of dispensed droplets the number of agglomerated droplets and their exact spatial distribution can vary significantly from PMCL to PMCL. This of course would have a deleterious effect on functionalization uniformity and increase variability in PMCL response if it could not be corrected through post-deposition droplet swelling.

(a) **(b)**

Figure 3-6: 8-PMCL array spotted with various bBSA solutions (a) before and (b) after 19 hours of incubation at room temp with the first 7 hours ramping from 24 to 94 %RH.

The effects of droplet swelling just after incubation are shown in Fig. 3-6(b). The same humidity ramping schedule as Fig. 3-5(b) is used over a 19 hour incubation period. Note that in all cases the final fluid coverage includes nearly all of each MCL surface with only a small variation in the tip region. Since this region contributes very little to static deflection, this variation is insignificant. Also note that for all except PMCL 8 the fluid volume increase is such that the final agglomerated drop spills off the base of the MCL, forming a relatively large bulb. In the case of PMCL 8, which is the only one for which three agglomerated droplets formed immediately after inkjetting, the water uptake is not enough to form a bulb, the lack of which has a severe effect on receptor uniformity which will be discussed in Section 3.3.2. In any case,

droplet swelling is clearly an effective means of forcing uniform fluid coverage of each PCML. I now turn to an evaluation of uniformity and relative density of receptor active sites.

3.3.2 Receptor Uniformity and Relative Density

Following incubation, the sample is placed on a hotplate at 35 °C and droplets are allowed to completely dry. For PMCLs with a bulb at the base of the microcantilever, the droplet dries from the microcantilever tip down toward the bulb such that the bulb is the last part of the droplet to dry. The result is that buffer salts and suspended proteins accumulate in the bulb and are not deposited along the PMCL during drying. For PMCLs without a bulb at the base of the microcantilever, the droplet dries from the edges toward the center of the PMCL, which causes buffer salts and suspended proteins to be concentrated in the center of the PMCL as the final liquid evaporates.

The reason for drying the PMCL arrays is related to the next step, which is to align and bond, at room temperature and overnight [36], a 2-layer PDMS microfluidic piece with integrated flow channels, valves, and control channels [16]. If there is still liquid on the PMCLs, the liquid dries during the overnight bonding process. As it dries, the interfacial force exerted on the PMCLs cause them to bend up. The group found that the bending is large enough that the still-wet PMCLs actually touch the top of the PDMS flow channel and become stuck to the surface through stiction, thereby ruining the device.

Following bonding, fluid and control channel ports are connected to tubing and a syringe pump to individually control fluid flow over each PMCL array [16]. The following sequence of fluids is then flowed through each flow channel:

1. Initial rinse with 1X PBS (pH 7.4) at a flow rate of 5 µL/min for 5 min
2. Passivate flow channel with 5 mg/ml BSA in 1X PBS (pH 7.4) at 5 µL/min for 1 hour

3. Expose flow channel to 25 nM solution of Alexa Flour 514 labeled streptavidin in 1X PBS buffer (pH 7.4) at 5 µL/min for 3 min

4. Final rinse with 1X PBS (pH 7.4) at 5 µL/min for 5 min

To enable clear fluorescent imaging of the PMCLs, the PDMS microfluidic piece is removed from the die and fluorescent images are taken with the sample immersed in DI water. Figure 3-7 shows the final result, which allows qualitative assessment of the effects of droplet swelling, bulb formation, and fluid formulation.

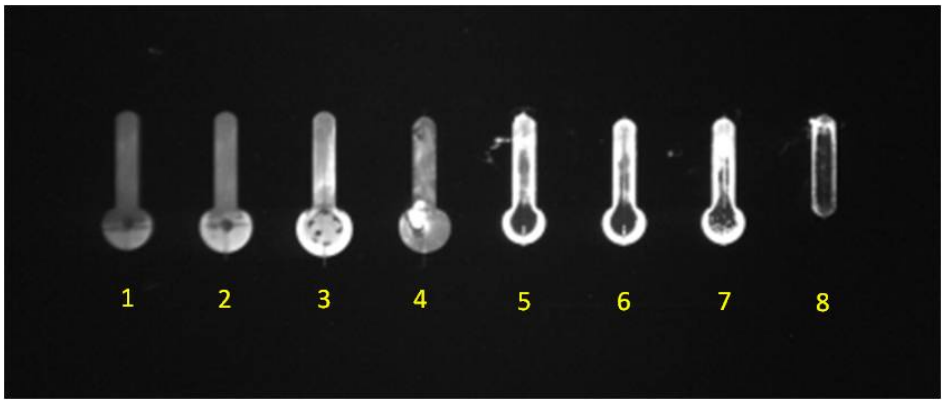

Figure 3-7: Fluorescence image of PMCL set shown in Figure 3-6 after exposure to Alexa Fluor 514 labeled streptavidin.

As illustrated by PMCL 8, lack of bulb formation during droplet swelling results in fluorescently tagged ligand being captured only around the edges of the PMCL. The interior remains quite dark in comparison. I observed the same phenomenon many times on numerous PMCL samples with a wide range of fluid formulations. I concluded that receptor active site density is severely limited in the interior of the PMCL. This is most likely due to interference from precipitation of salt and/or residual unbound protein as the drop dries.

The rest of the PMCLs show much improved fluorescence uniformity with dark regions primarily confined to the bulb area. Analysis of video of during fluid drying shows that the drop recedes from the MCL tip toward the base until it is confined only to the base where it continues

to evaporate until fully dried. Salts and unbound protein therefore end up primarily in this region where they do not affect receptor site uniformity on the PMCLs themselves. Hence bulb formation in conjunction with droplet swelling is a very useful tool in achieving improved uniformity.

Careful examination of each pair of PMCLs shows that the best fluorescence uniformity occurs for PMCLs 1 and 2, spotted with dilute citrate buffer. However, the fluorescence intensity is significantly less than for PMCLs 3-7, indicating that receptor site density is likely smaller. The next best uniformity is for PMCLs 3 and 4, spotted with phosphate buffer. Moreover, quantitative analysis shows 80% higher average fluorescence intensity. It should be noted that the bright spot in the bulb for PMCL 4 is a piece of debris that started on the PMCL and was wicked to the bulb region during drying. This may have affected the overall brightness and uniformity of PMCL 4 compared to PMCL 3. PMCLs 5-7 spotted with carbonate buffer show regions of highest fluorescence intensity, but poor uniformity on the PMCL surface compared to MCLs 1-4 (although much better than PMCL 8). If uniformity is more important than achieving maximum active site density, the results from Fig. 3-7 indicate that a phosphate buffer-based functionalization fluid may be superior. However, further experimentation in conjunction with surface stress generation studies (i.e., PMCL deflection) are needed to determine the best buffer species and pH for the functionalization fluid in order to maximize receptor site density and uniformity.

3.4 Summary

I demonstrated single-sided functionalization of a silicon photonic microcantilever array using a Dimatix inkjet printer. I found that an excellent fluid formulation for jetting dissolved proteins is 61% glycerol, 39% aqueous buffer and Triton X-100 or Tween 20 at their respective

critical micelle concentrations. I demonstrate that fluid coverage of the PMCL surfaces can be maximized through droplet swelling during a controlled ramp up of relative humidity due to water uptake by hygroscopic glycerol in the jetted droplets. I also show that continued swelling to form a liquid bulb just off the base of each PMCL offers dramatic improvement in receptor surface site density by largely confining buffer salts and unbound protein to the bulb region during drying. The next steps are to use the results of this study to investigate fluid formulation to maximize microcantilever deflection for a given receptor/ligand system, and to apply this to actual biosensing scenarios.

4 STREPTAVIDIN SENSING WITH IN-PLANE PHOTONIC MICROCANTILEVER SENSOR ARRAY

4.1 Motivation

As in Chapter 3, this chapter is adapted from a peer reviewed article publised in IEEE Sensors.

A label-free and highly-specific bio-diagnostic sensor capable of multiplexed assays and parallel readout could satisfy many of the requirements for remote point-of-care medical use, reduce the cost and processing time of medical laboratory diagnostics in metropolitan areas, and open a way to use newly discovered biomarkers for medical testing. Integration with microfluidics provides the additional benefit of on-chip sample handling which reduces the amount of sample and reagent consumed and improves response time through advection-dominated transport of target molecules (analyte) to the sensor surface. Moreover, a device consisting of large arrays of tens to hundreds of individual sensors can improve redundancy and detection limits, allowing the statistical analysis of measurements and enabling calibration standards.

Microcantilevers (MCLs) have received significant attention to fill this diagnostic role, but there are a number of potential drawbacks to overcome before this can be realized. For example, the two most commonly used methods to measure the deflection state of a MCL in bio-sensing scenarios are the optical lever method in which a laser beam reflects off the MCL onto a position sensitive detector, or embedding a piezoresistive element in the MCL to measure small

changes in resistance due to MCL deflection. Of the two, the optical lever method is more sensitive, with reported responsivities of 10^{-3} nm^{-1} vs. ~ 4 x 10^{-6} nm^{-1} for the piezoresistive detection method [12]. However, the optical lever method does not conveniently scale to simultaneously read out large arrays of MCLs. Also, the optical lever method can be challenging to implement for sensing in liquid environments where the assay solution may either absorb or scatter the laser beam and small changes in solution refractive index cause undesirable changes in refraction.

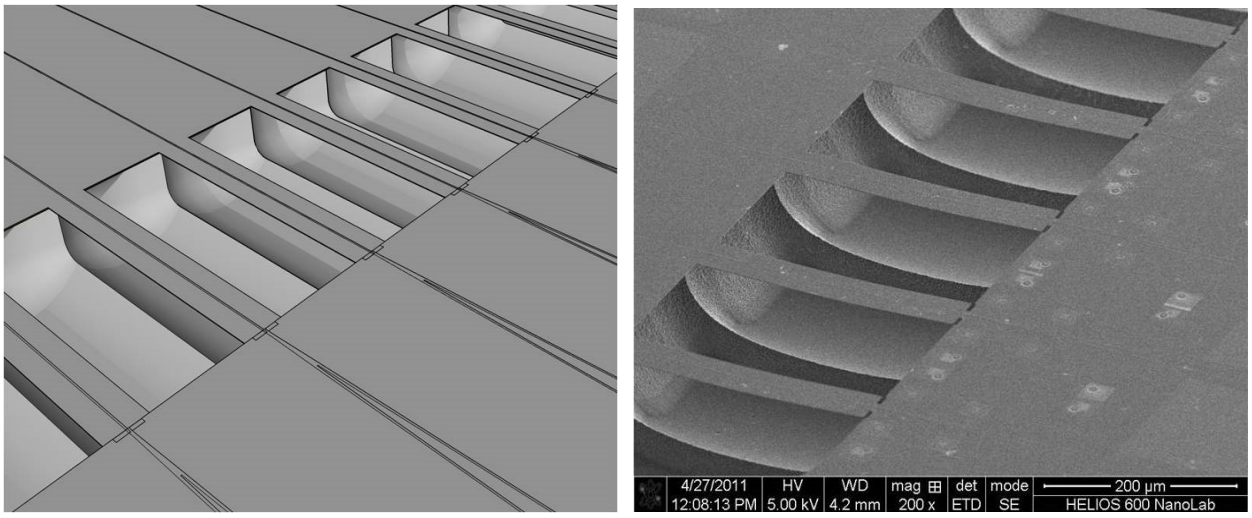

(a) **(b)**

Figure 4-1: (a) Sketch of deeply etched channel under PMCL array with single mode wave guides transitioning to differential splitter across the gap at the free end of the PMCL. (b) SEM image of deeply etched microfluidic channel under PMCL array.

Most research groups involved in MCL biosensing use a gold-thiol attachment chemistry, which requires deposition of a thin (typically <40 nm) gold layer on one MCL surface followed by exposure to thiolated receptor molecules such as DNA, proteins, antibodies, and/or molecular linkers [2-10,17-20,46]. This method is a very simple and convenient way to selectively attach reactive molecules to just the gold-coated side of a MCL due to the favorable reaction kinetics of the gold-thiol interaction. However, the presence of the gold layer presents additional complications such as deflection sensitivity to changes in temperature [21, 22], instability of the

receptor gold-thiol linkage in the presence of other thiols in complex sample media such as blood plasma [47], and the susceptibility of the gold-thiol bond to air oxidation [23].

To address these issues and exploit the MCL's unique advantages, the Nordin research group recently developed a scalable in-plane photonic technique to simultaneously read out an array of MCLs on a single chip, [12, 13-15] which I will refer to as a photonic microcantilever (PMCL). This technique is compatible with direct attachment of receptors to the native oxide on the PMCLs such that a gold adhesion layer is avoided. In this chapter, I briefly review the operation of the PMCL transduction method, recent device improvements, and integration with microfluidics. I then characterize the PMCLs as label-free biosensors using biotin/streptavidin as a convenient molecular receptor/target system in which the biotin is attached to the native oxide layer of silicon. I found that the maximum surface stress generated is quite limited for direct attachment of biotin to the native oxide, even for high analyte concentration (6 mN/m for 4.7 μM streptavidin). I also investigated an alternate biotin linker molecule and the effects of a PEG passivation agent.

4.2 Photonic Microcantilever and Microfluidics

PMCLs are designed to measure changes in static deflection (static mode) due to adsorption-induced differential surface stress via molecular interactions, rather than measuring a shift in resonance frequency (dynamic mode) via mass accumulation due to adsorption. Static mode is better suited for sensing in liquid due to a decrease in the quality factor, Q, of the vibration modes of a microcantilever in liquid. The reduced quality factor limits the minimum detectable frequency shift for dynamic mode measurements [17]. Static mode sensing measurements require sensitizing one surface, either top or bottom, of the MCL to the target analyte, usually by immobilizing receptors to that surface. Upon specific adsorption of the

analyte to the bound receptor, the molecular interaction at the surface results in surface stress which causes the MCL to deflect [46]. The change in static deflection can then be measured by the in-plane differential photonic transduction method.

The in-plane photonic transduction method, as described in Refs. 1, 20-22, is based on a rib waveguide directly fabricated in the PMCL. Light exiting the waveguide at the free end of the PMCL is coupled into an asymmetric multimode waveguide and differential splitter which splits light into two outputs. The relative amount of light that is coupled into each output is a function of the deflection state of the PMCL. By taking the normalized difference between the optical powers of the two outputs, a differential signal is formed that varies monotonically with deflection over a ±500 nm detection range. The responsivity of the PMCL is comparable to the best reported for the optical lever method, which has enabled me to readily measure differential surface stress changes in the range of 0.1 mN/m with a 16-PMCL array [16].

Figure 4-1 shows a schematic illustration of part of an array of PMCLs and a corresponding scanning electron microscope (SEM) image of a fabricated sample. PMCL arrays are fabricated on 10 mm x 14 mm SOI chips. The PMCLs are 300 μm long, 45 μm wide and dry-etched down from 750 nm to 650 nm thick to form rib waveguides. The 1 μm thick oxide layer underneath the PMCLs is removed as well as ~60 μm of the underlying silicon handle wafer. This locates the PMCLs vertically in the approximate middle of what will be a microfluidic channel (MFC) once the PDMS microfluidic piece is bonded to the sample. The fluid velocity profile is highest in the middle of the MFC, thus maximizing mass transport of the analyte to all surfaces of the PMCL (thereby decreasing response time) and eliminating transient deflections that might cause ambiguity in deflection measurements [16, 48].

The silicon device is designed for simultaneous readout of tens to hundreds of PMCLs on a single SOI chip and can be arranged in multiple arrays for multiple sensing opportunities per chip [15], which the group demonstrates in this chapter. For example, Fig. 3-2(a) shows a schematic illustration of the microfluidic layout over two 16-PMCL arrays. Pneumatically actuated PDMS valves, shown in green, direct fluid flow within the desired MFCs, shown in red. This enables me to load an analyte solution in the MFC through the input inlet on the left of the die and transport the solution quickly to specific PMCL arrays, shown in black. New fluids can be queued up in Bypass Channel #2 in preparation for their introduction to one or both of the 16-PMCL arrays. This allows two independent sensing experiments per chip. Figure 4-2(b) shows a fully integrated PMCL chip with PDMS microfluidics. The layout is different from Fig. 4-2(a) and has one 16-PMCL array and two 8-PMCL arrays per chip, demonstrating the inherent flexibility of the PMCL and MFC platform. For purposes of illustration, the MFCs are filled with red dye and the control valves are filled with green dye.

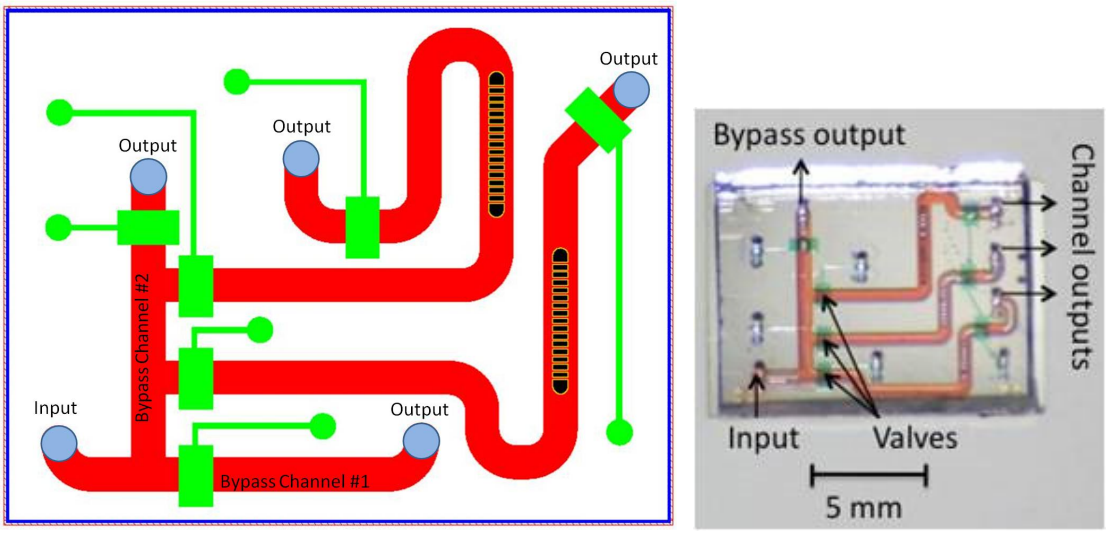

(a) **(b)**

Figure 4-2: (a) Schematic of the layout of PDMS microfuidics for a die with 2 x 16 PMCL arrays. (b) Photo of a PDMS microfluidic piece and valve network bonded to a silicon die properly aligned over the PMCL arrays (1 x 16, 2 x 8) using curing agent as an adhesive.

4.3 Sensor Functionalization

4.3.1 Functionalization Approach

Many research groups have investigated MCLs for label-free detection and quantification of proteins and other bio-molecules in aqueous solutions. These studies employ DNA hybridization [2-4], DNA-protein [5,6], protein-protein [7,8], or antibody-antigen [3,7,9,10] for molecular recognition of target biomolecules. For initial characterization of the PMCL arrays, I elected to use the biotin-streptavidin interaction since the binding efficiency and strength of the reaction is high and the relative cost of the reagents is low. Based on past experience (unpublished), I found that immobilizing large biotinylated proteins such as bovine serum albumin (BSA) as receptors does not result in measureable amounts of surface stress. The strategy is therefore to bind the analyte as close to the surface as possible to maximize the induced surface stress and thus PMCL deflection. Fortunately, there are numerous small-molecule, biotin-based reagents commercially available due to their common usage in bio-conjugation and molecular labeling.

I first prepared the silicon surface with an aminosilane in order to covalently link the biotin receptor to the silicon substrate [42]. I then use an inkjet process to selectively attach receptor molecules to the top surface of the PMCLs [41] and functionalize only half of the PMCL array with biotin and leave the other half unfunctionalized to serve as references, which allows me to subtract out deflection due to other environmental effects, such as flow dynamics, unrelated to analyte adsorption. After functionalization with biotin receptors, the two-layer PDMS microfluidic piece is bonded to the silicon die. Since in general receptor molecules can be temperature sensitive (e.g., proteins), the group employed a recently developed room temperature bonding technique in which PDMS curing agent is used as the adhesive [36].

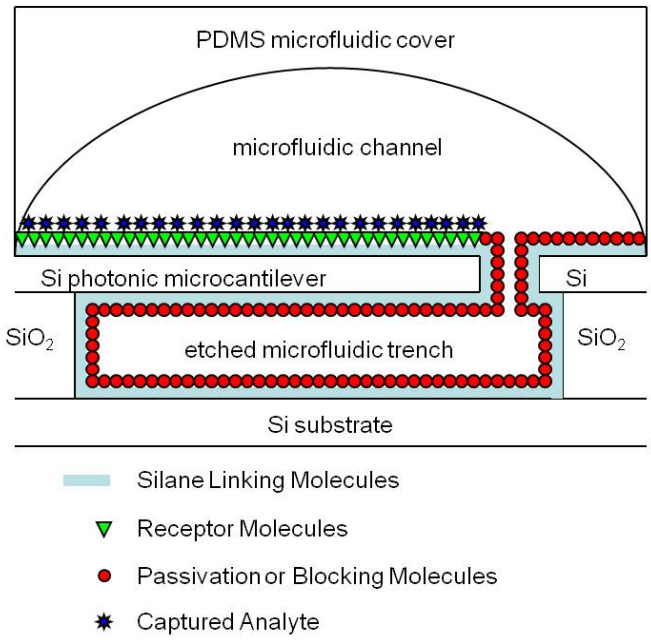

Figure 4-3: Functionalization and Passivation Approach.

Ideally, it would be best to eliminate non-specific binding of the target analyte (streptavidin) to all non-sensor surfaces in the MFC. This is especially true for the bottom surface of functionalized PMCLs, so as to maximize the differential surface stress upon analyte adsorption to the receptor-coated top surface. To accomplish this, I investigated several possible passivation molecules and chose one that would readily bind with the aminosilane-coated surface and afterward be resistant to non-specific protein adsorption. The result of this general approach of functionalization, passivation, and capture of a target analyte is shown in Fig. 4-3 with a cross-sectional view of a PMCL in a MFC.

4.3.2 Surface Chemistry

To deposit a monolayer of amino-silane, a variety of organosilanes were tested, and two different methods of silane deposition were developed, one based on chemical vapor deposition (CVD) and the other on liquid phase deposition. This was done to determine the chemistry and

process that yields a high density of active receptor sites and a large induced surface stress. Figure 4-4 illustrates the steps involved in functionalizing the sensor surface for both the liquid and CVD processes.

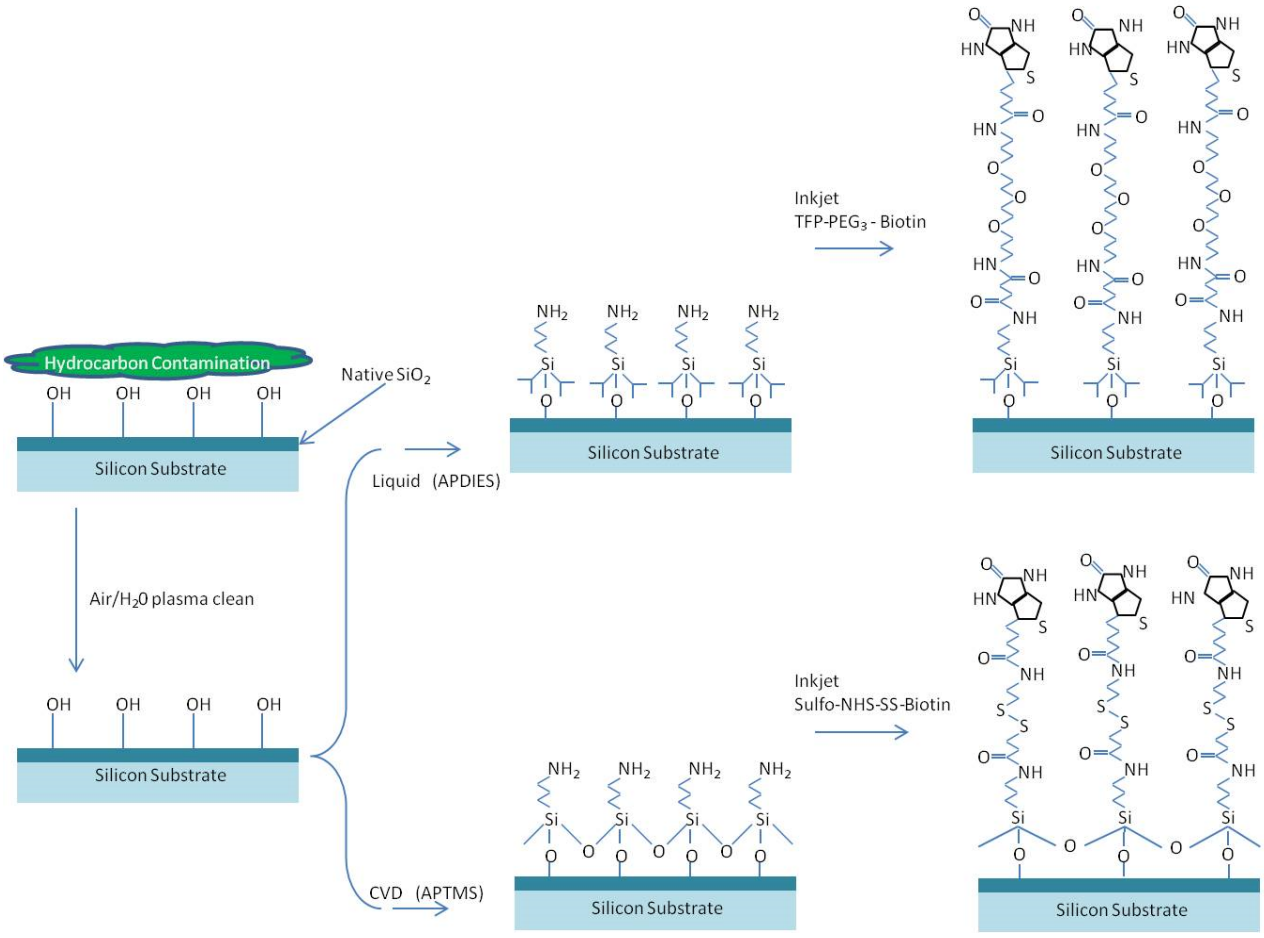

Figure 4-4: Sensor surface functionalization chemistry for APDIES and APTMS organosilane linkers and biotin functional groups.

The CVD process is based on the one reported in Ref. [41], except that (3-aminopropyl) trimethoxysilane (APTMS) instead of (3-glycidoxypropyl) trimethoxysilane (GOPS) is used as the anchor molecule to the silicon surface. Additionally, sulfo-NHS-SS-biotin (Pierce Biotech) is used in place of biotinlyated-BSA as the receptor molecule and is inkjetted on the PMCL surface. The inkjet solution contains 15 mg/ml Sulfo-NHS-SS-biotin in 61% glycerol/39% 50

mM PBS buffer (pH 7.0) with 0.66 mg/ml Triton X-100. Prior to loading the solution into the inkjet cartridge, I filter out any aggregates with a PTFE 0.2 μm syringe filter.

Liquid phase deposition is performed in an anhydrous toluene solution with 5% (w/w) (3-aminopropyl) diisopropylethoxysilane (APDIES). The deposition jar is rinsed with acetone and isopropyl alcohol (IPA), plasma cleaned, dehydrated at 150 °C for four hours, and then, while still hot, filled with fresh toluene and APDIES. In the meantime, the PMCL die is cleaned in Nanostrip at 90 °C for 1 hour, followed by a de-ionized water rinse. The die is then transferred into IPA and dried in a Tousimis Autosamdri-815 Series B supercritical point dryer. Next, the die surface is activated with silanol groups by placing it in a Harrick Plasma Cleaner (PCD-32G) at 18 W for 3 min. Immediately thereafter, it is placed in the prepared APDIES/toluene solution, covered and incubated. To measure the deposited film thickness after incubation, a J.A. Woollam manual angle M-2000 spectroscopic ellipsometer set at an angle of 65° is used in conjunction with a 1 cm x 2 cm plain silicon witness slide that accompanies the PMCL die during processing. The liquid deposition process with APDIES (which is a monofunctional silane) is found to be self-limiting and obtains 98% of the steady-state thickness of 0.9 nm (+/- 0.3 nm) within 2 hours of incubation. After liquid deposition of the aminosilane, I rinsed the die in fresh toluene and transfered it to IPA for another cycle in the supercritical point dryer. A solution of 10 mg/ml TFP-PEG_3-biotin (Pierce Biotech) is mixed in an inkjetting solution (61% glycerol, 39% 50 mM MOPS, 51 mM NaCl (pH 7.0) buffer, 0.15 mg/ml Triton X-100). I then removed aggregates with a 0.2 μm syringe filter as the solution is loaded into the inkjet cartridge.

Following deposition of aminosilane using either process, the corresponding receptor molecule is inkjetted onto the MCL surface [41]. After jetting the receptor molecule solution on select PMCLs the die is incubated for 2 hours at 85% relative humidity (RH) and room

temperature and then dried on a hot plate at 37 °C. Members of the group then aligned and attached the PDMS microfluidics and allow the bonding adhesive to cure for ~18 hours at room temperature [36].

If passivation of the non-functionalized surfaces is desired, this process is done after integration with the PDMS microfluidics. I typically used a 30 mM solution of NHS-PEG_{24}-methyl ($MS(PEG)_{24}$ from Pierce Biotech) in 25% DMSO and 75% 50 mM MOPS Buffer (pH 7.0), that was injected through all or select MFCs of any given die, as part of a sensing experiment. Figure 4-5 shows the chemical reactions for the passivation process of the silicon surfaces.

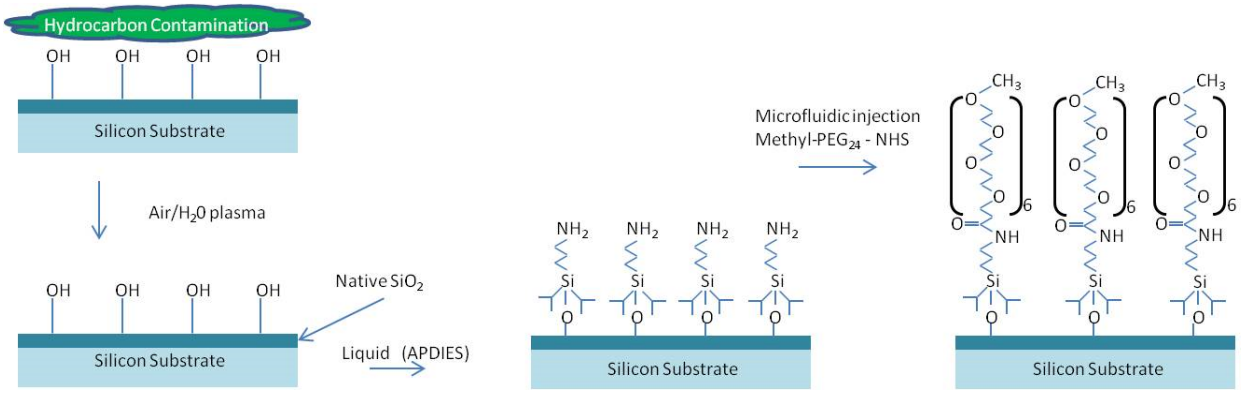

Figure 4-5: Passivation chemistry to reduce non-specific binding of streptavidin to the silicon surface.

4.3.3 Etched vs. Un-etched Sensor Surfaces

During fabrication of the silicon die, rib waveguides are defined by etching 100 nm everywhere except over the waveguides. To determine whether the additional surface roughness induced by the dry etch process affects surface stress generation on functionalized PMCLs, members of the group patterned a die with alternating etched and un-etched PMCLs. Figure 4-

6(a) shows an overhead, out-of-plane view of a portion of a PMCL array where etched and unetched PMCLs have been fabricated in the same array.

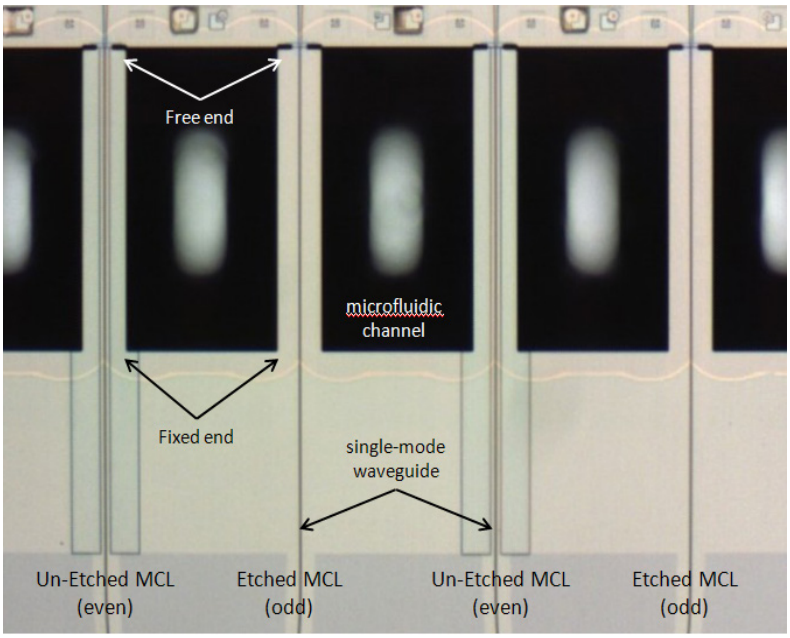

(a)

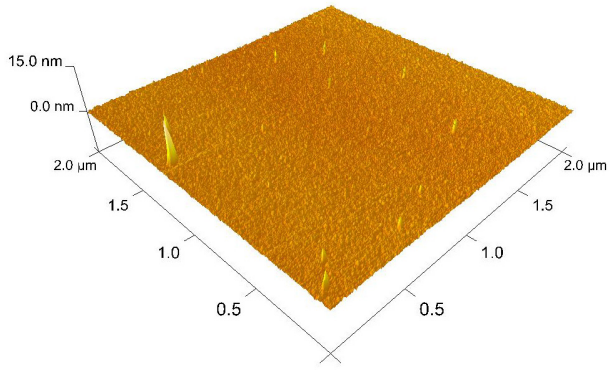

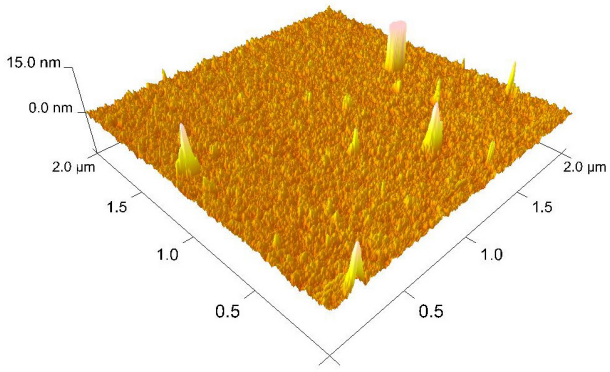

(b) **(c)**

Figure 4-6: (a) Microscope image of a section of a PMCL array with alternating etched and un-etched PMCLs. (b) AFM image of unetched PMCL surface. (c) AFM image of etched PMCL surface.

Atomic force microscopy (AFM) is used to quantify the difference in surface roughness between etched and unetched silicon surfaces. The AFM images in Figs. 4-6(b) and 4-6(c) clearly indicate increased surface roughness for etched as compared to unetched silicon. The AFM measurements are taken over a 2 μm x 2 μm area with a Veeco Dimension V AFM system and model TESPDW tip with a nominal 15 nm radius. The RMS surface roughness (R_q) for the unetched PMCL is 0.340 nm (+/- 0.050 nm) while for the etched surface it is 0.570 nm (+/- 0.068 nm). The image resolution for the AFM images in Fig. 4-6 is 3.91 nm/pixel (512 lines over 2 μm x 2 μm area) and the outlying points shown in the images are due to debris on the surface and are not included in the R_q calculations.

4.4 Sensing: Biotin/Streptavidin

4.4.1 Experimental Equipment and Set-up

Once an SOI chip is processed and prior to functionalization and PDMS integration, operation of the PMCLs is inspected and calibrated by physically deflecting each PMCL up and down and measuring its differential signal response [15]. During this step, damaged and unresponsive PMCLs are identified. Following inspection and calibration, the die is functionalized, assembled, and then mounted in a holder and integrated on an optical alignment bench where a single-mode optical fiber couples light to the chip input waveguide, which has a series of waveguide optical splitters to source light to each PMCL in the arrays. Light is provided by a SLED with a 1550 nm center wavelength. Fluid is introduced to the chip with a syringe pump routed through a 10-channel selector valve. Different fluids can be presented in each MFC depending on the selector valve and on-chip PDMS valve settings. Output tubes leading to waste collection containers are cut to consistent lengths and fixed at the same elevation above the

device each time an experiment is run to create repeatable flow dynamics. Control tubes run from the ports for the PDMS control valves to a solenoid valve manifold and pressurized air source.

Individual waveguide array outputs from the differential splitters are imaged onto separate pixels of a linear InGaAs focal plane array camera [15]. During a sensing experiment, custom in-house developed LabVIEW software controls and synchronizes the syringe pump, selector valve, PDMS fluid handling valves, and data capture from the camera. When post-processing the data (typically captured at a line scan rate between 1 and 4 kHz), a 251 point moving-average filter is applied to reduce noise.

Although the PMCL sensing mechanism is label-free, I used Alexa Fluor 488 or 514 tagged streptavidin as the analyte. The fluorescent tags serve as a debugging tool by allowing me to determine where in the MFC the analyte begins and ends, what time the analyte reaches the PMCL array during an experimental flow, and to what degree streptavidin non-specifically binds to the MFC surfaces. A Navitar Video ZFL Scope, Infinity 2-2M 2.0 Megapixel CCD Monochrome Camera, X-Cite 120Q microscope light source, liquid light guide, and appropriate Chroma filter sets comprise the fluorescence imaging system.

4.4.2 APTMS/Sulfo-NHS-SS-Biotin Experiment

Each experiment with each device began by first introducing liquid into all of the MFCs in the form of an initial rinse buffer that consists of 1X PBS with 0.2% Triton-X100 (pH 7.4) at a flow rate of 100 μL/min for 2 min, followed by a 1X PBS solution without surfactant for a 30 min period at a rate of 10 μL/min Next the input fiber and camera optics are aligned and a solution of 4.7 μM Alexa Fluor 514 labeled streptavidin in 1X PBS is loaded into Bypass Channel #2. The device is now prepared for sensing streptavidin.

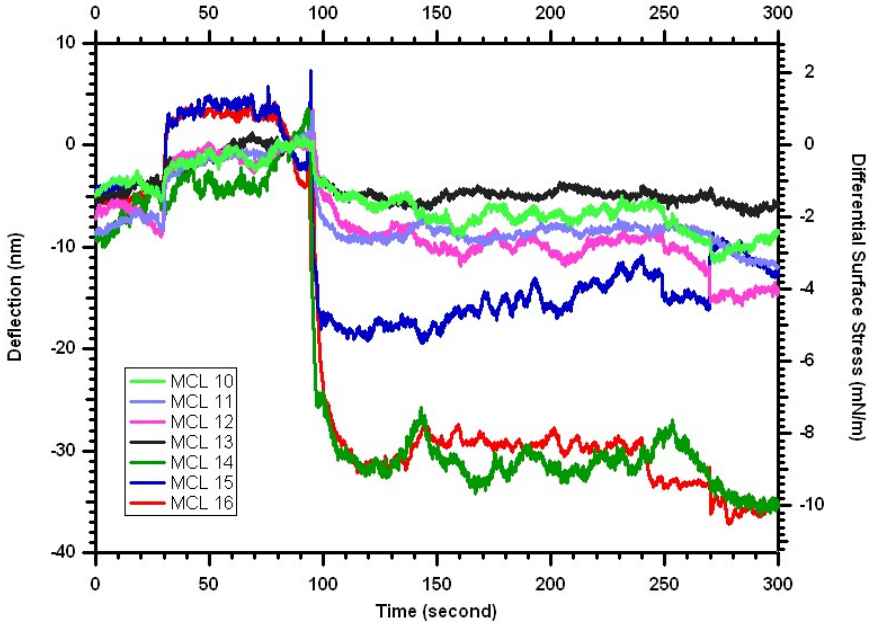

(a)

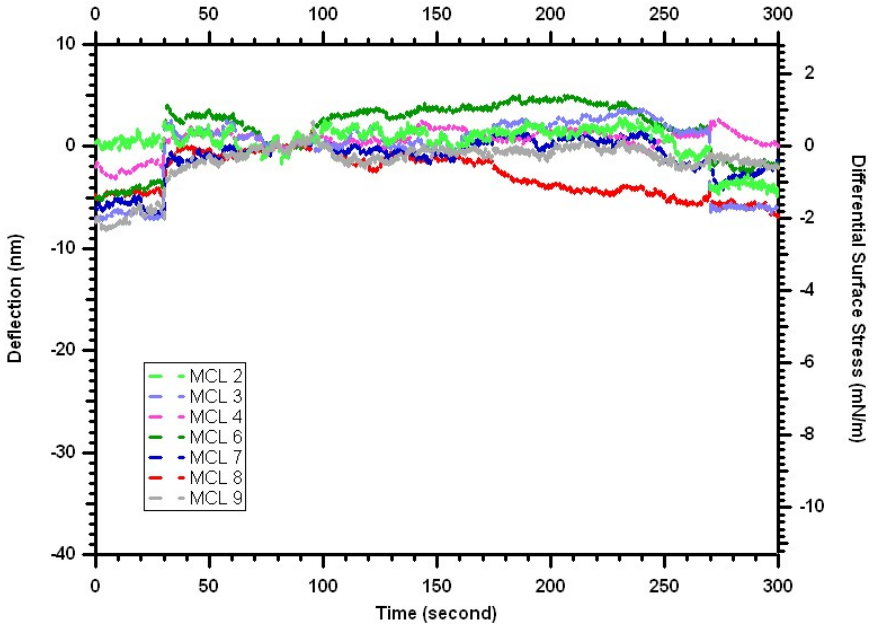

(b)

Figure 4-7: (a) Output of sensor PMCLs (b) Output of reference PMCLs.

During a sensing run, data was captured for a total of 5 min: at 30 sec the valve at the entrance to the MFC opens, at 60 sec the syringe pump initiates flow, at 240 sec the syringe pump is stopped

to end the flow, and at 270 sec the entrance valve closes. This experiment is performed on a die similar to that shown in Fig. 4-2(b) in which the group use only the 16 PMCL array where the even numbered PMCLs are etched and the odd numbered PMCLs are unetched. Initial inspection of the die revealed that PMCLs 1 and 5 were damaged so the data from these (unetched) PMCLs was discarded.

Figures 4-7(a) and 4-7(b) show the individual deflection curves of seven PMCLs functionalized with sulfo-NHS-SS-biotin and seven unfunctionalized PMCLs that serve as references. All reference PMCLs are upstream from the sensor PMCLs, so that the direction of flow is from low to high numbered PMCLs. At a flow of 2 μL/min, the 4.7 μM streptavidin solution reaches the PMCL array at approximately 92 sec. Note the pronounced change in deflection for the sensor PMCLs while the reference PMCLs are relatively unaffected and more tightly grouped.

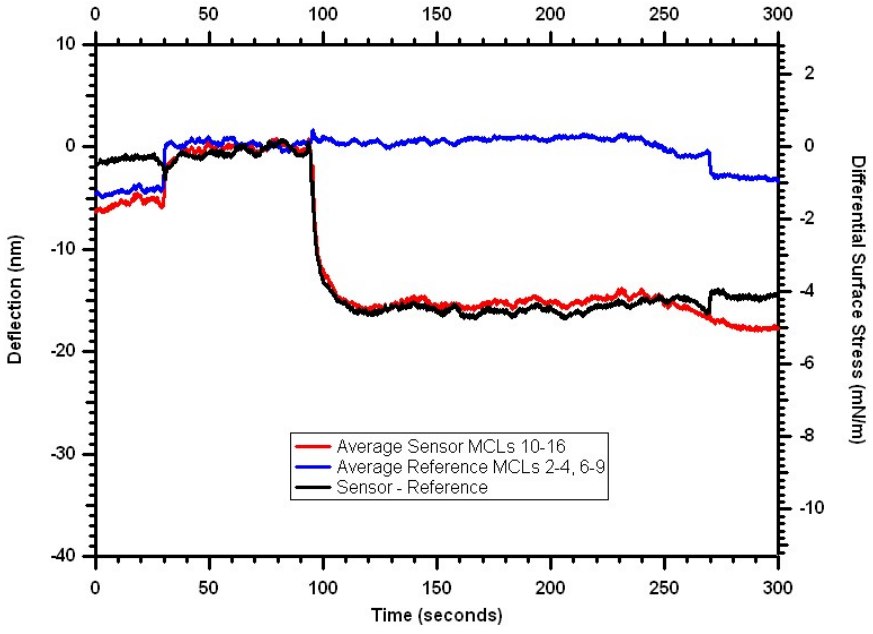

Figure 4-8: Averaged sensor and reference PMCL outputs and the average difference.

Figure 4-8 shows how the average of these signals (i.e., the average of the sensor PMCL deflection and the average of the reference PMCL deflection) gives a clearer picture of the sensor response through reduction of noise and PMCL response variability. The average sensor PMCL deflection is 16 nm while the average reference PMCL deflection is essentially zero. Based on our PMCL dimensions and assuming full coverage of binding sites, one can calculate the average adsorption-induced surface stress to be -4.5 mN/m (compressive) for the sensor PMCLs.

From this same experiment, I noticed that the etched and unetched PMCLs respond differently. Since deflection goes as the inverse square of MCL thickness, one would expect unetched PMCLs (750 nm thick) to exhibit only 75% of the deflection of etched (650 nm thick) PMCLs for the same applied surface stress.

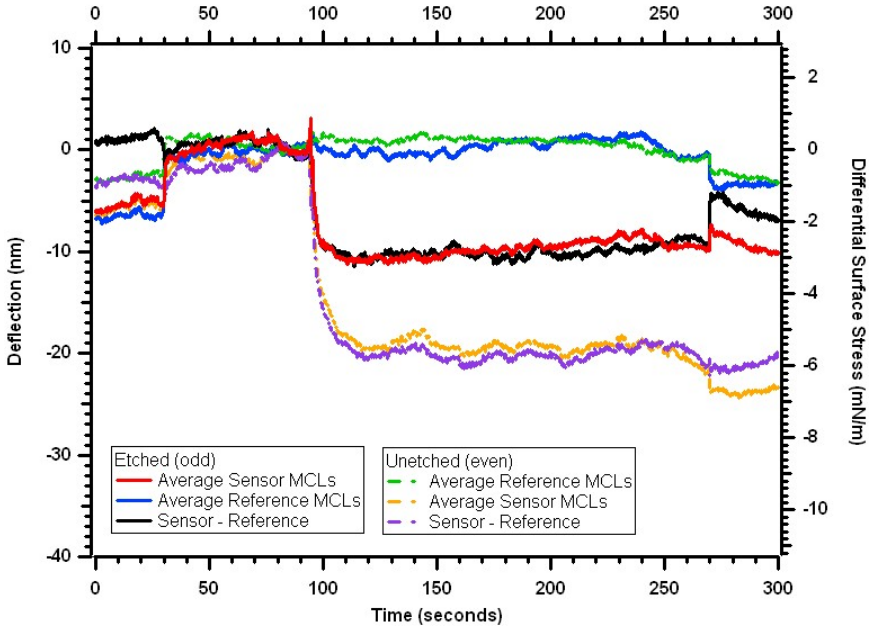

Figure 4-9: Etched vs. Unetched PMCL responses.

However, as shown in Fig. 4-9, the etched PMCLs exhibit an average deflection of ~10 nm (3 mN/m), while the unetched PMCLs have a response twice as big at ~20 nm (6 mN/m). This indicates that the smoothness of the silicon surface significantly affects the surface stress generated by streptavidin uptake on the surface. Possible mechanisms include reduction of active biotin site density and hence captured streptavidin surface density if streptavidin intermolecular interactions are important in causing surface stress, or reducing streptavidin/surface interactions if these are the dominant cause of surface stress. In any case, surface smoothness clearly affects the effective generated surface stress.

4.4.3 APDIES/TFP-PEG$_3$-Biotin Experiment

I had the group repeat the sensing experiment using a different surface chemistry and introduce a passivation agent into one of the PMCL arrays on the die. Additionally, the overall layout of the PMCL die was modified to use the design shown in Fig. 4-2(a) which has two 16-PMCL arrays wherein all PMCLs are un-etched.

Again, an initial rinse buffer is introduced into all MFCs on the die. The rinse buffer consists of 20 mM Tris, 140 mM NaCl, 0.26% Triton X-100 (pH 7.0) and flows at a rate of 50 μL/min for 5 min. The Tris buffer solution is chosen for the initial rinse as it contains amines to bind with any active TFP-PEG$_3$-biotin molecules that might detach from a functionalized PMCL during the rinse and thereby prevent binding to the underside of a downstream PMCL. This is followed by a solution of 10 mM MOPS, 140 mM NaCl (pH 7.0) buffer without surfactant that flows at a rate of 10 μL/min for 30 min. Next, the input fiber and camera optics are aligned and a solution of 5.7 μM Alexa Fluor 488 streptavidin in the same buffer is loaded into the bypass channel. The device is now prepared for sensing streptavidin. During a sensing run, the group captures data for a total of 5 min: at 15 sec the entrance valve opens, at 30 sec the syringe pump

begins flow, at 240 sec the syringe pump is stopped, and at 270 sec the valve closes. Initial inspection of the die indicates that PMCLs 2, 3 and 16 in Array #1 and PMCLs 7 and 11 in

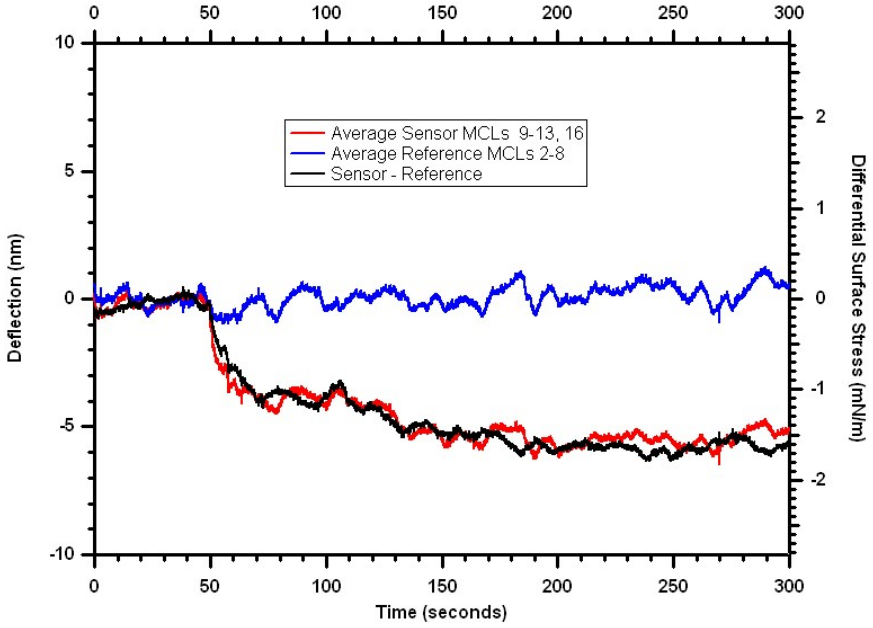

(a)

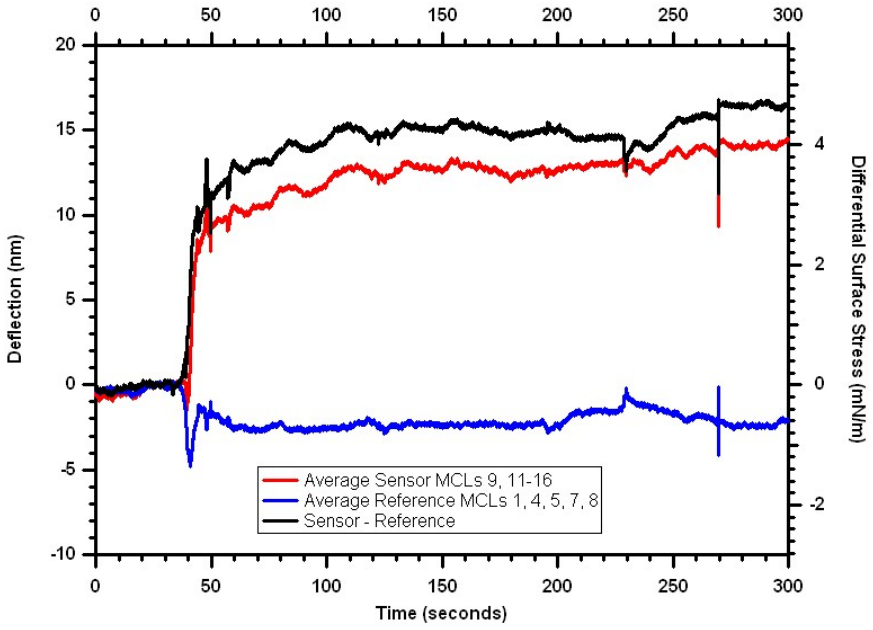

(b)

Figure 4-10: (a) Averaged streptavidin response for unpassivated PMCLs. (b) Averaged sensor and reference signals during passivation with $MS(PEG)_{24}$.

Array #2 are damaged, so one may discard the data from these PMCLs.

Figure 4-10(a) shows the average deflection of 6 PMCLs functionalized with biotin and 7 unfunctionalized PMCLs that serve as references for Array #1, which was not exposed to the passivation agent. Flowing at 2 μL/min, the 5.7 μM streptavidin solution reaches the PMCL array at approximately 45 sec. The deflection response is less than that observed for the previous surface chemistry and generates a differential surface stress of only -1.5 mN/m.

For Array #2, I had the group introduce passivation (30 mM $MS(PEG)_{24}$ in 25% DMSO and 75% 50 mM MOPS Buffer (pH 7.0)) prior to doing a streptavidin sensing run. The PMCL response monitored during the first 5 min of the passivation cycle to determine any change in deflection due to binding of $MS(PEG)_{24}$ to PMCL surfaces. As seen in Fig. 4-10(b), the reference PMCLs show little deflection since the $MS(PEG)_{24}$ binds to both the top and bottom PMCL surfaces. However, the sensor PMCLs deflect because the $MS(PEG)_{24}$ binds primarily to the bottom of the PMCLs since the top surfaces are already functionalized thereby occupying many,

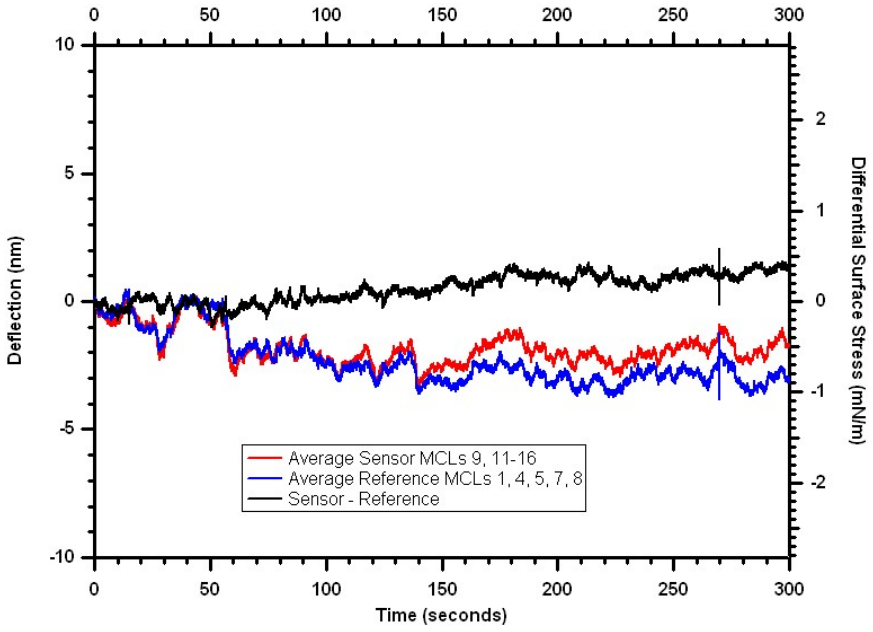

Figure 4-11: Averaged streptavidin response for passivated PMCLs.

if not most, of the possible binding sites. The net deflection (signal minus reference) is ~15 nm, corresponding to a differential surface stress of ~4.5 mN/m. The deflection is also positive (i.e., in the opposite direction of the deflection observed during the sensing with Array #1), consistent with the $MS(PEG)_{24}$ adsorbing and binding more so to the underside of the functionalized PMCLs.

Next, the passivation solution in the MFC is rinsed away with the same buffer used for the streptavidin solution, and 5.7 μM streptavidin is introduced. By looking at the fluorescence video capture, the streptavidin reaches the PMCL array at 47 sec, but as seen in Fig. 4-11, there is no discernible deflection response that can be attributed to a streptavidin-biotin binding interaction. One possibility is that biotin immobilization may not be sufficiently dense to prevent $MS(PEG)_{24}$ from filling in between active biotin sites. Since the passivator is longer than the biotin tether (8.8 nm vs. 2.4 nm), it may block streptavidin binding to biotin. Alternatively, if streptavidin does bind to biotin, $MS(PEG)_{24}$ may interfere with intermolecular interactions (streptavidin-streptavidin and/or streptavidin-surface) responsible for surface stress generation.

4.5 Discussion

Many different mechanisms have been postulated as contributing, to a larger or lesser degree, to surface stress induced by adsorption for static-mode MCL-based biosensors. These mechanisms include intermolecular repulsive forces, surface reconstruction, substrate interaction, and charge density redistribution [2-10, 43]. In the work reported here, I do not focus on specific mechanisms, but, rather, experimentally investigate the magnitude of surface stress that can be generated when receptor molecules are directly attached to silicon MCLs instead of to an intermediate gold layer. The group used the highly sensitive in-plane photonic microcantilever readout mechanism in conjunction with averaging multiple identically

functionalized sensor and unfunctionalized reference PMCLs to accurately measure small surface stresses.

The results indicate that the generated surface stress is quite limited—6 mN/m or less for 4.7 μM streptavidin. This is in contrast to Shu et al. [8] who investigated streptavidin binding to biotin tethered to an intermediate gold layer on single MCLs. They reported that the generated surface stress is dependent on the specific biotin thiol attached to the gold layer. For example, use of biotin-HPDP with 10 nM streptavidin resulted in a compressive stress of 88.7 mN/m, which is 15 times larger than the maximum surface stress that I observed using ~500 times higher streptavidin concentration. Interestingly, they also used biotin-SS-NHS but got a tensile stress of 17.8 mM/m for 10 nM streptavidin, a factor of three larger than ours but in the opposite direction.

A recent study by Godin et al. [44] gives insight into the relative contributions of various surface stress effects for molecules attached to a gold intermediate layer. Their focus was vapor deposited alkanethiols. They found that by far the largest contributor is change in the electronic charge density at the gold surface (on the order of 1 N/m), followed by electrostatic interactions (on the order of 0.1 N/m), and Lennard-Jones effects (1 – 10 mN/m). The magnitude of surface stress I observed is comparable to the weakest interaction, i.e., Lennard-Jones-type, studied for alkanethiols.

Oliveiro et al. [45] examined DNA hybridization with static-mode MCLs in which a gold layer is not used. Instead, a thin polymer adhesion layer was attached to the MCLs. Probe single strand DNA (ssDNA) was inkjetted onto one side of the MCLs to bind to the polymer layer. For two slightly different conditions, they measured surface stress changes of 3.6 and 5.1 mN/m upon hybridization with 1 μM complementary ssDNA. The corresponding molar Gibbs free

energy change is consistent with the calculated change. Note that the magnitude of surface stress change in the absence of a gold intermediate layer is comparable to what the group observed for streptavidin-biotin.

These results also suggest that a small increase (~0.2 nm) in silicon surface roughness has a deleterious effect on effective surface stress generation. Moreover, the amount of surface stress generated seems to depend on the specific linker that is used to attach biotin to the silicon surface. Attachment of $MS(PEG)_{24}$ as a passivating agent in and of itself results in measureable surface stress (4.5 mN/m) for functionalized PMCLs, but seems to block surface stress generation when the PMCLs are exposed to streptavidin.

4.6 Conclusion

I have presented new modifications to the group's chip layout that improved its performance. I also presented the results of experiments wherein streptavidin effectively binds to biotin immobilized directly on silicon PMCL arrays with integrated microfluidics on an SOI chip. The measurements indicate that streptavidin binding to biotin results in a compressive surface stress in the top functionalized surface, thus producing a downward deflection. It is unclear exactly what mechanism is primarily responsible for the compressive surface stress. However, the amount of surface stress generated is quite limited (6 mN/m or less for 4.7 μM streptavidin), which raises questions about the feasibility of this approach for practical MCL-based biosensors. I also found that an increase in surface roughness decreases the amount of generated surface stress. In addition, binding of the passivation agent $MS(PEG)_{24}$ to functionalized PMCLs produces a compressive surface stress (4.5 mN/m), but since it adsorbs to the bottom of the PMCL more than the top, the deflection is in an upward direction. Moreover,

application of the passivation agent prevents surface stress generation on functionalized PMCLs upon exposure to streptavidin.

5 ORIENTED F(AB') FRAGMENT IMMOBILIZATION ON PMCL SENSOR

5.1 Motivation

From Fig. 2-17, one can see that immunoglobulin proteins, IgG in particular, are one of the more abundant proteins in human serum. They provide the much of antibody-based immunity against invading pathogens and hence their use in immunoassays for medical and reseach applications is very common. While we saw only a small amount (~ 5-15 nm) of deflection from a biotin/streptavidin system, there is reason to suspect from past experiments with a biotin-BSA/streptavidin system that we may see a larger amount of deflection from an IgG system if the receptors can be immobilized closer to the surface.

Figure 5-1 shows the general structure of an IgG protein. The antigen binding site is located at the end of each Fab portion of the IgG. With pepsin digestion of the IgG, the Fc portion can be discarded. This provides an opportunity to immobilize the F(ab') portion of the IgG in an oriented fashion that brings the active binding site closer to the surface and yet still pointing away from the surface. This can be done by selectively reducing the disulfide bonds at the hinged region of the $F(ab')_2$, which are then free to react to a number of possible linker molecules previously applied to the sensor surface.

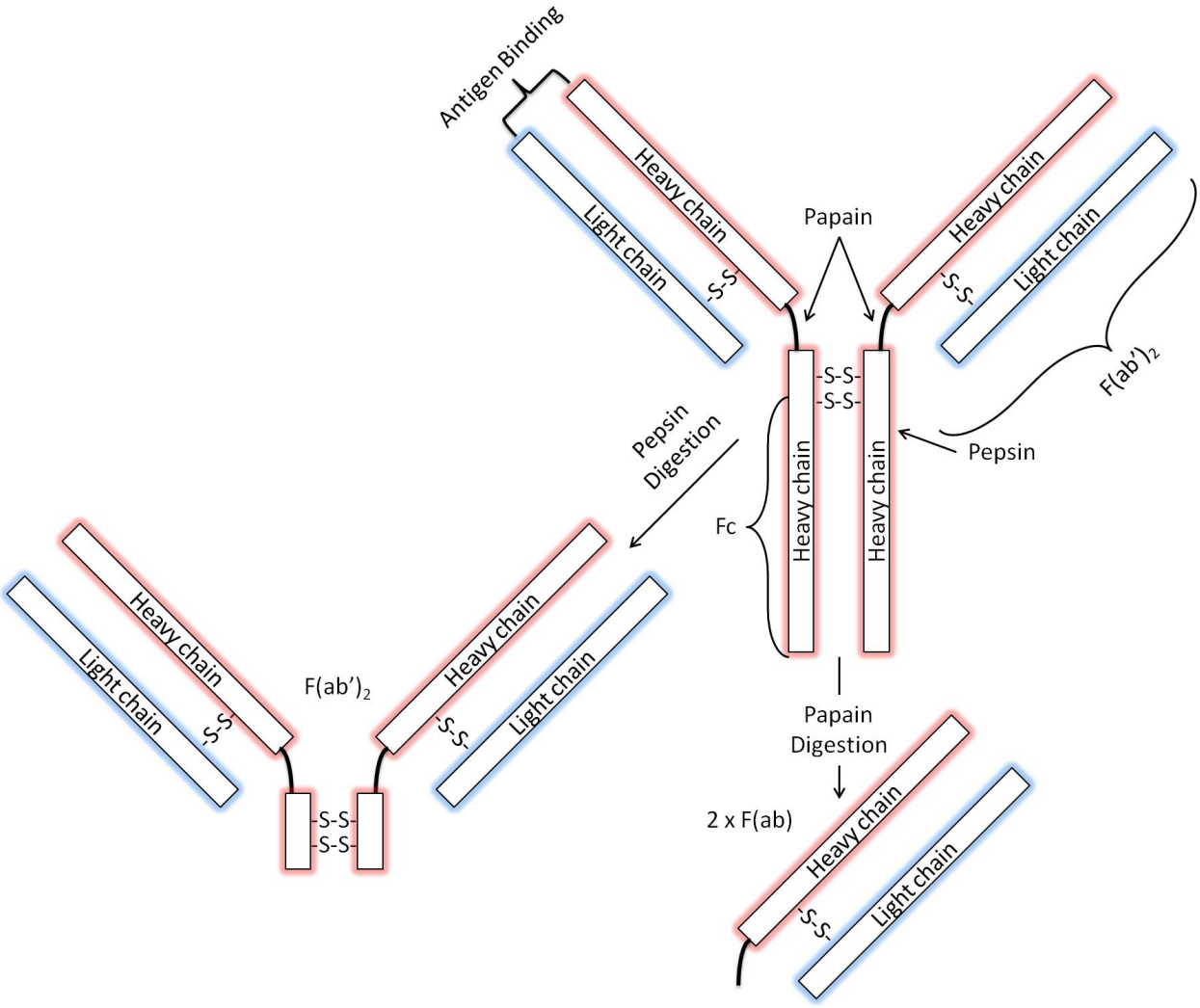

Figure 5-1: Generalized diagram of an IgG and two possible ways to digest an IgG into F(ab) and F(ab')$_2$ fragments.

The IgG antigen to antibody association rate constant of 2–3×10^5 $M^{-1}s^{-1}$ [39] is less than that of the biotin/streptavidin system which is in the range of 3.0 × 10^6–4.5 × 10^7 M^{-1} s^{-1} [40], therefore one may see a decrease in the slope of the response at the same concentration (~ 6 µM) and flow rate (2 µL/min). To ensure binding of the IgG analyte to the immobilized F(ab') receptor in the event that the immobilized F(ab') are inactive, it was determined to use rabbit anti-goat F(ab') as the receptor and Alex Fluor 488 labeled goat anti-rabbit IgG as the analyte. F(ab') fragments are difficult to keep stable for long periods of time due to oxidation and

recombination of their free sulfhydryl groups, but prepared rabbit anti-goat F(ab')$_2$ fragments are stable up to 3 months and can be purchased from biotech companies (Thermo Scientific: Pierce Biotech).

There are several linking molecules that may work to perform the final immobilization of the F(ab') receptors. With consistent success forming a monolayer of amino-silane using APDIES, primary consideration was given to heterobifunctional cross-linkers containing N-hydroxysuccinimide (NHS) esters. NHS based amine-to-sulfhydryl crosslinking reagents with maleimide, haloacetyl or pyridyldithiol reactive groups that are able to bind with an –SH group are commercially available. An example of each of these is sulfosuccinimidyl-4-(N-maleimidomethyl)cyclohexane-1-carboxylate (Sulfo-SMCC), sulfosuccinimidyl (4-iodoacetyl)aminobenzoate (Sulfo-SIAB) and 2-Pyridyldithiol-tetraoxaoctatriacontane-N-hydroxysuccinimide (PEG_{12}-SPDP), respectively. All of these can be utilized under physiological conditions making them suitable for protein immobilization. Iodoacetyl groups react with the -SH by nucleophilic substitution of iodine and results in a stable thioether bond. Specificity towards –SH groups is achieved by using a slight stoichiometric excess of iodoacetyl groups and by maintaining the reaction at pH 7.5-8.5, with optimal specificity at pH 8.3. However, the iodoacetyl group can react with amino acids if there are no free sulfhydryls available or if there is a gross excess of iodoacetyl group over sulfhydryls [50]. This may cause a problem for immobilization strategies, since a monolayer of iodoacetyl group would have a inherently high concentration of iodoacetyl groups at a local level. PEG_{12}-SPDP is a multifunctional crosslinker for protein conjugation via amine-to-amine or amine-to-sulfhydryl crosslinks when the pH is between pH 7 and 8, making it less than ideal for our application. Sulfo-SMCC is soluble in aqueous solutions to a concentration of about 10 mM and will link to

an amino-silane surface via an NHS ester leaving a maleimide group to selectively react with the –SH group after reduction of the disulfide bonds ajoining the two halves of the $F(ab')_2$. The maleimide group in (Sulfo-SMCC) reacts with sulfhydryl groups when the pH is between pH 6.5 and 7.5 and forms a stable thioether bond [50]. Although maleimides will react with primary amines at pH 7, the rate is 1000 times slower than the reaction with sulfhydryls [50].

A number of reducing agents can be used to break the disulfide bonds at the hinged region to create two F(ab') for immobilization. These include 2-mercaptoethanol (2-ME), 2-mercaptoethylamine-HCl (2-MEA), Cysteine-HCl, dithiothreitol (DTT), and Tris(2-carboxyethyl)phosphine hydrochloride (TCEP). Of these, 2-MEA and TCEP are of greatest interest. 2-MEA has been shown to seletively reduce disulfide bonds at the hinged region of antibodies [50], but since it contains –SH groups, a 2-MEA/F(ab') solution will require desalting before introduction to the maleimide surface or it will interfere with the reaction. TCEP is a very effective reducing agent that does not require protection of the free sulfhydrls from oxidation and does not interfere with the maleimide to sulfhydryl reaction. However, because TCEP is such an effective reducing agent, it may also reduce the disulfide bond adjoining the heavy and light chains of the F(ab')2, thereby suppressing antigen binding activity. Either case may require the use of a spin column to remove either the 2-MEA salt or excess TCEP and IgG framents smaller than a F(ab').

5.2 Experimental Procedures and Results

Based on the available options presented above, test experiments on quartz slides were accomplished first to test the viability of using APDIES with sulfo-SMCC as the linker molecule and TCEP as the reducing agent. The results seem reasonable, so a PMCL die was then prepared with an amine monolayer by liquid deposition of 5% APDIES in dry toluene (HPLC grade),

inkjet printing of a solution of sulfo-SMCC onto select PMCLs, flowing a solution containing $MS(PEG)_4$ for passivation and flowing a solution of reduced F(ab') fragments after microfluidic integration to complete the functionalization of the sensor surfaces. The following sections outline the procedures of the various experiments to functionalize and test the PMCL sensor with F(ab') as receptors and IgG as analytes.

5.2.1 Fluorescence Experiments

Fluorescence experiments on quartz slides, indicated that differential adsorption of tagged IgGs to the intended sensor surface could be increased by using a passivation agent. Theoretically, passivation should increase surface stress over a non-passivated scenario if the passivation agent is shorter than the F(ab'), thus precluding interference. An additional caveat to this would be that the adsorption of the tagged IgG does indeed induce a surface stress.

The processing steps for two quartz dies (labeled Q1 and Q2) plus a silicon witness slide for this experiment are as follows:

1) Clean quartz and silicon slides in acetone, then with IPA and N_2 dry
2) Plasma clean for 3 min at 18 W in Harrick Plasma Cleaner
3) Clean in Nanostrip at 90 °C for 30 min, remove and rinse in DI water
4) Plasma clean for 3 min at 18 W in Harrick Plasma Cleaner
5) Measure SiO_2 thickness of silicon witness slide with spectroscopic ellipsometer
    a. Initial: 2.054 nm (MSE: 2.712 °)
6) Plasma clean for 1 min at 18 W in Harrick Plasma Cleaner
7) Place slides in jar containing 5% APDIES solution (~9.5 gm toluene, 0.5 ml APDIES) for 19 hours.

8) Mix sulfo-SMCC in jettable solution: ~ 6.5 mg/ml Sulfo-SMCC (61% glycerol, 39% 40 mM MOPS Buffer (pH 7.0), 0.15 mg/ml TX-100)
9) Remove and dip in two rinse jars of fresh toluene, then rinse in an jar of IPA, remove and N_2 dry
10) Use Dimatix inkjet printer to spot sulfo-SMCC on quartz slides in large area arrays where fluid channels will be once covered with PDMS piece
11) Let stand for 30 min at room temp for NHS ester to $-NH_2$ reaction to proceed
12) Measure SiO_2 thickness of silicon slide
    a. After APDIES deposition: 3.243 nm (MSE: 2.215 °)
    b. Estimated APDIES thickness: 1.189 nm
13) Attach PDMS piece, glass piece and cure at 70 C for 60 min for each quartz die, in turn
14) Rinse away excess sulfo-SMCC with 40 mM Tris buffer (pH 7.0) + 0.2% TX100 for 10 min @ 10 µl/min.
15) Rinse and buffer exchange to 75% 50 mM MOPS buffer (pH 7.0) / 25% DMSO
16) Passivate one set on each quartz slide with 30 mM $MS(PEG)_4$ in 75% 50 mM MOPS buffer (pH 7.0), 25% DMSO for 15 min.
17) Rinse and buffer exchange to $F(ab')_2$/TCEP drive buffer (pH 7.0)
18) Flow 0.35 mg/ml rabbit anti-goat $F(ab')_2$ solution consisting of 50 µL of $F(ab')_2$ stock (7 µM) with 50 µL 0.4 mM TCEP solution (2 µl/min for ~30 min switching between sets every 60 sec) for each quartz die.
19) Rinse and buffer exchange with 100 mM sodium phosphate, 100 mM NaCl, 5 mM NaN_3 -- pH 7.5
20) Flow 200 nM Alexa Fluor 488 IgGs at 2 µl/min for ~10 min

21) Set #1: 200 nM Alexa Fluor 488 Goat Anti-Human IgG

22) Set #2: 200 nM Alexa Fluor 488 Goat Anti-Rabbit IgG

23) Rinse and capture fluorescence images, remove PDMS and re-image

Figure 5-2 shows two sets of printed line where Sulfo-SMCC was inkjeted on two quartz slides Q1 and Q2. These images are after they were passivated and non-passivated, respectively, exposed to 200 nM Alexa Fluor 488 Goat Anti-Rabbit IgG and then had the PDMS removed. The average intensity from these images shows that passivation provides 75% more differential binding over the non-passivated case for goat anti-rabbit IgG to an immobilized rabbit anti-goat F(ab') receptor.

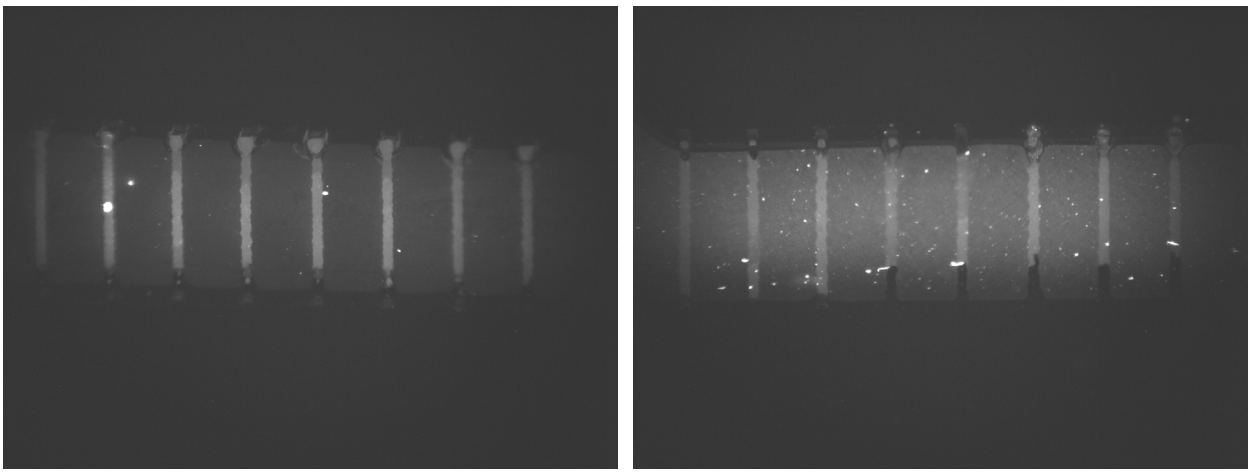

(a) ***(b)***

Figure 5-2: Fluorescent microscope image of a set of lines from deposited sulfo-SMCC which were (a) passivated with MS(PEG)4 (Q1) and (b) non-passivated (Q2) after exposure to 200 nM Alexa Fluor 488 Goat Anti-Rabbit IgG (PDMS removed, exposure: 150 ms, gain: 24, gamma: 1, magnification: X7).

To estimate to what degree the immobilized F(ab') retained their activity for binding antigens, the other sets were exposed to Alexa Fluor 488 Goat Anti-Human IgG. Figure 5-3 shows set #1 for quartz slide Q2 with the PDMS removed which was passivated at the same time as the other set. The average intensity from these images demonstrates that the activity is very

low with only 17% over the intensity of its passivated background where as the same scenario with Alexa Fluor 488 goat anti-rabbit IgG is 162% over its passivated background. This experiment was repeated with new reagents a second time and again the activity was only 18% for anti-human IgG and 156% for the anti-rabbit IgG.

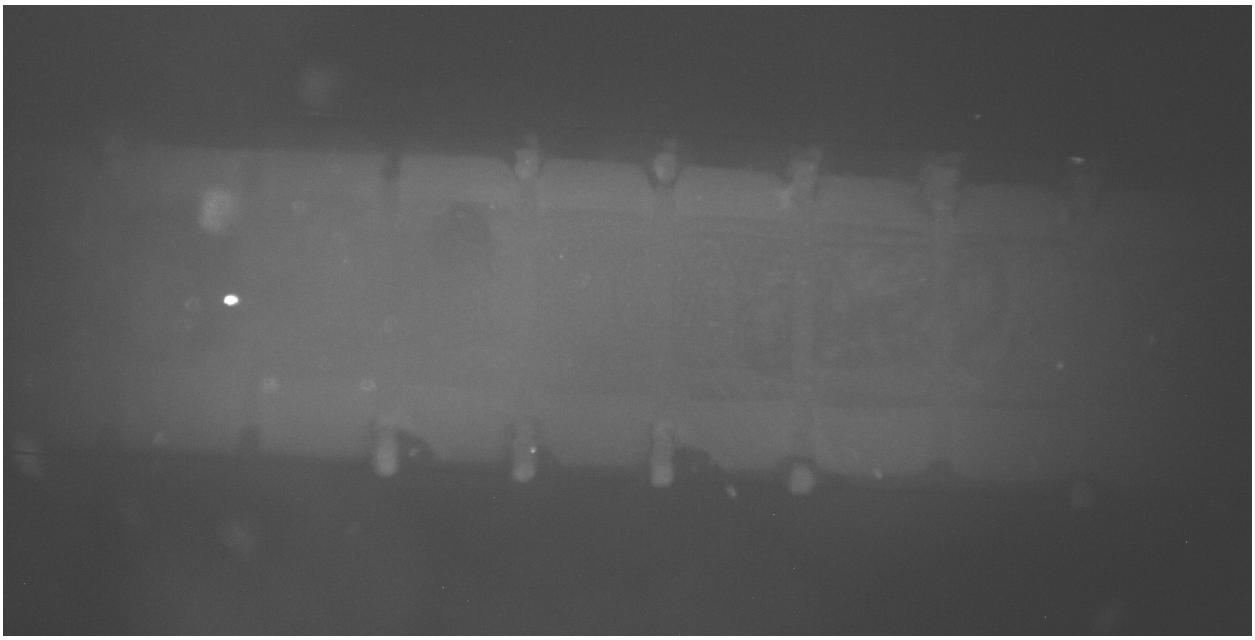

Figure 5-3: Fluorescent microscope image of a set of lines from deposited sulfo-SMCC which were passivated with MS(PEG)4 (Q2) after exposure to 200 nM Alexa Fluor 488 Goat Anti-Human IgG (through the PDMS, exposure: 150 ms, gain: 24, gamma: 1, magnification: X7).

While this clearly shows that my immobilization technique is not functionalizing the sensor surface with a sufficient density of active receptors, it also provides evidence that an experiment following this protocol on a real PMCL die should indicate whether or not sufficient binding stress could be generated upon adsorbtion of active IgG antibodies, namely the Alexa Fluor 488 goat anti-rabbit IgG. This experiment might also indicate that F(ab') fragements are being split into their separate heavy and light chains, allowing inactive fragments to compete for space on the sensor surface. Therefore, it was determined to use this protocol on a real PMCL

die, with one set being functionalized with a solution of un-filtered F(ab') fragments and the other with a solution that is filtered to remove fragments smaller than a F(ab').

5.2.2 Reagent Preparation

Sulfo-SMCC, $MS(PEG)_4$ and rabbit anti-goat IgG $F(ab')_2$ fragments (adsorbed against human serum proteins to minimize cross-reactivity) were purchased from Thermo Scientific (Pierce Biotechnologies). The Alexa Flour 488 goat-anti rabbit IgG antibodies were purchased from Life Sciences Corp. (Invitrogen). To minimize cross-reactivity, these were adsorbed against human IgG, human serum, mouse IgG, mouse serum and bovine serum. The Alexa Flour 488 goat-anti human IgG antibodies were also purchased from Life Sciences Corp. (Invitrogen) and were adsorbed against mouse, rabbit and bovine serum to minimize cross-reactivity. Alexa Fluor stock solutions were received at 2 mg/ml (13.3 μM) -- 100 mM $NaPO_4$, 100 mM NaCl, 5 mM NaN_3, pH 7.5 with 6 mole dye/mole IgG. $F(ab')_2$ fragments were received at 0.7 mg/ml (7 μM) in phosphate buffer (10 mM $NaPO_4$, 250 mM NaCl, pH 7.6). The following protocol outlines the steps used to reduce and filter (if desired) $F(ab')_2$ to F(ab').

1) Make TCEP reaction buffer: 50 mM MOPS, 210 mM NaCl, 5 mM EDTA, pH 7.0
    a. For 500 ml of buffer, 730 mg of EDTA is required for a 5 mM solution
    b. Place 100 ml of 100 mM NaOH solution in beaker with stir bar and place on stirring plate.
    c. Weigh out 730 mg of EDTA, add to beaker and stir
    d. Insert calibrated pH meter into solution
    e. Add NaOH to solution to maintain pH above 8.0 until EDTA is fully dissolved

f. Transfer EDTA solution to 500 ml beaker with larger stir bar and place on stir plate

g. Add 400 ml DI H_2O

h. Add 5.230 gm of MOPS acid (50 mM in 500 ml)

i. Add 6.14 gm NaCl (210 mM in 500 ml)

j. Insert calibrated pH meter into solution, stir and adjust with HCl or NaOH solution until a pH 7.0 is achieved.

2) Mix TCEP stock reducing solution -- 4 mM TCEP-HCl in 50 mM MOPS, 210 mM NaCl, 5 mM EDTA, pH 7.0

a. Add 80.3 mg of TCEP-HCl to 70 ml of reaction buffer

b. Stir and adjust to pH 7.0 with HCl or NaOH solution

c. Dilute a portion to 0.4 mM with reaction buffer

3) Reduce F(ab')2:

a. Equilibrate 30kDa centrifuge filter (Millipore Amicon Ultra-4, MWCO: 30 kDa) by passing 1 ml of reaction buffer through it.

b. Buffer exchange:

i. Combine 200 µL $F(ab)_2$ stock to spin filter and 1 ml of reaction buffer

ii. Spin at 4000 RPM for 10 min in centrifuge filter (Millipore Amicon Ultra-4, MWCO: 30 kDa)

iii. Repeat Steps i and ii

iv. Dilute back to 200 µL of F(ab)2 (0.7 mg/ml).

c. Remove 50 µL of buffer exchanged F(ab')2 stock from spin filter and place in 1.5 ml centrifuge tube

d. Add 50 µL of the 0.4 mM TCEP reducing solution

e. Incubate for 30 min at room temperature

4) Filter out low molecular weight fragments

a. Return 150 µL reaction mixture back to centrifuge filter to remove heavy and light chain fragments.

b. Add 1 ml of reaction buffer to centrifuge filter

i. Spin at 4000 RPM for 10 min in centrifuge filter (Millipore Amicon Ultra-4, MWCO: 30 kDa)

ii. Repeat Steps 1 and 2

c. Dilute to desired concentration with reaction buffer (0.35 mg/ml)

Extra buffer solutions to match that which was used to carry IgG and F(ab') fragments were made and introduced before reagent solutions to eliminate any PMCL response due to changes in pH, buffer species or concentration. Filtered and un-filtered solutions were tested in an SDS-PAGE 10% acrylamide gel run at 150 V for ~ 1 hour with non-reducing loading buffer as shown in Figure 5-4. The following list indicates each lane assignment:

1) **M.W. Control Scale:** All Blue Standards
2) **Stock only:** 25 µL $F(ab')_2$ stock solution (0.7 mg/ml) + 25 µL 50 mM MOPS buffer, pH 7.0
3) **0.4 mM TCEP after 1 hour incubation:** 25 µL $F(ab')_2$ stock solution (0.7 mg/ml) + 25 µL 0.4 mM TCEP in 50 mM MOPS, pH 7.0
4) **0.4 mM TCEP after 1 hour incubation, filtered at 30 kDa MWCO:** 50 µL $F(ab')_2$ stock solution (0.7 mg/ml) + 50 µL 0.4 mM TCEP in 50 mM MOPS, pH 7.0, filtered in 30 kDa MWCO filter unit, reconstituted with stock/MOPS buffer to 0.35 mg/ml.

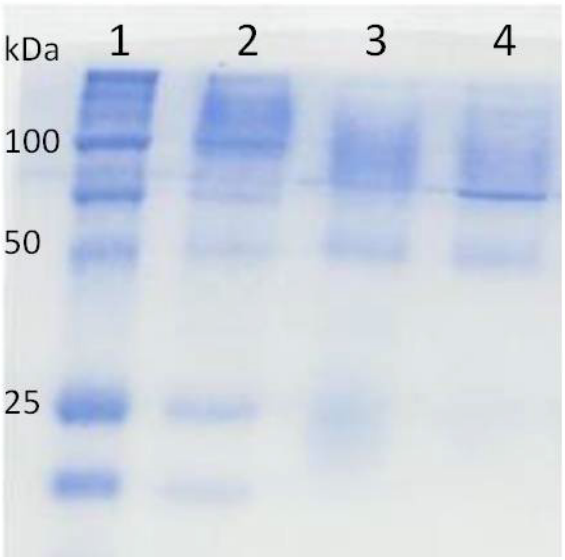

Figure 5-4: SDS-PAGE 10% acrylamide gel of molecular weight reference (lane 1), stock F(ab')2 (lane 2), reduced F(ab') solutions both unfiltered (lane 3) and filtered (lane 4).

The $F(ab')_2$ portion of an IgG has a molecular weight around 100, so the molecular weight for a F(ab') is around 50. Fragments in the 25 range are likely F(ab') fragment that had their heavy and light chains split, making them inactive. As seen from the gel, the filtering protocol was not only effective at removing split F(ab') fragments but also removing smaller fragments already present in the stock solution.

5.2.3 PMCL Die Preparation

Starting with a newly fabricated 2 x 16 array PMCL die, measurement of the PMCLs response with respect to deflection state was performed on a custom auto-alignment system and optical bench. During this pushdown experiment, PMCLs #1 and #4 on set #1 of the PMCL die showed small slopes in their output differential signals and other anomalous behavior, thus the data from these are excluded from the results.

After the pushdown experiments, the die was cleaned in fresh Nanostrip at 90 °C for 18 hours, rinsed with DI water, IPA and then dried in the supercritical point dryer (CPD). A glass

reaction jar was cleaned with acetone, IPA and a 5 min plasma at 18 W in a Harrick plasma cleaner. After dehydrating the jar for 4 hours at 150 °C, 9.5 mg of toluene and 500 µL of APDIES were combined in the dehydrated jar freshly removed from the dehydration oven. The PMCL die was then given a final treatment in the Harrick plasma at 18 W for 3 min and immediately placed in the reaction jar and covered with a PTFE-lined lid. With spectroscopic ellipsometry measurements of a witness slide, the thickness of the APDIES layer was estimated to be 0.892 nm, which corresponds to a monolayer. After silane deposition, the die was rinsed twice in fresh toluene, then in IPA and dried in the CPD. After removing from the CPD, a freshly prepared solution of 5.2 mg/ml sulfo-SMCC in 1 ml of spotting solution (61% Glycerol, 39% 40 mM MOPS 0.15 mg/ml TX100) was inkjet-printed onto the first nine PMCLs for Set #1 and first eight PMCLs for Set #2. Improvements in microfluidic integration technique allowed for assembly without first drying the sulfo-SMCC functionalization fluid. After microfluidic integration, excess sulfo-SMCC was rinsed away with a buffer/surfactant solution (40 mM Tris (pH 7.0) + 0.2% Triton X-100) for 2 min at 100 µL/min A stabilization rinse was then performed overnight with 40 mM Tris buffer (pH 7.0) flowing through the microfluidics at 2 µL/min switching between PMCL arrays every 60 sec.

5.2.4 PMCL Sensing Experiment

This IgG sensing experiment provided three opportunities to see adsorption-induced surface stress during the introduction of $MS(PEG)_4$, rabbit anti-goat F(ab') fragment, and Alexa Fluor 488 goat anti-rabbit IgG solutions. The passivation run proceeds at 2 µL/min, spans 5 min of data capture and is timed as follows: At the 15 sec mark the valve opens, at the 30 sec mark the flow starts, at the 240 sec mark the flow stops, and at the 270 sec mark the valves closes. The F(ab') and IgG exposures proceed at 2 µL/min, span 10 min of data capture and are timed as

follows: At the 15 sec mark the valve opens, at 30 sec the flow starts, at 540 sec the flow stops, and at 570 sec the valves closes.

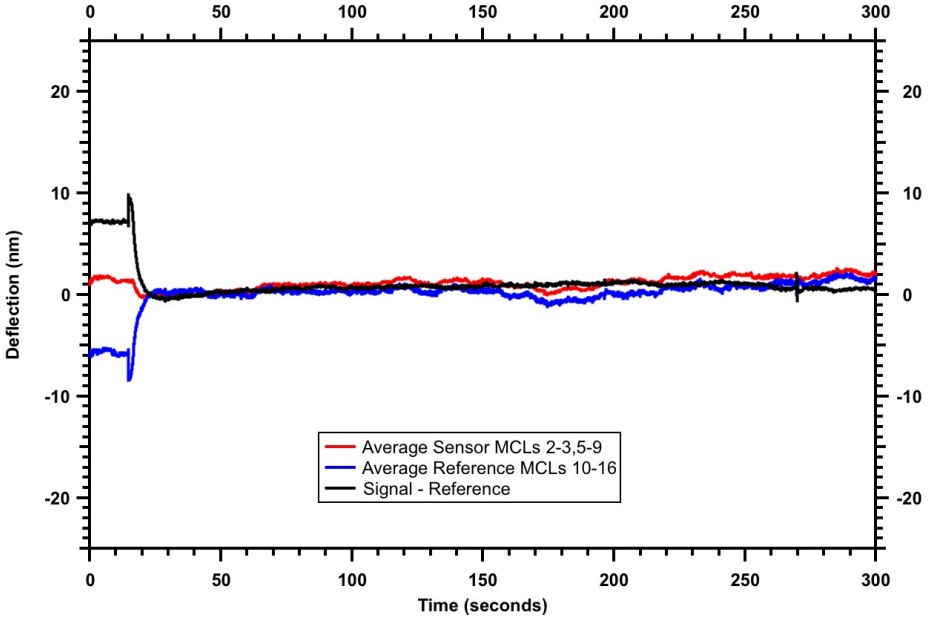

(a)

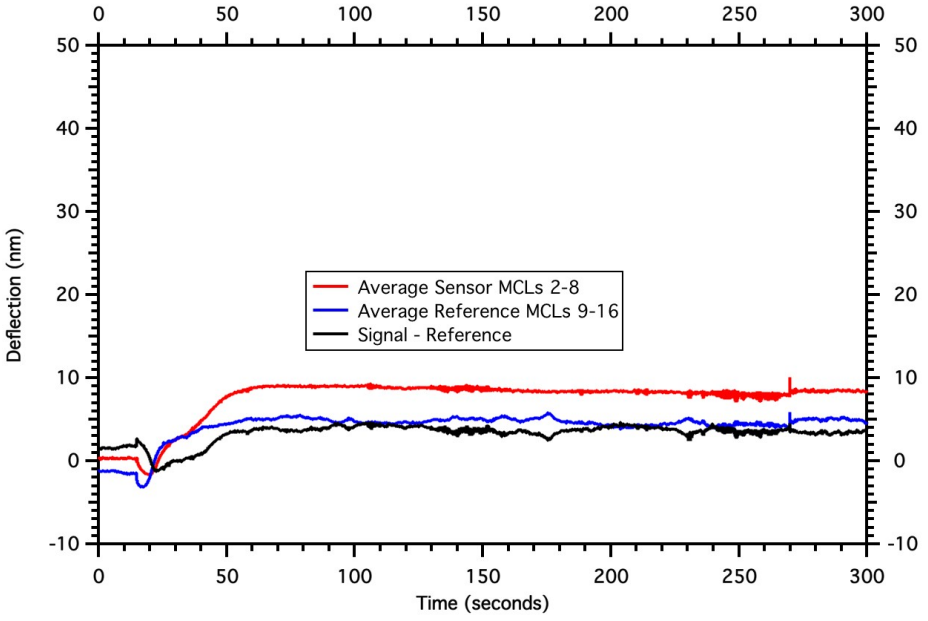

(b)

Figure 5-5: Average passivation (30 mM MS(PEG)$_4$) response of sensor and reference PMCLs for (a) Set#1 and (b) Set #2.

There are often spurious spikes in the data caused by heavy geo-technical construction close to the laboratory building where the experiments were conducted and can be disregarded.

Starting from the stabilization rinse of 40 mM Tris buffer (pH 7.0), the first step performed was to exchange the buffer with 75% 50 mM MOPS/NaOH buffer (pH 7.0) / 25% DMSO and flow this through each channel at 100 uL/min for 20 sec in preparation to see any deflection when introducing the passivation agent. The passivation was done with 30 mM $MS(PEG)_4$ in 75% 50 mM MOPS/NaOH buffer (pH 7.0) and 25% DMSO. Figure 5-5 shows the average sensor and reference response to adsorption of the passivation agent for both PMCL arrays. Set #1 shows a transient response followed by an average negative response (downward deflection) of 7 nm over a relatively short period of ~10 sec, followed by a stable response the remainder of the test. Set #2 also shows a transient response followed by an average positive response of ~ 4 nm.

The next step was a control/stabilization run, which produced a flat uneventful response, so the results are omitted. In preparation for F(ab') functionalization, the buffer is exchanged for 50 mM MOPS, 210 mM NaCl, 5 mM EDTA at pH 7.0. Set #1 was exposed to a 0.35 mg/ml rabbit anti-goat F(ab') filtered solution and set #2 was exposed to the un-filtered version of the same solution as described in Section 5.2.2. Figure 5-6 shows the average sensor and reference response to adsorption of F(ab') fragments for both PMCL arrays. The response for both sensor and reference PMCLs for both filtered and unfiltered cases was mixed with about half moving in a positive direction and the other half in a negative direction, although the filtered solution on set #1 seems to have more of a negative deflection on average.

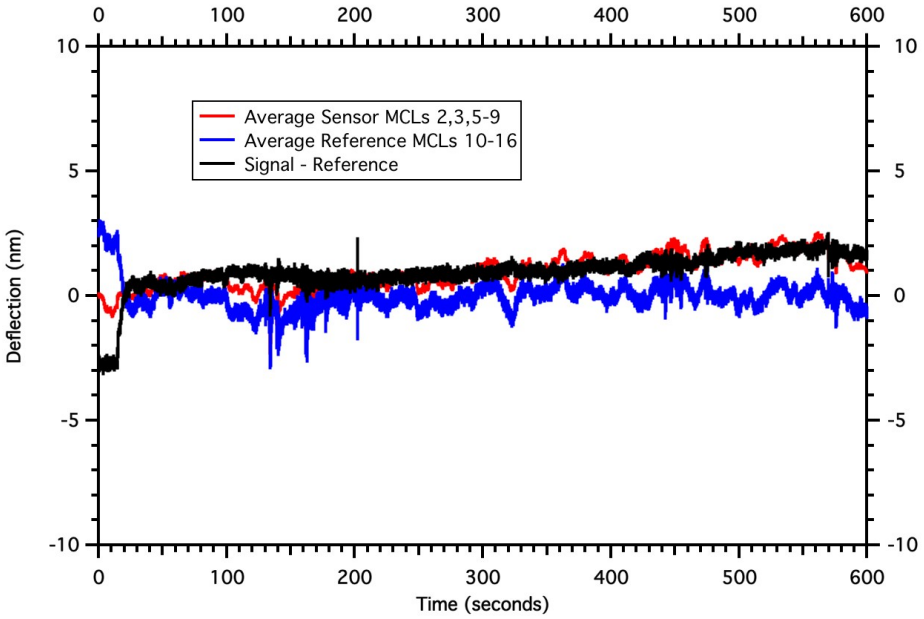

(a)

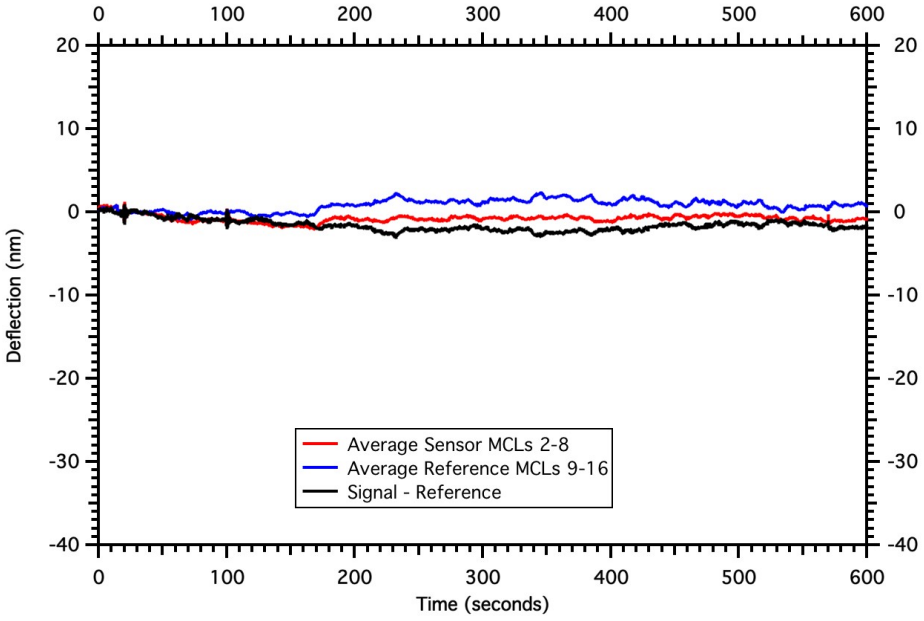

(b)

Figure 5-6: Average F(ab') response of sensor and reference PMCLs for the (a) filtered F(ab') solution on Set #1 and the (b) un-filtered F(ab') solution on Set #2.

Next, the buffer was exchanged again with 100 mM sodium phosphate, 100 mM NaCl, 5 mM NaN_3 (pH 7.5) in preparation for the IgG sensing run using 6.7 μM Alexa Fluor 488 goat

anti-rabbit IgG. For Set #1, the fluorescence appeared in the array microchannel at the 41 sec mark. For Set #2 the fluorescence appeared at the 42 sec mark.

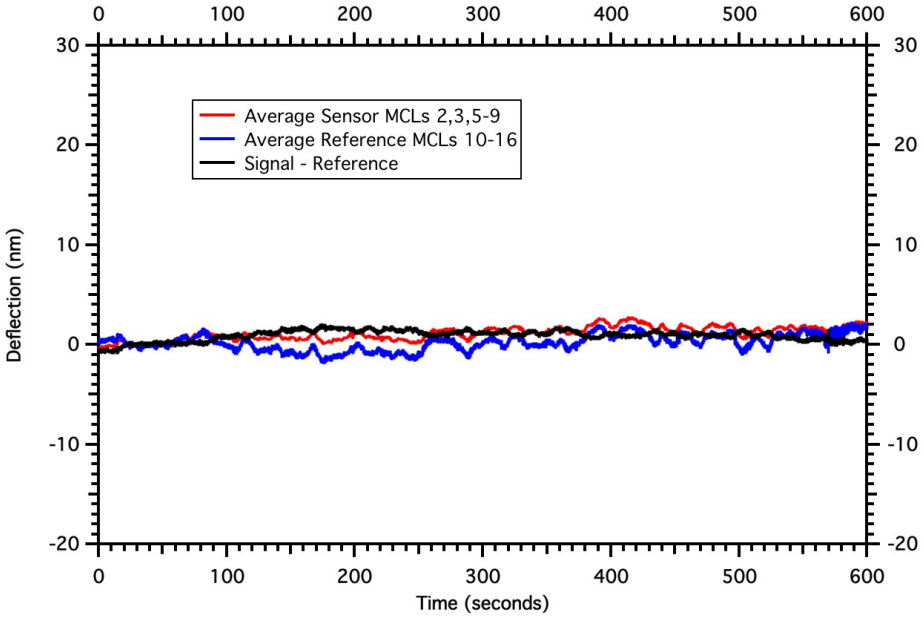

(a)

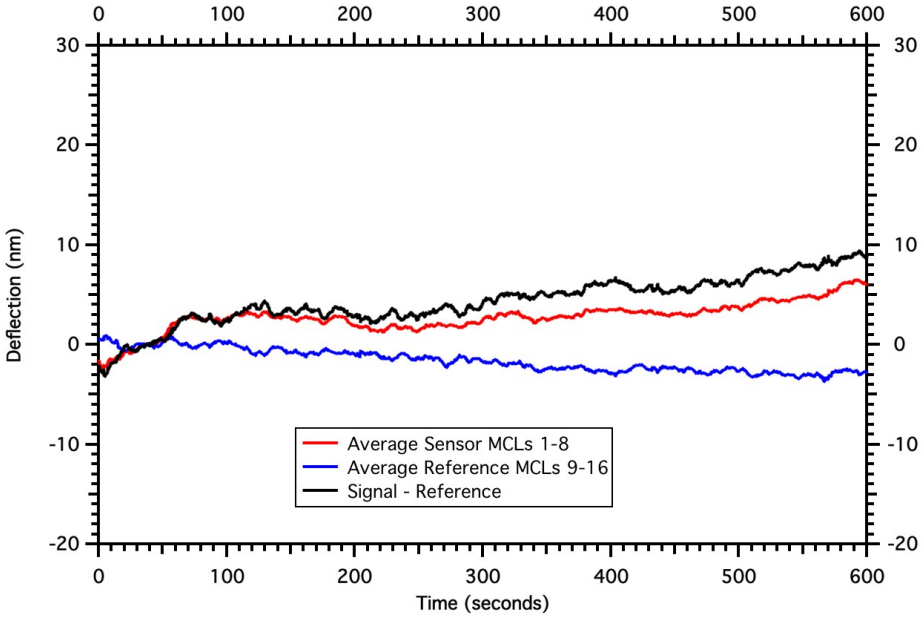

(b)

Figure 5-7: Average response of sensor and reference PMCLs to 6.7 µM Alexa Fluor 488 goat anti-rabbit IgG for the (a) filtered F(ab') receptors on Set #1 and the (b) un-filtered F(ab') receptors on Set #2.

5.3 Discussion

The passivation data in Figure 5-5 for both Sets #1 and #2 might appear to indicate deflection upon adsorption of the $MS(PEG)_4$. Based on past experiments, one would expect passivation to provide a upward (positive) deflection of around 10-15 nm (Figure 4-9(b)). However, Set #1 shows a larger response for the reference PMCLs and the net deflection difference is in the negative direction with a magnitude of about 7 nm. The response may also be too early, as seen in the AF 488 IgG run that the analyte front seems to be reaching the PMCL arrays around the 40-45 sec mark. Set # 2 also seems to have some sort of response, with a slight change in the responds of about 3-4 nm upward (positive) at the 40 sec mark that might be measuring $MS(PEG)_4$ adsorption.

Data for F(ab') sensing on Set #1 (filtered F(ab') solution), shows a similar pattern, with a larger average response for the reference PMCLs but this time the average net response of the array is positive. The increase in noisy behavior of Set #1 may have been due to the geo-technical construction (pile driving) under way near the laboratory during the test. Set #2 (un-filtered F(ab') solution) shows absolutly no deflection or indication of a binding event.

The IgG sensing tests show a practically flat response for Set #1 with slight construction vibrations noted at 267, 512, 560-595 sec. Set #2 for the un-filtered F(ab') solution might indicate some sort of adsorption event, however the slope of the reponse is rather linear and begins before fluorescence indicates the IgG's even reach the PMCL array. Construction vibrations at 225 sec are noted for Set #2.

5.4 Conclusion

I have demonstrated the ability to immobilize IgG proteins on the quartz surface. While the activity of the immobilized F(ab') fragments was very low (17-18%), I was able to move

forward with a preliminary sensing test to see if a larger molecule would provide greater PMCL deflection. I demonstrated an effective passivation agent that increases differential binding by 75% over the a non-passivated scenario. A protocol for the reduction of $F(ab')_2$ and isolation of F(ab') fragments was tested and shown to be effective through SDS-PAGE. The results of three sensing tests on two separate arrays with ~0.35 mg/ml rabbit anti-goat F(ab') filtered and un-filtered (for isolation) solutions are rather inconclusive and may be an indication of variation in reagent or die processing. Further testing would be required to be certain whether IgG are indeed adsorbed on the PMCL surface and if that adsorption would result in surface stress and deflection. Also, futher exploration of $F(ab')_2$ reduction and purification need to be accomplished.

6 CONCLUSION

6.1 Summary

Cost savings in healthcare, the potential for expanded options for human blood serum testing and enhanced diagnosis of disease states provide motivation to develop a packaged lab-on-chip device capable of detecting sub-pM protein concentrations. MCLs have been successfully transformed into nanomechanical biosensors based on a variety of biomolecular interactions, but have yet to reach this limit of detection. The development of a functionalization technique to transform an all-silicon in-plane PMCL into a working biosensor included applied knowledge of MCL operational theory, surface chemistry analysis, deposition methods, bio-conjugation techniques, biochemistry and the technical requirements for non-contact deposition of biological materials as reviewed in Chapter 2.

I demonstrated the non-contact single-sided functionalization of a silicon PMCL array using a Dimatix inkjet printer and improved drop placement accuracy from +/- 25 μm to +/- 7.5 μm. I developed a jettable fluid (61% glycerol, 39% aqueous buffer, 0.15 mg/mL Triton X-100) suitable for biological molecules and presented a method to maximize fluid coverage of the PMCL surfaces through droplet swelling during a controlled increase in ambient humidity by water uptake of hygroscopic glycerol in the jetted droplets. I also demonstrated a method to improve the surface site density by removing buffer salts and excess proteins from the sensor surface during functionalization. This was accomplished by swelling the functionalization fluid

to form a liquid bulb just below the base of each PMCL and allowing surface tension to wick dissolved solids off the PMCL upon drying.

I effectively immobilized biotin as a receptor and improved the monolayer silane deposition from 1.14 nm (+/- 0.23 nm) with GOPS to the more stable APDIES at 0.9 nm (+/- 0.3 nm). With immobilized biotin on the sensor surface, the group experimentally tested a solution containing 4.7 μM of Alexa Fluor 488 streptavidin and reported adsorption induced surface stress of 6 mN/m or less and corresponding PMCL deflection of 5 – 15 nm. In the process, the group discovered that increased surface roughness decreases the amount of generated surface stress. In addition, binding of the passivation agent $MS(PEG)_{24}$ to functionalized PMCLs produces a compressive surface stress (4.5 mN/m) and the application of the passivation agent prevents surface stress generation on functionalized PMCLs upon exposure to streptavidin.

I demonstrate that passivation with $MS(PEG)_4$ provides 75% more differential binding over the non-passivated case for goat anti-rabbit IgG ligand to immobilized rabbit anti-goat F(ab') fragments (receptors). A protocol for the reduction and isolation of F(ab') fragments was tested and shown to be effective through SDS-PAGE. Fluorescent query and imaging of immobilized F(ab') fragments indicates that my protocol for reduction and/or immobilization renders the F(ab') virtually inactive. The group performed a test to passivate two PMCL arrays, immobilize F(ab') fragments on the PMCL sensor surfaces, and determine the potential for adsorption induced surface stress with Alexa Fluor 488 goat anti-rabbit IgGs. Insufficient differential surface stress was generated during any of these tests to conclusively determine the ability of adsorped IgG's to induce a differential surface stress on a silicon PMCL.

6.2 Future Research

The end goal of the Nordin group's microcantilever project was to create a viable lab-on-chip diagnostic device for bio-medical sensing applications. This dissertation demonstrates a technique and approach to functionalize PMCLs and provides a baseline characterization of the PMCL. While these are important milestones in the PMCL research and development, further research is required to enhance the adsorption-induced surface stress before a viable sensor platform based on a PMCL can be realized. It is likely that this will involve a non-metallic thin film coating that undergoes a structural change at the atomic level upon adsorption of a nearby molecule. Once this occurs, a sensing demonstration of real world bio-molecules can be undertaken. This will include development of an immobilization strategy for the receptor of interest and an appropriate passivation scheme before sensor characterization can begin. This characterization should include the development of an ambiguity function, or receiver operating characteristic (ROC) curve, to eliminate false positives in multiplexed sensing scenarios.

In addition to improvement and characterization of the PMCL as a biosensor, other research efforts need to be undertaken in the way of fluid delivery and on-chip processing specific for the group's PMCL device. This has partially begun with the design and development of on-chip PDMS reflow pumps with the goal to more efficiently utilize small sample volumes and detect even lower concentrations (e.g. sub-fM).

Considerable cost could be avoided if the sulfo-NHS esters or TFP esters used in the reactive group of our biotin receptor could be replaced with stable variant. Due to hydrolysis, these esters are unstable in aqueous solutions with a half life of about two hours. Consequently, I had to use a new Dimatix inkjet cartridge for each die, at a cost of $100 each not including the prep time and reagents. A more stable option, such as a photoreactive biotinylation reagent (e.g.

TFPA-PEG$_3$-Biotin) should be investigated. The optimal wavelength for photoactivation of the Tetrafluorophenyl Azide (TFPA) moiety is in the UV range at 320nm (Figure 6-1).

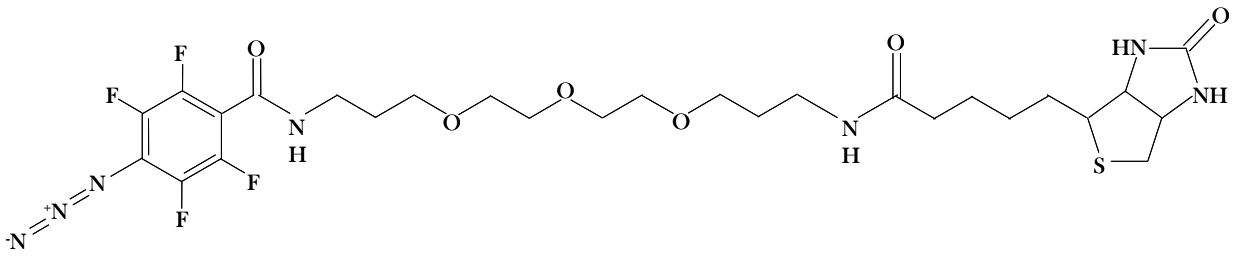

Figure 6-1: Model of TFPA-PEG3-Biotin

Finally, other applications for the PMCL sensor, such as a seismic sensor or a chemical vapor sensor, should be considered.

REFERENCES

[1] Organisation for Economic Co-operation and Development (2009), "OECD Health Data", *OECD Health Statistics* (database), accessed on 18 April 2012.

[2] J. Fritz, M. K. Baller, H. P. Lang, H. Rothuizen, P. Vettiger, E. Meyer, H.J. Guntherodt, C. Gerber, and J. K. Gimzewski, "Translating biomolecular recognition into nanomechanics," *Science* 288, 316-318 (2000).

[3] G. Wu, H. Ji, K. Hansen, T. Thundat, R. Datar, R. Cote, M. F. Hagan, A. K. Chakraborty, and A. Majumdar, "Origin of nanomechanical cantilever motion generated from biomolecular interactions," *Proceedings of the National Academy of Sciences* 98, 1560-1564 (2001).

[4] R. McKendry, J. Zhang, Y. Arntz, T. Strunz, M. Hegner, H. P. Lang, M. K. Baller, U. Certa, E. Meyer, and H. J. Guntherodt, "Multiple label-free biodetection and quantitative DNA-binding assays on a nanomechanical cantilever array," *Proceedings of the National Academy of Sciences* 99, 9783-9788 (2002).

[5] C. A. Savran, S. M. Knudsen, A. D. Ellington, and S. R. Manalis, "Micromechanical detection of proteins using aptamer-based receptor molecules," *Anal. Chem*. 76, 3194-3198 (2004).

[6] F. Huber, M. Hegner, C. Gerber, H. J. Guntherodt, and H. P. Lang, "Label free analysis of transcription factors using microcantilever arrays," *Biosens. Bioelectr.* 21, 1599-1605 (2006).

[7] R. Raiteri, M. Grattarola, H. J. Butt, and P. Skladal, "Micromechanical cantilever-based biosensors," *Sensors and Actuators B: Chemical* 79, 115-126 (2001).

[8] W. Shu, E.D. Laue, and A.A. Seshia, “Investigation of biotin–streptavidin binding interactions using microcantilever sensors,” *Biosens. Bioelectron.* 22, 2003–2009 (2007).

[9] Y. Arntz, J. D. Seelig, H. P. Lang, J. Zhang, P. Hunziker, J. P. Ramseyer, E. Meyer, M. Hegner, and C. Gerber, "Label-free protein assay based on a nanomechanical cantilever array," *Nanotechnology* 14, 86-90 (2003).

[10] N. Backmann, C. Zahnd, F. Huber, A. Bietsch, A. Pluckthun, H. P. Lang, H. J. Guntherodt, M. Hegner, and C. Gerber, "A label-free immunosensor array using single-chain antibody fragments," *Proceedings of the National Academy of Sciences* 102, 14587-14592 (2005).

[11] K.M. Goeders, J.S. Colton, and L.A. Bottomley, "Microcantilevers: sensing chemical interactions via mechanical motion," *Chem. Rev.*108522–42 (2008).

[12] J.W. Noh, R.R. Anderson, S. Kim, W. Hu, and G.P. Nordin, "Sensitivity enhancement of differential splitter-based transduction for photonic microcantilever arrays," *Nanotechnology* 21, 155501 (2010).

[13] J.W. Noh, R.R. Anderson, S. Kim, J. Cardenas and G.P. Nordin, "In-plane photonic transduction of silicon-on-insulator microcantilevers," *Optics Express* **16** (16), pp. 12114-12123 (2008).

[14] J.W. Noh, R.R. Anderson, S. Kim, W. Hu, and G.P. Nordin, "In-plane all-photonic transduction with differential splitter using double-step rib waveguide for photonic microcantilever arrays," *Optics. Express* 17 (22), 20012–20 (2009).

[15] W. Hu, R.R. Anderson, Y. Qian, J. Song, J.W. Noh, S. Kim and G.P. Nordin, "Demonstration of microcantilever array with simultaneous readout using in-plane photonic transduction method," *Rev. Sci. Instr.* 80, 085101, pp. 1-7 (2009).

[16] R.R. Anderson, W. Hu, J.W. Noh, W.C. Dahlquist, S.J. Ness, T.M. Gustafson, D.C. Richards, S. Kim, B.A. Mazzeo, A.T. Woolley and G.P. Nordin, "Transient deflection response in microcantilever array integrated with polydimethylsiloxane (PDMS) microfluidics," *Lab Chip* , vol.11, pp. 2088-2096, (2011).

[17] P.S. Waggoner and H.G. Craighead, "Micro- and nanomechanical sensors for environmental, chemical, and biological detection," *Lab Chip*, vol. 7, no. 10, p. 1238, (2007).

[18] Y. Yang, H.F. Ji, and T. Thundat, "Nerve agents detection using a Cu_2/L-cysteine bilayer-coated microcantilever," *J Am Chem Soc* 125, 1124-1125 (2003).

[19] J. Thaysen, A. Boisen, O. Hansen, and S. Bouwstra, "Atomic force microscopy probe with piezoresistive read-out and a highly symmetrical Wheatstone bridge arrangement," *Sensors Actuators* 83, (2000) 47-53.

[20] X. Yan, H.-F. Ji, and T. Thundat, "Microcantilever (MCL) biosensing," Current Analytical *Chemistry* 2, (2006) 297-307.

[21] J. Mertens, E. Finot, T. Thundat, A. Fabre, M.-H. Nadal, V. Eyraud, and E. Bourillot, "Effects of temperature and pressure on microcantilever resonance response," *Ultramicroscopy* 97, (2003) 119-126.

[22] R. Zhang, A. Best, R. Berger, S. Cherian, S. Lorenzoni, E. Macis, R. Raiteri, and R. Cain, "Multiwell micromechanical cantilever array reader for biotechnology," *Review of Scientific Instruments* 78, (2007) 084103.

[23] M.J. Tarlove and J.G. Newman, "Static secondary ion mass spectrometry of self-assembled alkanethiol monolayers of gold," *Langmuir* 8, (1992) 1398-1405.

[24] A. Bietsch, J. Zhang, M. Hegner, H.P. Lang, and C. Gerber, "Rapid functionalization of cantilever array sensors by inkjet printing," *Nanotechnology* 15, (2004) 873-880.

[25] R.C. Zangar, D.S. Daly and A.M. White, "ELISA microarray technology as a high throughput system for cancer biomarker validation", *Expert Rev. Proteom*. 3 (2006) 37–44.

[26] A. Densmore, M. Vachon, D.-X. Xu, S. Janz, R. Ma, Y.-H. Li, G. Lopinski, A. Delage, J. Lapointe, C.C. Luebbert, Q.Y. Liu, P. Cheben and J.H. Schmid, "Silicon photonic wire biosensor array for multiplexed real-time and label-free molecular detection", *Opt. Lett.* 34 (2009) 598–600.

[27] D. Xu, A. Densmore, A. Delâge, P. Waldron, R. McKinnon, S. Janz, J. Lapointe, G.Lopinski, T. Mischki, E. Post, P. Cheben and J.H. Schmid, "Folded cavity SOI microring sensors for high sensitivity and real time measurement of biomolecular binding", *Opt. Express* 16 (2008) 15137.

[28] A.M. Armani, R.P. Kulkarni, S.E. Fraser, R.C. Flagan and K.J. Vahala, "Label-free, single-molecule detection with optical microcavities," *Science* 310 (2007) 783–787.

[29] M. Bisoffi, B. Hjelle, D.C. Brown, D.W. Branch, T.L. Edwards, S.M. Brozik, V.S. Bondu-Hawkins and R.S. Larson, "Detection of viral bioagents using a shear horizontal surface acoustic wave biosensor," *Biosens. Bioelectron.* 23 (2008) 1397–1403.

[30] A.K.Y. Wong and U.J. Krull, "Surface characterization of 3-glycidoxypropyl trimethoxysilane films on silicon-based substrates," *Anal. Bioanal. Chem.* 383 (2005) 187–200.

[31] S. Taylor, S. Smith, B. Windle and A. Guiseppi-Elie, "Impact of surface chemistry and blocking strategies on DNA microarrays," *Nucleic Acids Research*, 2003, Vol. 31, No. 16 e87.

[32] Y. Lvov and H. Mohwald, *Protein Architecture: Interfacing Molecular Assemblies and Immobilization Biotechnology*, Marcel Dekker, Inc., New York, 2000, p. 36.

[33] A.K. Gaigalas, J.B. Hubbard, M. McCurley and S. Woo, "Diffusion of bovine serum albumin in aqueous solutions," *J. Phys. Chem.* 96 (5) (1992) 2355–2359.

[34] J.M. Andreas, E.A. Hauser and W.B. Tucker, "Boundary tension by pendant drops", *J. Phys. Chem.* 42 (8) (1938) 1001–1019.

[35] A.K. Wright and M.R. Thompson, "Hydrodynamic structure of bovine serum albumin determined by transient electric birefringence", *Biophys. J.* 15 (2 (Pt 1)) (1975 February) 137–141.

[36] B. Tsai, W.C. Dahlquist, S. Kim and G.P. Nordin, "Bonding of Polydimethylsiloxane (PDMS) Microfluidics to Silicon-Based Sensors," *J. Micro/Nanolith. MEMS MOEMS* 10 (2011), 043009, doi:10.1117/1.3659139.

[37] G. G. Stoney "The Tension of Metallic Films Deposited by Electrolysis," *Proceedings of the Royal Society of London. Series A*, (1909). 82(553), 172-175.

[38] R.R. Andersen, W. Hu, J.W. Noh, W.C. Dahlquist, S.J. Ness, T.M. Gustafson, D.C. Richards, S. Kim, B.A. Mazzeo, A.T. Woolley and G.P. Nordin. "Transient deflection response in microcantilever array integrated with polydimethylsiloxane (PDMS) microfluidics." *Lab Chip*, (2011), **11**, 2088-2096.

[39] M. Srisa-Art, E.C. Dyson, A.J. deMello, and J.B. Edel "Monitoring of Real-Time Streptavidin-Biotin Binding Kinetics using droplet microfluidics," *Anal. Chem.* (2008), 80, 7063–7067.

[40] A. Malmborg, A. Michaelsson, M. Ohlin, B. Jansson and C. A. K. Borrebaeck, "Real time analysis of antibody-antigen reaction kinetics" *Scandinavian journal of immunology*, (1992) Vol.35 (6), pp.643-50.

[41] S. J. Ness, S. Kim, A. T. Woolley, and G. P. Nordin, "Single-Sided Inkjet Functionalization of Silicon Photonic Microcantilevers," *Sens. Actuators B* 161 (2012) 80-87.

[42] F. Zhang, K. Sautter, A. M. Larsen, D. A. Findley, R. C. Davis, H. Samha, and M. R. Linford, "Chemical vapor deposition of three aminosilanes on silicon dioxide: surface characterization, stability, effects of silane concentration, and cyanine dey adsorption," *Langmuir* (2010), 26 (18), 14648-14654

[43] A.G. Mathad. "The origin of surface stress experienced by a micro-cantilever beam," *Proceedings of the 2010 IEEE Students' Technology Symposium*, 3-4 April 2010, IIT Kharagpur.

[44] M. Godin, V. Tabard-Cossa, Y. Miyahara, T. Monga, P.J. Williams, L.Y. Beaulier, R.B. Lennox and P. Grutter. "Cantilever-based sensing: the origin of surface stress and optimization strategies," *Nanotechnology* 21 (2010) 075501 (8pp).

[45] G. Oliviero, P. Bergese, G. Canavese, M. Chiari, P. Colombi, M. Cretich, F. Damin, S. Fiorilli, S. L. Marasso, C. Ricciardi, P. Rivolo, and L. E. Depero, "A biofunctional polymeric coating for microcantilever molecular recognition," *Analytica chimica acta*, vol. 630, no. 2, pp. 161–167, Dec. 2008.

[46] M. Alvarez and L. M. Lechuga, "Microcantilever-based platforms as biosensing tools," *Analyst*, vol. 135, pp. 827-836, (2010).

[47] S. Mittal, F. Bushman and L.E. Orgel, "Thiol-mediated degradation of DNA adsorbed on a colloidal gold surface," *J Chem Technol Biotechnol* 78:471–473 (2003).

[48] T. M. Squires, R. J. Messinger, and S. R. Manalis, "Making it stick: convection, reaction and diffusion in surface-based biosensors," *Nature Biotechn*., vol. 26, pp. 417-426, (2008).

[49] K. Kitahara, "General Formula for the Deformation of a Plate due to Surface Stress," *Jpn. J. of Appl. Phys*., Vol 33. (1994), 3673–3674.

[50] G.T. Hermanson, *Bioconjugate Techniques, 2nd edition*. Academic Press Inc. (2008).

[51] Anderson, N.L. and Anderson, N.G., "The Human Plasma Proteome", *Molecular & Cellular Proteomics, 1,* (2003) *845-867.*

[52] S.J. Ness, R.R. Anderson, W. Hu, D.C. Richards, J. Oxborrow, T.M. Gustafson, B. Tsai, S. Kim, B.A. Mazzeo, A.T. Woolley and G.P. Nordin, "Weak Adsorption-Induced Surface Stress for Streptavidin Binding to Biotin Tethered to Silicon Microcantilever Arrays," *IEEE Sensors* (accepted for publication).